HGS™
Verification Manual

aquanty

aquanty

Contents

List of Figures

List of Tables

Chapter 1

Verification Examples

In order to verify the numerical techniques and demonstrate the applicability of **Hydro-GeoSphere** via simulation examples, verification is performed by comparison with available analytical solutions, published numerical solutions of simulators with some equivalent features, and field or experimental applications.

Many of the verification problems discussed in this manual correspond to verification test models that are included as part of your **HydroGeoSphere** installation (see the `verification` directory under the **HydroGeoSphere** installation directory). Before diving in, we recommend taking a look at Table 1.1, which provides a useful reference for navigating between the test models included with your installation and the sections in this manual.

1.1 Subsurface Flow

1.1.1 Level 1: Drawdown in a Theis Aquifer

Note: the verification problem described in this section corresponds to the `theis` test case found in the `verification` directory under the **HydroGeoSphere** installation directory.

In order to verify the accuracy of **HydroGeoSphere** in simulating drawdown due to pumping in a Theis aquifer, it was compared with an exact analytical solution. The example is taken from Freeze and Cherry (1979), to which the reader is referred for detailed information regarding the Theis solution. The input parameters for the analytical solution are shown in the Table 1.2.

In the numerical model, a circular grid of 28596 prism elements which was 10000 m in diameter and 1 m thick was generated. The pumping well was simulated with a single vertical line element which was located at the center of the grid. The discharge was specified at the lowermost node in the well. A prescribed head boundary condition was maintained at the outer edge of the domain.

For comparison, the same problem was run using the axisymmetric option with a graded

Table 1.1: Verification test and section cross-reference.

Verification Test	Section Reference
1D_backwards_transport	1.8.1
1D_structures\1_theis_sat_common	1.3.1
1D_structures\2_theis_sat_dual	1.3.1
1D_structures\3_theis_unsat_common	1.3.1
1D_structures\4_theis_unsat_dual	1.3.1
1D_structures\5_HW_pipe_leaks_uniform	1.3.2
1D_structures\6_HW_pipe_leaks	1.3.2
1D_structures\7_fipps	1.3.3
1D_structures\8_fipps_transient	1.3.3
1D_structures\9_channel_rect_const_inflow	1.3.4
abdul	1.4.1
abdul_snowmelt	1.4.1
abdul_thermal	1.4.1
abdul_transport	1.4.1
digiammarco	1.2.3
dual	1.5.4
elder	1.6.1
forsyth	1.1.3
f_cd	1.5.2
gerke	1.5.5
hm_1d	1.1.5
hm_1d_coupled	1.1.6
meyer	1.7.3
olf1	1.2.1
one_well_injection	1.5.6
one_well_pumping	1.5.6
panday	1.4.2
pm_cd	1.5.1
pm_tvs	1.5.3
point_source_case1	1.5.7
point_source_case2	1.5.7
saltpool1	1.6.2
shikaze	1.6.3
smith_woolhiser	1.2.2
tempf	1.7.2
theis	1.1.1
thermal_molson	1.7.5
two_well	1.5.8
two_well_het_ss	1.5.9
two_well_het_trans	1.5.10
unsat_slab	1.5.11
u_1d	1.1.2
wang	1.1.4
ward	1.7.1
yang	1.7.4

Table 1.2: Parameter Values for Simulation of Theis Problem.

Parameter	Value	Unit
Pumping rate	4.0×10^{-3}	m s^{-1}
Hydraulic conductivity	0.0023	m s^{-1}
Aquifer thickness	1.0	m
Aquifer storativity	7.5×10^{-4}	
Radial distance to observation point	55	m
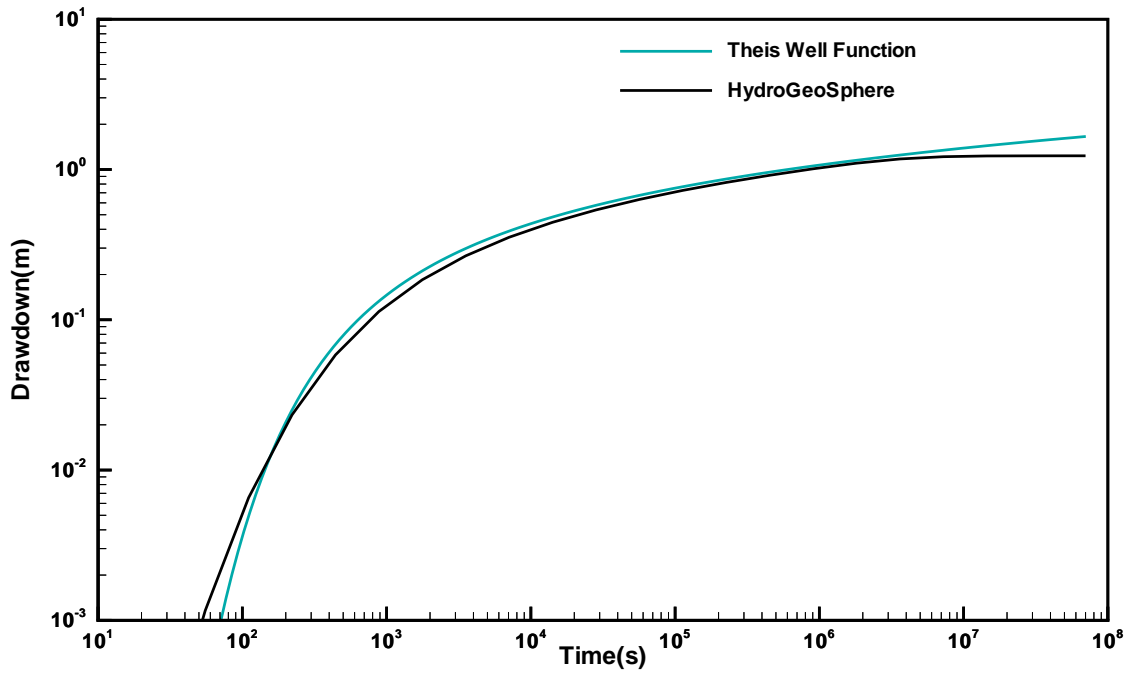
Figure 1.1: Results for Pumping in a Theis Aquifer.

mesh consisting of 33 block elements, ranging from 0.01 m near the well to 1000 m near the outer boundary.

Drawdown versus time data for a node located 55 m from the pumping well is shown in Figure 1.1.

The results from both the full 3-D grid and axisymmetric grid are very close to those obtained from the analytical solution. Both solutions drop below the Theis solution at late time due to the influence of the constant head boundary condition. Although both approaches give essentially identical results, the axisymmetric option results in a 2 order-of-magnitude decrease in CPU time.

1.1.2 Level 2: Unsaturated Flow Through a Column

Note: the verification problem described in this section corresponds to the `u_1d` test case found in the `verification` directory under the **HydroGeoSphere** installation directory.

This verification example consists of one-dimensional transient infiltration in an unsaturated vertical column. The specifications of the problem are taken from Huyakorn et al. (1986, Example 4). The physical system is 200 cm long in the vertical (z) direction, with the top face corresponding to the soil surface and the bottom face corresponding to the water table. The column has dimensions of 50 cm in each of the horizontal (x and y) directions. Initially, the pressure head at the water table is zero, it is -90 cm at the soil surface and equals -97 cm in the remainder of the domain. Infiltration at the rate of 5 cm d^{-1} is then applied for a period of 10 days. The saturated hydraulic conductivity of the soil is 10 cm d^{-1} and its porosity is 0.45. The constitutive relationships for the soil are given by:

$$k_{rw} = \frac{(S_w - S_{wr})}{(1 - S_{wr})}$$

and:

$$\frac{(\psi - \psi_a)}{(-100 - \psi_a)} = \frac{(1 - S_w)}{(1 - S_{wr})}$$

where the residual saturation, S_{wr}, is 0.333 and the air entry pressure , ψ_a, is 0.0 cm. Substituting these values in the equations given above yields simple linear relationships which can be input to the model in tabular form. The input values of water saturation versus pressure head are shown in Table 1.3. The input values of relative permeability versus

Table 1.3: Water Saturation Versus Pressure Head Relationship for the Unsaturated Column Example.

ψ(cm)	S_w
-0.01	.333
0.0	1.0

water saturation are shown in Table 1.4.:

Table 1.4: Relative Permeability Versus Water Saturation Relationship for the Unsaturated Column Example.

S_w	K_{rw}
.333	0.0
1.0	1.0

The column is discretized in three dimensions with 2 nodes in each of the x- and y-directions and 41 nodes in the z-direction. The mesh thus consists of a total of 164 nodes and 40 elements. The time steps are identical to Huyakorn et al. (1986) with an initial value equal to 0.1 days, which is increased by a factor of 1.2 until a maximum of 1.0 days is attained. The tolerance on pressure head for the Newton-Raphson iteration is set to 0.01 cm.
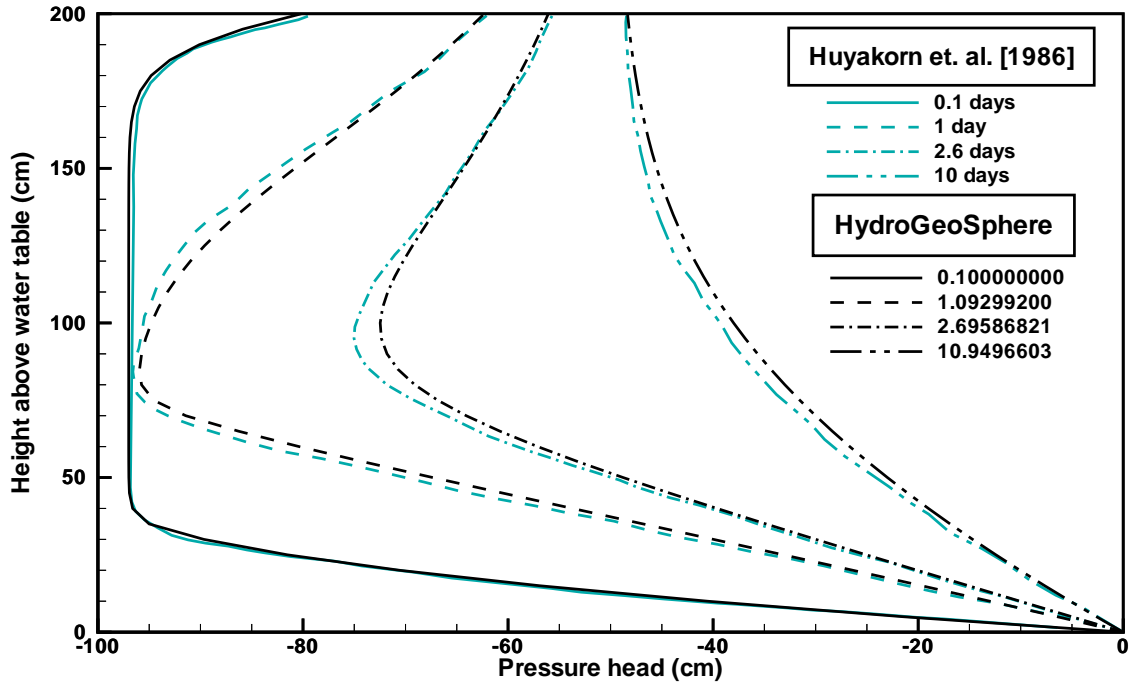
Figure 1.2: Pressure Head Profiles for the Unsaturated Flow Verification Example.

Figure 1.2 shows pressure head profiles at 4 different times during the infiltration event from Huyakorn et al. (1986). For comparison, results from **HydroGeoSphere** are also presented. It can be seen that the results are almost identical.

1.1.3 Level 2: Very Dry Initial Conditions

Note: the verification problem described in this section corresponds to the `forsyth` test case found in the `verification` directory under the **HydroGeoSphere** installation directory.

This verification problem is taken from Forsyth et al. (1995), Example 2, which was developed to compare the performance of numerical simulators for very dry initial conditions. The computational domain is shown in Figure 1.3. All boundaries are no flow except for the zone of infiltration at the top left corner. Table 1.5 provides the material properties for the 4 soil zones. They report using a 90 × 21 finite volume grid to discretize the domain, but the exact grid coordinates were unavailable. The initial pressure head was set to -734 cm, and water infiltration occurred for 30 days.

Figure 1.4 compares saturation contours between **HydroGeoSphere** using upstream weighting and Forsyth's one phase, central weighting case. The saturation front produced by **HydroGeoSphere** is considerably sharper than that shown by Forsyth.
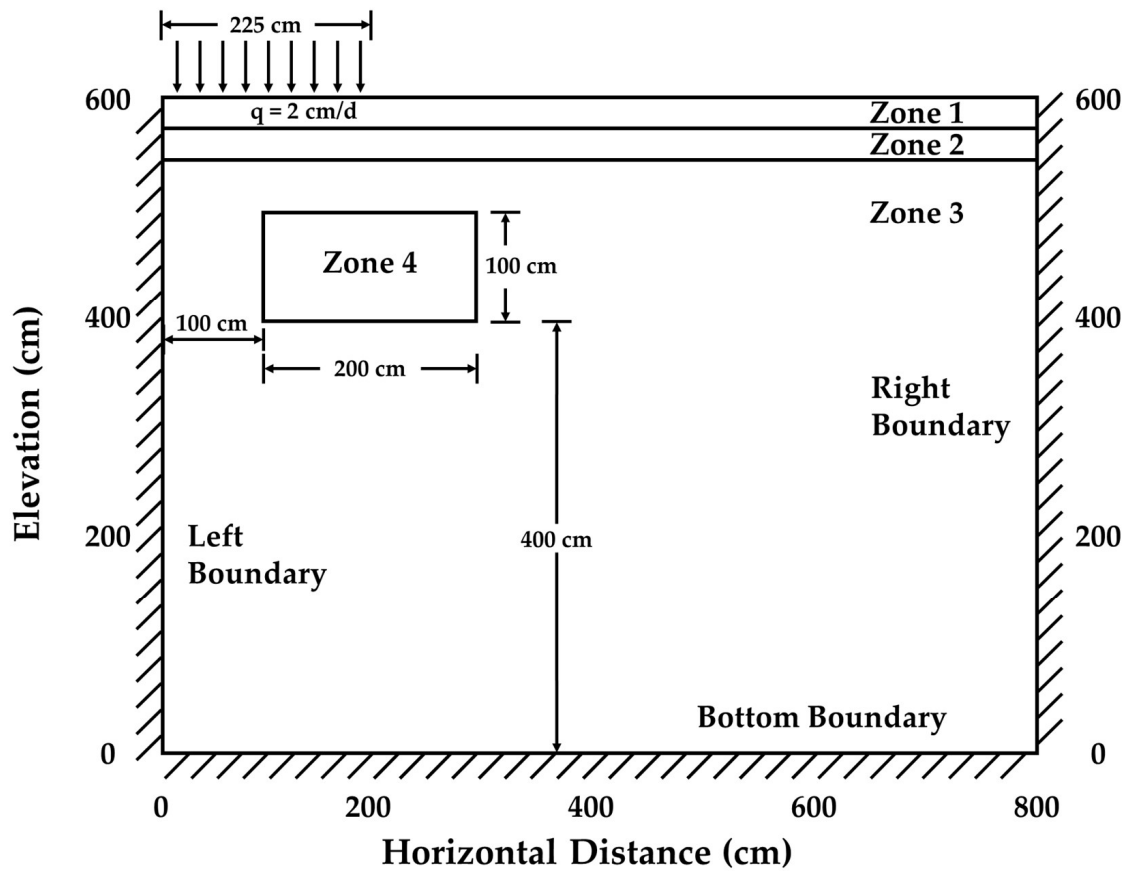
Figure 1.3: Schematic for Very Dry Initial Conditions Problem.

Table 1.5: Material Properties for the Simulation of Forsyth et al. (1995), Example 2.

Parameter	Value	Unit
Soil Zone 1		
porosity, n	0.3680	
permeability, k	9.3×10^{-12}	m^2
Van Genuchten parameter, α	0.0334	cm^{-1}
Van Genuchten parameter, β	1.982	
residual saturation, S_r	0.2771	
Soil Zone 2		
porosity, n	0.3510	
permeability, k	5.55×10^{-12}	m^2
Van Genuchten parameter, α	0.0363	cm^{-1}
Van Genuchten parameter, β	1.632	
residual saturation, S_r	0.2806	
Soil Zone 3		
porosity, n	0.3250	
permeability, k	4.898×10^{-12}	m^2
Van Genuchten parameter, α	0.0345	cm^{-1}
Van Genuchten parameter, β	1.573	
residual saturation, S_r	0.2643	
Soil Zone 4		
porosity, n	0.3250	
permeability, k	4.898×10^{-11}	m^2
Van Genuchten parameter, α	0.0345	cm^{-1}
Van Genuchten parameter, β	1.573	
residual saturation, S_r	0.2643	
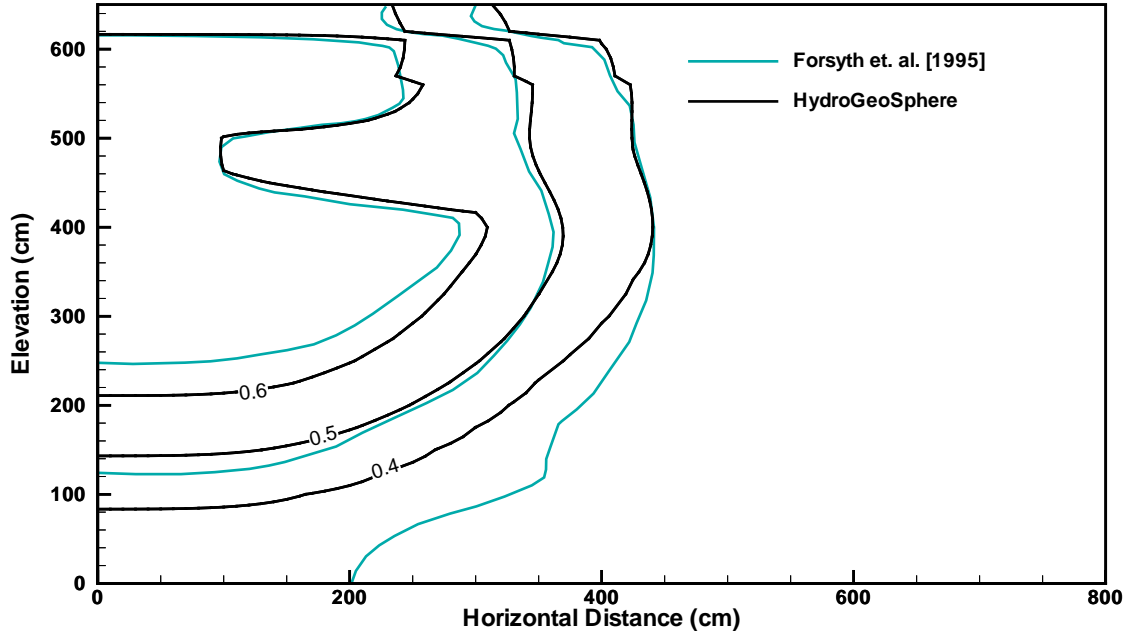
Figure 1.4: Results For Very Dry Initial Conditions Problem

1.1.4 Level 2: Drainage of a Fractured Tuff Column

Note: the verification problem described in this section corresponds to the `wang` test case found in the `verification` directory under the **HydroGeoSphere** installation directory.

An example is now presented to verify the variably-saturated flow solution in discretely-fractured porous media. Because the variably-saturated flow equation is nonlinear and analytical solutions are at best approximate, the numerical formulation was verified by comparison to the numerical solution presented by Wang and Narasimhan (1985) for an example problem which involves the vertical drainage of a three-dimensional fractured tuff column.

Analytical expressions describing the fracture relative permeability, k_r, saturation, S and effective fracture-matrix flow area, σ, as presented by Wang and Narasimhan (1985) have the following forms:

$$k_r(\psi) = \frac{1}{6(4 + \beta b_c)}\{[24 - \exp(-\beta b_s)(24 + 24\beta b_s + 12\beta^2 b_s^2 + 4\beta^3 b_s^3 + \beta^4 b_s^4)]$$

$$+\beta b_c[6 - \exp(-\beta b_s)(6 + 6\beta b_s + 3\beta^2 b_s^2 + \beta^3 b_s^3)]\} \tag{1.1}$$

$$S(\psi) = \frac{1}{2 + \beta b_c}\{[2 - \exp(-\beta b_s)(2 + 2\beta b_s + \beta^2 b_s^2)] \tag{1.2}$$

$$+\beta b_c[1 - \exp(-\beta b_s)(1 + \beta b_s)]\} \tag{1.3}$$

Table 1.6: Parameter Values Used for Wang and Narasimhan (1985) Relationships.

Parameter	Value	Unit
Fluid density ρ	1000	kg m^{-3}
Acceleration due to gravity g	9.80665	m s^{-2}
Surface tension γ	0.07183	kg s^{-2}
Solid/liquid surface angle Θ	0.0	
Fracture contact area ω	12	%
Horizontal fracture contact cutoff aperture $b_{c(H)}$	0.074	mm
Vertical fracture contact cutoff aperture $b_{c(V)}$	0.057	mm
β_H	0.804×10^4	m^{-1}
β_V	1.04×10^4	m^{-1}

$$\sigma(\psi) = 1 - \exp(-\beta b_c - \beta b_s)(1 + \beta b_c + \beta b_s) \tag{1.4}$$

where the β values are parameters determined from fracture spacing. The variable b_c is the contact cutoff aperture for the fracture and can be determined by the root of the equation:

$$1 - \exp(-\beta b_c)(1 + \beta b_c) = \omega \tag{1.5}$$

ω being the fraction of contact area for a fracture.

The variable b_s represents the saturation cutoff aperture and is given by:

$$b_s = -\frac{2\chi \cos \Theta}{\rho g \psi} \tag{1.6}$$

where g is the acceleration due to gravity, ρ is the density of water, χ is the surface tension, Θ represents the angle between the solid and liquid surface and ψ is the pressure head.

The values of the above variables that are used in this simulator are based on the values presented in the Wang and Narasimhan (1985) study, and are show in Table 1.6. They examined flow in a fractured porous tuff unit, the Topopah Spring Member at Yucca Mountain, and developed a theory for computing the unsaturated flow properties of fractures which was then applied to this rock unit. Based on observations, they obtained values for all the parameters needed to describe unsaturated flow in the fractured tuff unit. They used an intrinsic permeability of $1.02 \times 10^{-11} m^2$ for the fractures. Note that they identified two sets of fractures, vertical fractures, for which the subscript V is used, and horizontal fractures denoted by subscript H.

The theoretical expressions developed by Wang and Narasimhan (1985) to describe the saturation, relative permeability and effective fracture-matrix flow area for the fractures, as functions of the fluid pressure, were implemented in this model and used for the simulation. The comparison was made for the case where the phase-separation constriction factor, which

was used by Wang and Narasimhan (1985) to represent the effects of the air phase on the flow of water, was neglected.

Figure 1.5 illustrates the geometry of the physical system. The porous tuff matrix contains three fracture sets, two sets are vertical with a constant fracture aperture equal to 240 μm and one set is horizontal, with a fracture aperture equal to 310 μm. It should be noted that the fractures have not been drawn to scale in Figure 1.5. The fractures partition the matrix into blocks, with each block having dimensions equal to 0.22 m × 0.22 m × 0.48 m. A total of 27 such blocks are represented in Figure 1.5. The saturated hydraulic conductivity of the tuff matrix is 3.2×10^{-8} cm s^{-1}, its porosity is 0.09 and its specific storage equals 1×10^{-6} m^{-1}. The constitutive relations describing matrix saturation and relative permeability are represented by the Van Genuchten relations (Equations 2.7 and 2.8), with $S_{wr} = 9.6 \times 10^{-4}$, $\alpha = 7.027 \times 10^{-3}$ m^{-1}, $m = 0.45$ and $n = 1.818$. The specific storage of the fractures is equal to 4.4×10^{-6} m^{-1}.

Due to the symmetry of the system, Wang and Narasimhan (1985) only considered one vertical column bounded by four vertical fractures. For this comparison, only one quarter of this column, i.e. total dimensions equal to 0.11 m × 0.11 m × 1.44 m, need be discretized, taking advantage of the horizontal symmetry of the drainage process. The column was discretized using 7 nodes in each of the horizontal directions and 31 nodes in the vertical direction, for a total of 1519 nodes (1080 three-dimensional elements). The nodal spacing used was identical to that reported by Wang and Narasimhan (1985). Each vertical fracture was represented by 180 two-dimensional elements and 36 elements were used to discretize each horizontal fracture.

The column was initially saturated, the fluid was static and its potential was everywhere zero. Drainage was performed by applying a suction equal to -112.0 m at the bottom of the column, all other boundaries being impermeable. This suction caused the fractures and the matrix to desaturate with time. Time stepping control was used to move the solution through time. A maximum change in pressure head of 1.0 m for each time step was used in conjunction with Equation 3.101. The total CPU time for the flow simulation was 6 minutes on the IBM RS/6000 Model 590 and a total of 511 variable time steps were necessary to reach the final simulation time of 10^5 years. It should be noted that convergence of the Newton procedure occurred typically after the first iteration for most time steps.

A comparison of the results obtained with this model and those of Wang and Narasimhan (1985) is presented in Figure 1.6, which shows the change in fluid pressure with time for four different locations in the column. Location A represents the middle of the porous block, location B is the middle of a vertical fracture bounding the matrix block and points C and D are in the middle of the horizontal fractures. It can be seen from Figure 1.6 that there is a very good agreement between the results obtained and those reported by Wang and Narasimhan (1985). The pressure head is seen to decrease gradually at early times for all observation points. The decrease is more rapid at point D, which is closer to the drainage boundary. The pressure at points A and B is identical, revealing that the drainage process for this case is mainly influenced by the porous matrix when unsaturated conditions prevail.

The drainage simulation was repeated using both the finite element and the finite difference
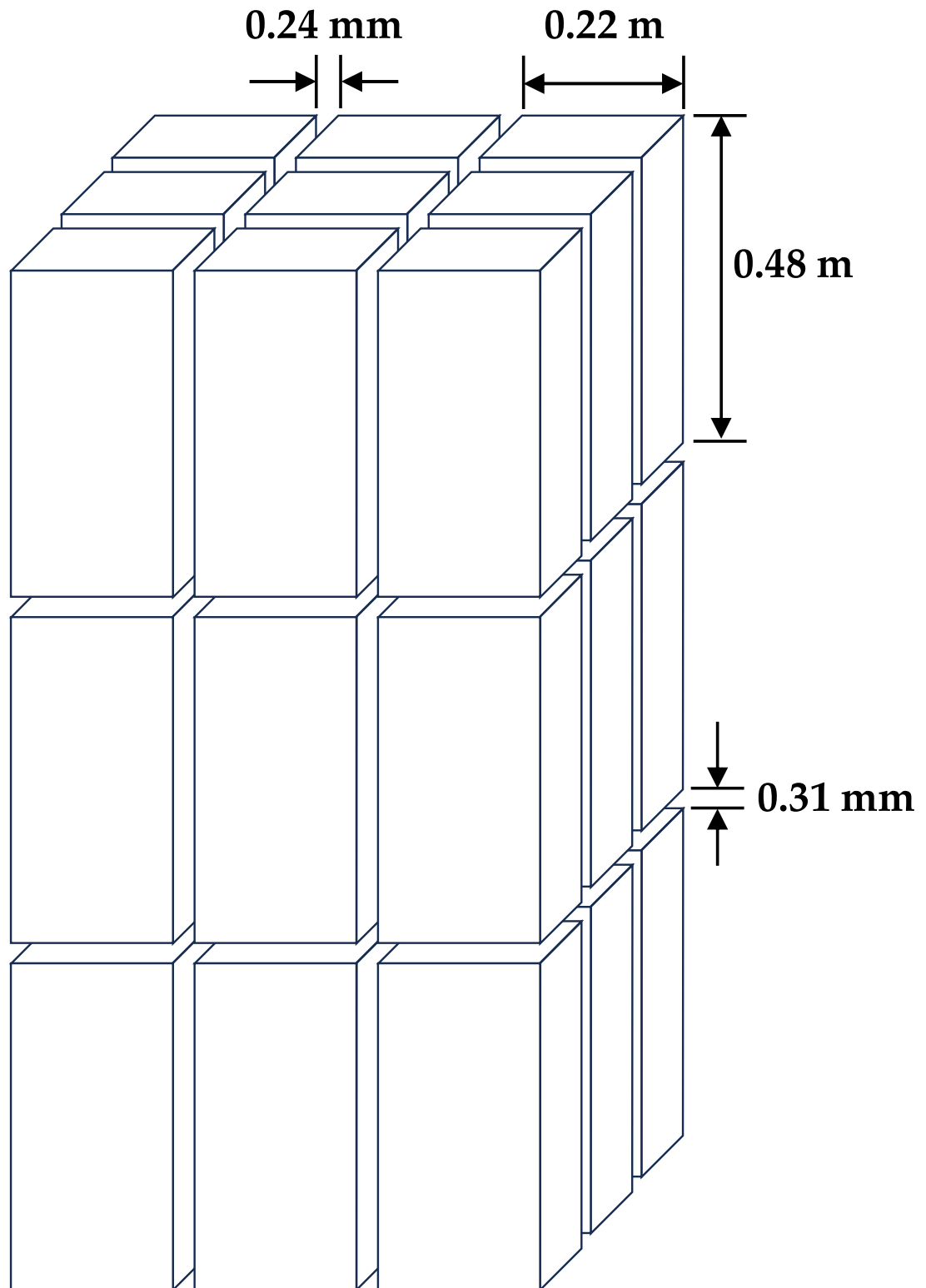
Figure 1.5: Verification Example Involving Fractured Porous Tuff (adapted from Wang and Narasimhan (1985)).
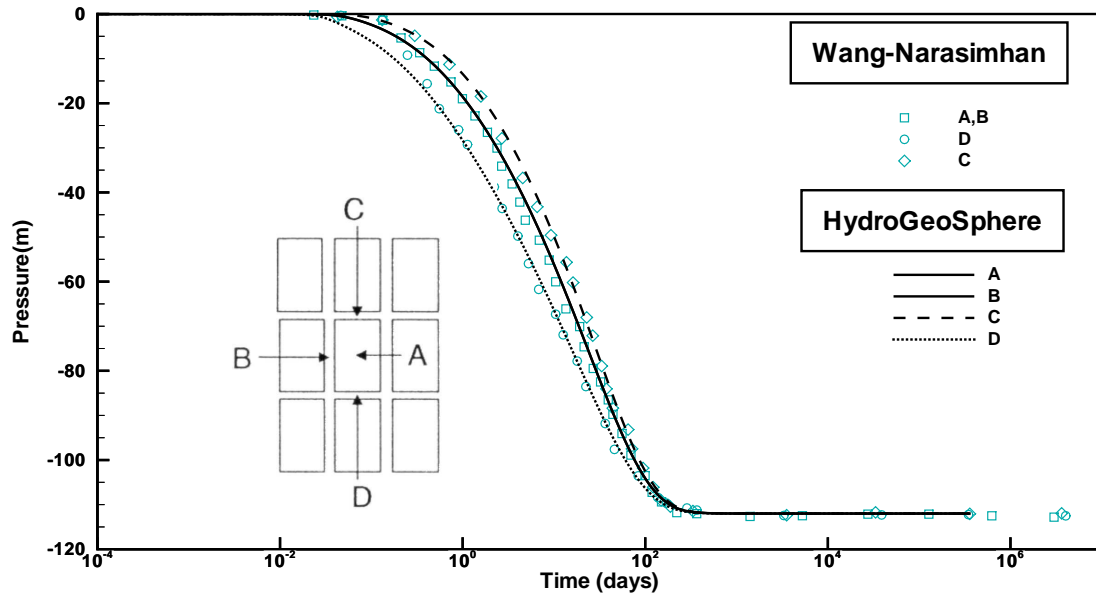
Figure 1.6: Pressure Drop at Selected Points During the Drainage of a Fractured Porous Tuff.

representations. Both representations produced identical results, although the finite difference representation required one quarter of the CPU time compared to the finite element scheme.

1.1.5   Level 1: 1-D Hydromechanical Coupling

Note: the verification problem described in this section corresponds to the `hm_1d` test case found in the `verification` directory under the **HydroGeoSphere** installation directory.

This verification example consists of the one-dimensional transient head response to uniform loading on the top of a saturated vertical column. The specifications of the problem are taken from Lemieux (2006), who developed an exact analytical solution for a column of semi-infinite length, which is subjected to loading by a mass M, added at constant intervals such that dM/dt is constant and where the top of the column is drained and the base is a no-flow boundary condition.

HydroGeoSphere was used to model this case and was compared to the analytical solution. A domain of 10,000 m length was used. A load of 0.3 m/yr was applied for a period of 10,000 years. Drainage at the top of the column is achieved by specifying a head of 0.0 m at the top of the column. The initial head along the length of the column was set to 0 m. The properties of the rock mass are described in Table 1.7.

Figure 1.7 shows the hydraulic head versus time at different depths in the column from Lemieux (2006). Also shown is the head response from **HydroGeoSphere** at a depth of 500 m below the top of the column. it can be seen that the numerical solution precisely corresponds to the analytical solution.

Table 1.7: Parameter Values for Simulation of 1-D Hydromechanical Coupling Problem.

Parameter	Value	Unit
Hydraulic conductivity	1×10^{-3}	m yr^{-1}
Specific storage	1×10^{-6}	m^{-1}
Loading efficiency	1.0	
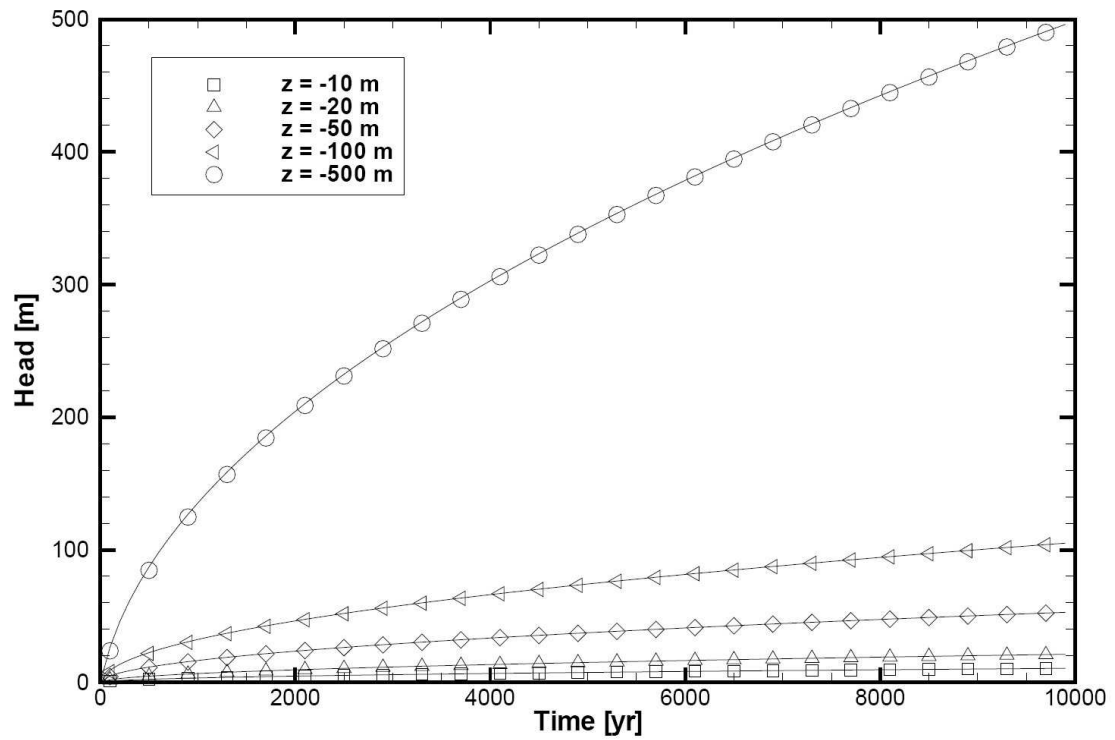
Figure 1.7: Results for 1D Hydromechanical Coupling Example.

Table 1.8: Parameter Values for Simulation of 1-D Hydromechanical Coupling Problem.

Parameter	Value	Unit
Hydraulic conductivity	0.1	m d^{-1}
Specific storage	0.0018	m^{-1}
Loading efficiency	1.0	

1.1.6 Level 1: 1-D Hydromechanical Coupling with Externally Computed Stresses

Note: the verification problem described in this section corresponds to the `hm_1d_coupled` test case found in the `verification` directory under the **HydroGeoSphere** installation directory.

This example is used to demonstrate that **HydroGeoSphere** could be used in conjunction with other hydromechanical models.

In general, because **HydroGeoSphere** cannot generate equilibrated hydromechanical total stresses for use in Equation 2.21, they must be generated by other models and used as input to **HydroGeoSphere**. Theoretically, time-dependent, average, element-specific total stresses are required.

As shown in Figure 1.8, a column of soil of height 1,000 metres supporting a load Φ_{zz} is confined laterally in a rigid sheath so that no lateral expansion can occur. It is assumed that no water can escape laterally or through the bottom while it is free to escape at the upper surface. The height of 1000 m is assumed to reflect the magnitude of depth that **HydroGeoSphere** is likely to be applied. Material properties for the soil are given in Table 1.8.

A vertical stress of 0.5 MPa was applied to the surface, which causes the water pressure head to rise by 50.9 metres at the onset.

For cases of purely vertical strain such as we have here, Guvanasen (2007) presents a method for computing the average hydromechanical stresses at any time from water pressures obtained from an analytical solution developed by Biot (1941). Details of the mathematical theory and procedures are not given here, but instead the reader is referred to Guvanasen (2007).

The analytical solution of Biot (1941) is based on the assumption that the vertical load is instantaneously applied and remains constant thereafter. In applying **HydroGeoSphere**, it was assumed that the load was increased in a linear fashion from 0 to 50.9 m in 0.1 days.

Average hydromechanical stresses versus time (expressed as water pressure in m) computed by Guvanasen (2007) at various elevations are plotted in Figure 1.9. These stresses were used as input to **HydroGeoSphere**

Figure 1.10 shows the hydraulic head versus time at different elevations in the column from
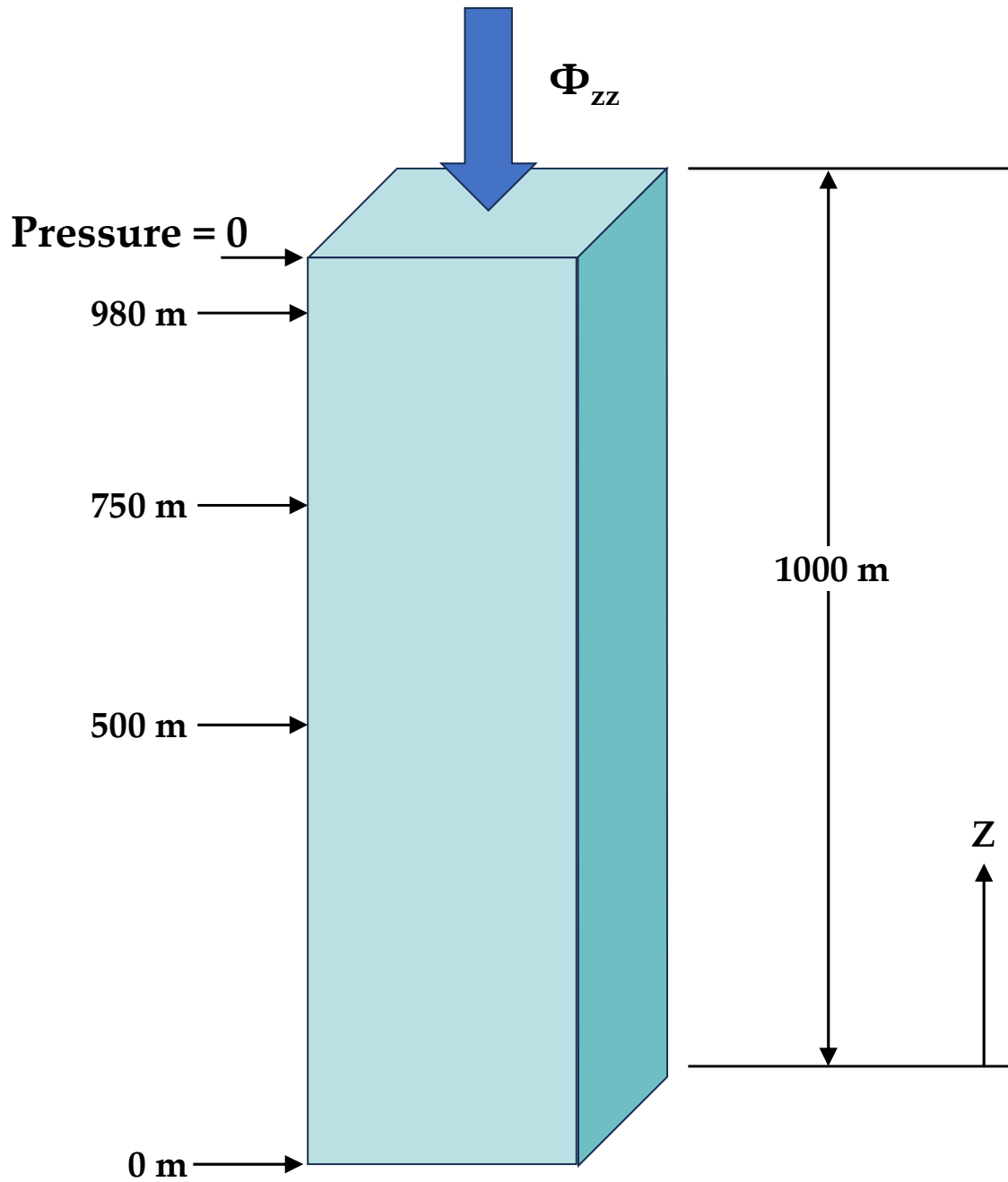
Figure 1.8: Schematic for 1D Hydromechanical Coupling with External Stresses Example.
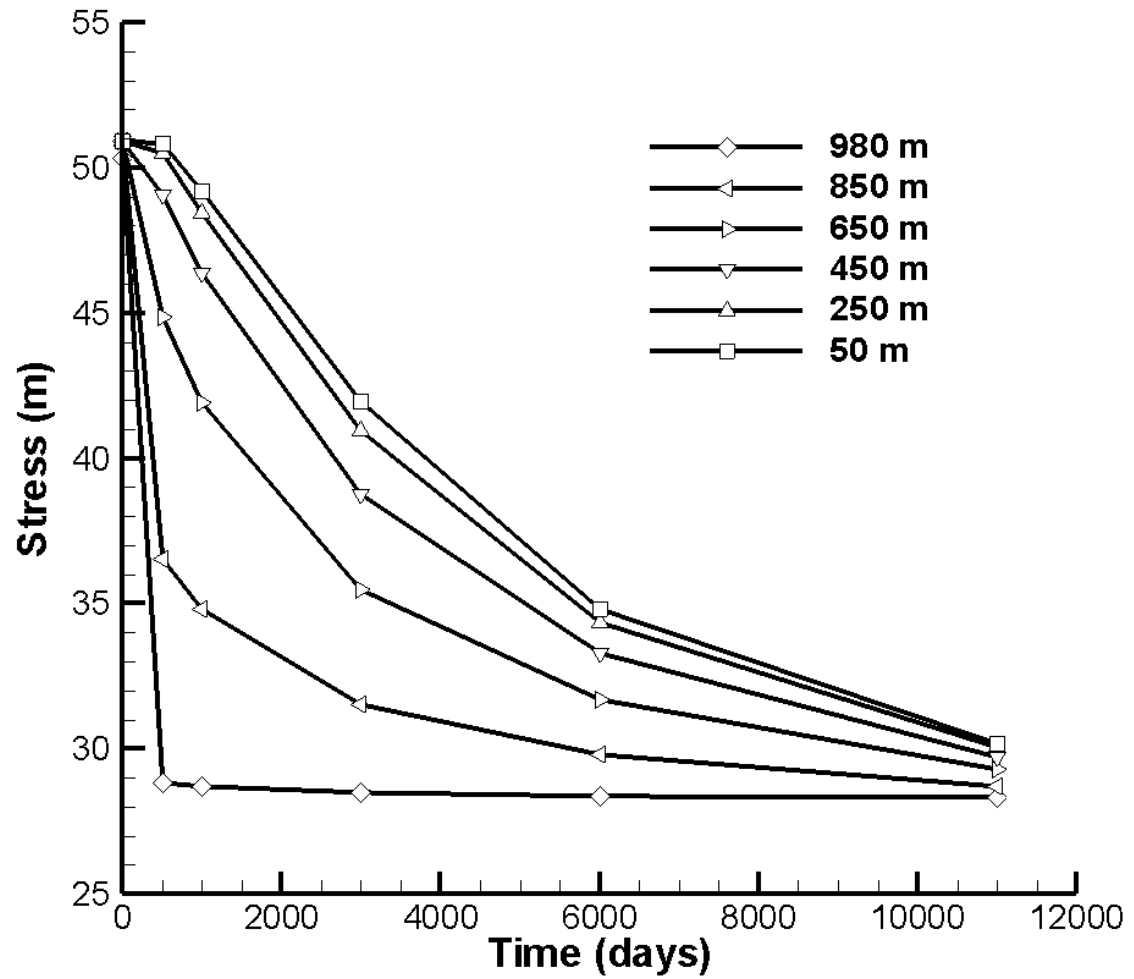
Figure 1.9: Mean Normal Stress Versus Time at Various Elevations.

Table 1.9: Parameter Values for Simulation of a 1-D Flow Example from Govindaraju et al. (1988a,b).

Parameter	Value	Unit
Froude number F_o	0.5	
Kinematic wave number K	10	m s^{-1}
Slope S_o	0.01	
Slope length L	100	m
Uniform recharge i_o	0.0040	m s^{-1}
Uniform velocity u_o	0.9905	m s^{-1}
Uniform depth d_o	0.4000	m
Manning's roughness coefficient n	0.0548	s m$^{-1/3}$

Biot (1941) and **HydroGeoSphere**. The agreement between **HydroGeoSphere** and the analytical solution is an indication that **HydroGeoSphere** can be interfaced with other hydromechanical models.

1.2 Surface Flow

1.2.1 Level 1: 1-D Surface Flow Study of Govindaraju

Note: the verification problem described in this section corresponds to the `olf1` test case found in the `verification` directory under the **HydroGeoSphere** installation directory.

The surface water flow capabilities of **HydroGeoSphere** are verified against analytical and numerical solutions of diffusive wave and dynamic wave equations, presented by Govindaraju et al. (1988a,b). The problem considered involves one-dimensional surface flow along a plane of one unit width (Figure 1.11). The authors presented numerical and analytical solutions for the different waves under a wide range of flow conditions ranging from highly subcritical flow (Froude number $F_o = u_o/\sqrt{gd_o} < 0.5$) to supercritical flow ($F_o = 1.5$) and at different kinematic wave numbers $K(= S_o L/d_o F_o^2)$ ranging from 3 to 50 ($K > 20$ indicates a kinematic wave), where u_o is the uniform velocity and d_o is the uniform depth at the downstream end, S_o is the bed slope, and L is the slope length.

We chose a single case for comparison, using the parameters shown in Table 1.9.

A zero-depth gradient boundary condition (see Equation 3.59) was applied at the downstream end of the system.

Modeling Approach and Results

The slope was discretized into 100 columns and 1 row of elements with dimensions 1 m × 1 m each. Only surface flow resulting from recharge was simulated and no interaction with ground water was considered. Adaptive time stepping was provided in the simulations with an initial time-step size of 1 s and a maximum time-step size of 2.5 s. Newton iteration
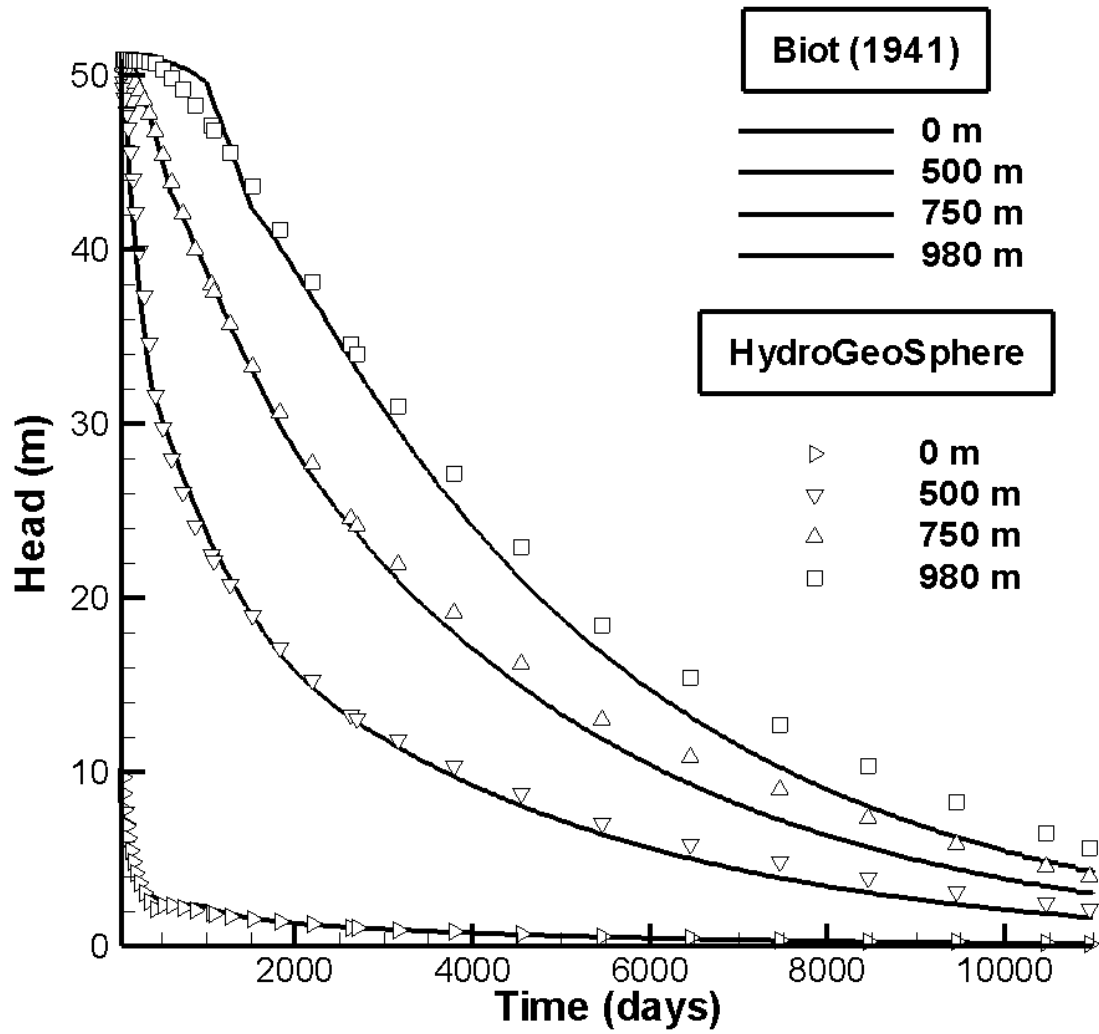
Figure 1.10: Results for 1D Hydromechanical Coupling with External Stresses Example.
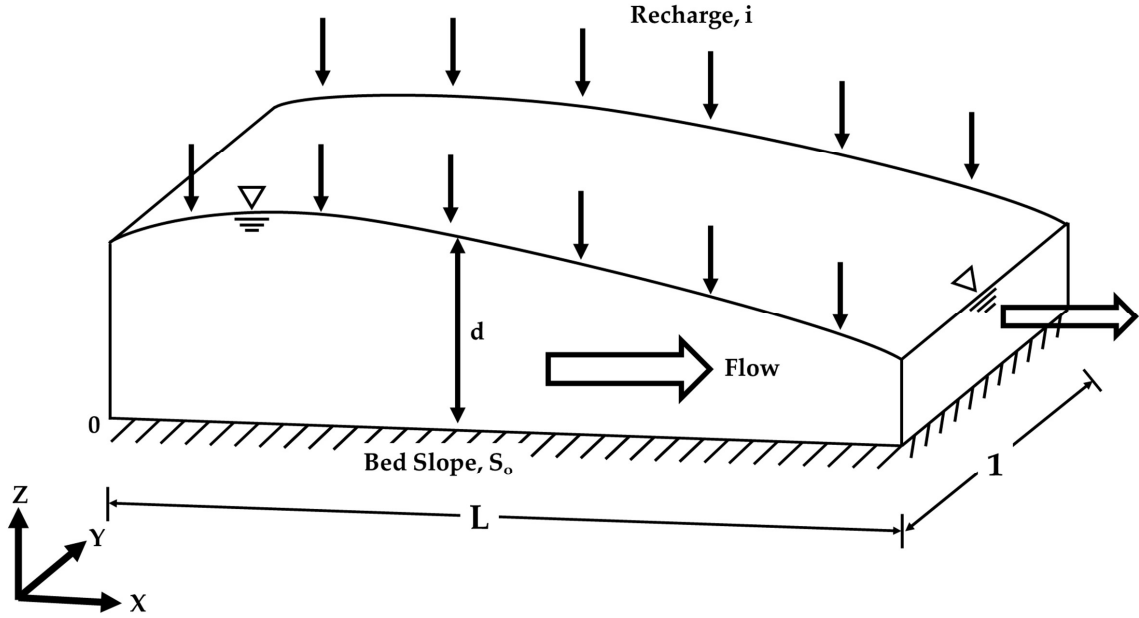
Figure 1.11: Schematic for the Govindaraju et al. (1988a,b) Problem.

considerations include a maximum of 20 iterations an absolute convergence tolerance of 10^{-4}. Figure 1.12 shows the discharge hydrograph at the downstream end of the slope. The hydrograph was normalized by dividing the discharge by the normal discharge Q_o, in this case 0.3962 m^3 s^{-1}, and time by $t_o(t_o = L/u_o)$.

The results obtained using **HydroGeoSphere** are in good agreement with both the diffusion wave solution of Govindaraju et al. (1988a,b), where Picard and Newton iterative approaches provide almost identical solutions, and the Modflow-Surfact solution. However, due to the limitations of the diffusive wave approximation, the solution deviates from the dynamic wave (i.e., the full Saint Venant solution) for the small value of the kinematic wave number K used in this example.

1.2.2 Level 2: Conjunctive Surface-Subsurface Flow Study of Smith and Woolhiser

Note: the verification problem described in this section corresponds to the `smith_woolhiser` test case found in the `verification` directory under the **HydroGeoSphere** installation directory.

Smith and Woolhiser (1971) present an experimental study of combined surface and subsurface flow which may be used to validate the surface and subsurface flow routines, and their interactions, in **HydroGeoSphere**. The experiments consisted of providing rainfall of 25 cm hour^{-1} for 15 minutes over a soil flume 1,220 cm long, 5.1 cm wide and 122 cm deep. The flume was inclined along its length at a slope of 0.01, and the moisture movement into
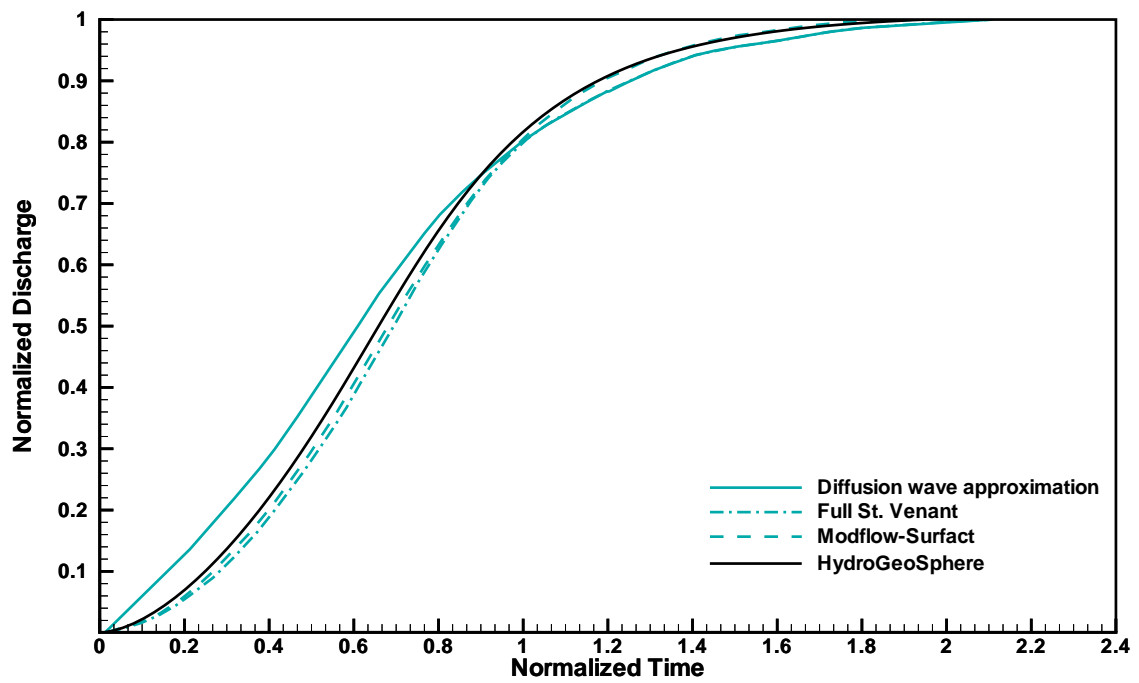
Figure 1.12: Comparison of Normalized Rising Hydrographs for Saint Venant Equations, the Diffusion Wave Approximation (Govindaraju et al., 1988a) and MSVMS for $F_o = 0.5$ and $K = 10$.
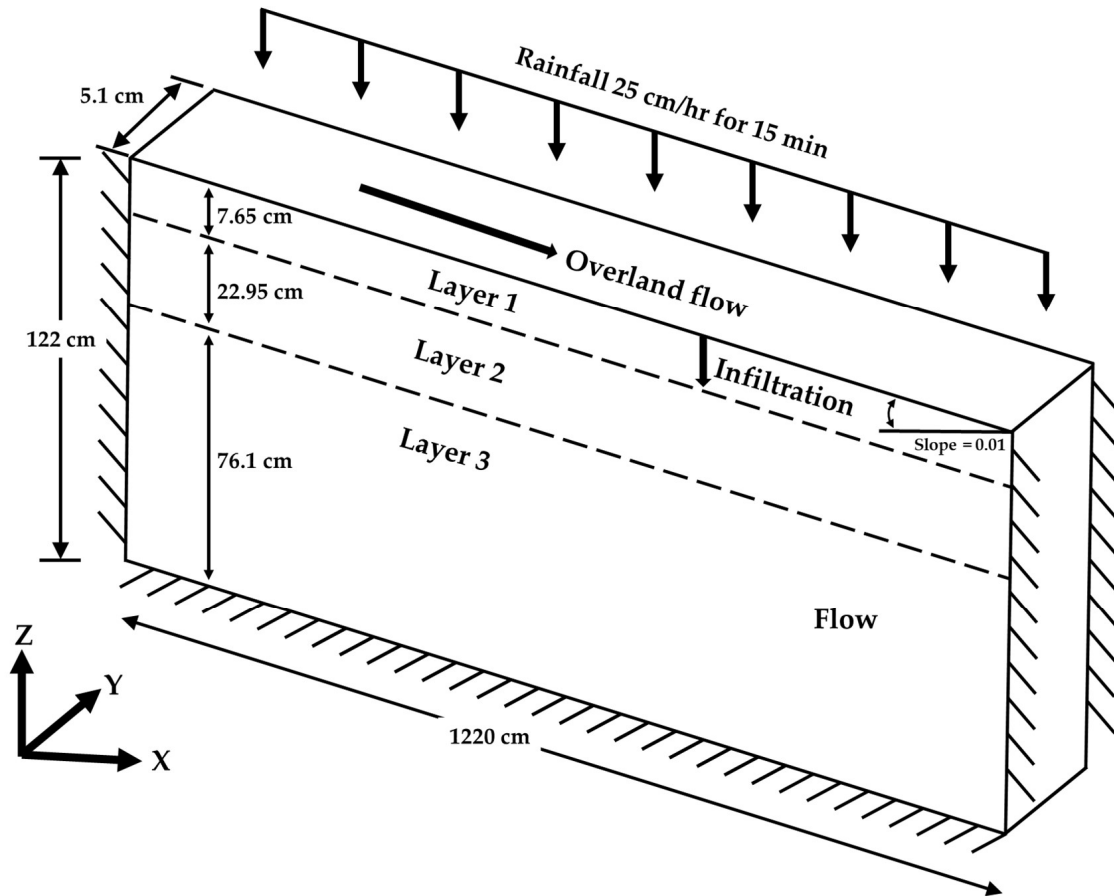
Figure 1.13: Experimental Setup of the Smith and Woolhiser (1971) Study.

the soil, and downstream discharge were measured. The experimental setup is schematically depicted in Figure 1.13. Several conjunctive models of surface and subsurface flow have selected this experiment as a test case. Smith and Woolhiser (1971) present a model using the kinematic wave approximation for surface flow. Akan and Yen (1981) and Singh and Bhallamudi (1998) solve the full dynamic wave equation for surface flow. Govindaraju and Kavvas (1991) solve the diffuse wave equation for surface flow for this case. All above models solve the Richards equation for flow in the subsurface, and use flux coupling between the surface and subsurface equations.

The case considered for simulation here, involves a dry soil. The soil, a Poudre fine sand, was placed in the flume in three layers of thickness 7.65 cm, 22.95 cm, and 76.1 cm from top to bottom (denoted as layers 1, 2, and 3, respectively). Hydraulic property curves provided by Smith and Woolhiser (1971) for the 3 soil layers were fit to the Van Genuchten functions using a regression code that adjusted the saturated moisture content and saturated hydraulic conductivity values. Figure 1.14 shows the observed moisture retention curve for soil layer 1, as provided by Smith and Woolhiser (1971), and the fitted Van Genuchten functions, and
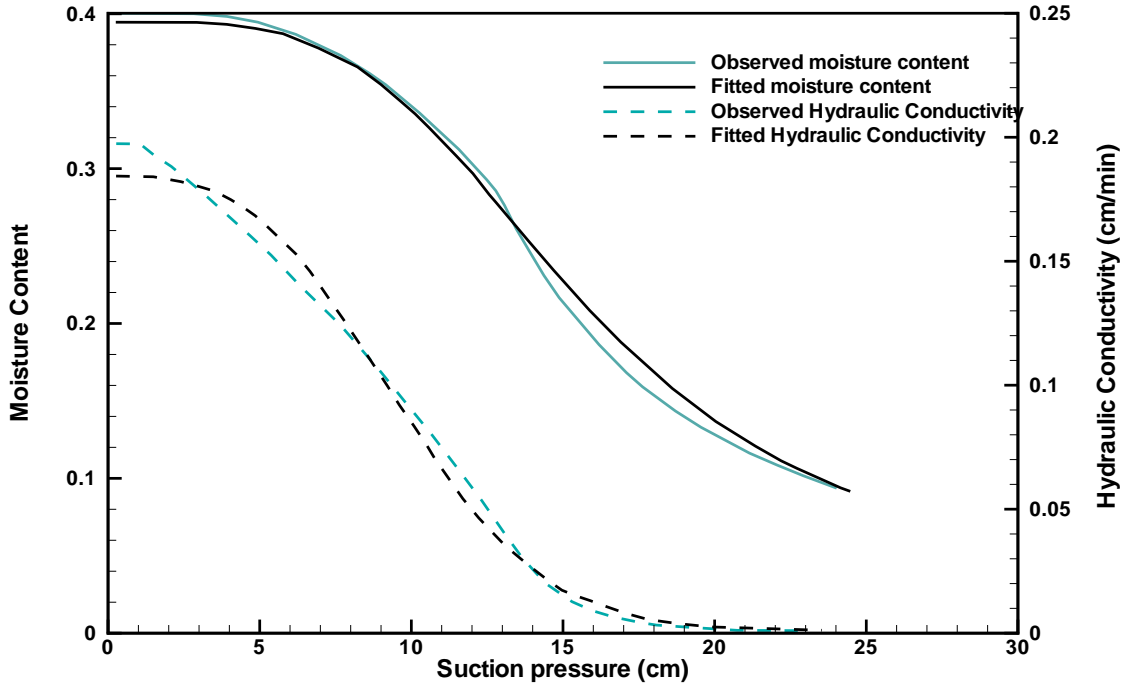
Figure 1.14: Moisture Retention Curve for Soil Layer 1.

indicates that the Van Genuchten parameters used for the simulation provide a good fit to the experimental data in the range of suction valid for this study. Figure 1.15 shows the observed and fitted relative hydraulic conductivity vs. moisture content curves for soil layer 1. The fitted Van Genuchten functions for the other two soil layers, not shown here, also had very good fits. Singh and Bhallamudi (1998) provide details of the Brooks-Corey relations fitted to the data of Smith and Woolhiser (1971). Table 1.10 provides a summary of the fitted Van Genuchten parameter values of the simulation for all three soil layers. Akan and Yen (1981) and Singh and Bhallamudi (1998) provide the Darcy-Weisbach friction factor used for the simulation as $f = C_L/R_e$ where the coefficient C_L is 92 for this laminar flow problem, and R_e is the Reynolds number defined as $R_e = q/\mu$, where q is the discharge per unit width and μ is the kinematic viscosity of the liquid. The liquid used in the experiments was a light oil with a kinematic viscosity of 1.94×10^{-6} m^2 s^{-1}. The average discharge for the experiments was approximately 1×10^{-5} m^3 s^{-1} for a flume width of 0.051 m, giving $q = 10^{-5}/0.051 = 1.96 \times 10^{-4}$ m^2 s^{-1} and thus $R_e = 101.07$, for an average number to determine the friction factor f as $92/101.07 = 0.91$. The Darcy-Weisbach equation, Chezy's equation and Manning's equation are related as $C_c = d^{1/6}/n = \sqrt{8g/f}$ where d is the depth and g is gravity, thus giving the Chezy constant for this problem as $C_c = \sqrt{8g/f} = 5569.1$ cm$^{1/2}$ minute^{-1} and the Manning constant as $n = d^{1/6}/C = 0.000180d^{1/6}$ minutes cm$^{-1/3}$. The depth of flow for this problem is less than 1 cm - assuming it to be 0.15 cm gives $d^{1/6}=0.6873$ (the one-sixth power brings it all closer to unity). Thus, Manning's n for this problem is 0.0001228 minutes cm$^{-1/3}$.

Modeling Approach and Results

Table 1.10: Parameter Values for Simulation of the Smith and Woolhiser (1971) Experiment.

Parameter	Value	Unit
Soil layer 1 [†]		
porosity, n	0.3946	
saturated conductivity, K_s	0.184	cm minute^{-1}
Van Genuchten parameter, α	0.07	cm^{-1}
Van Genuchten parameter, β	3.4265	
residual saturation, S_r	0.05068	
Soil layer 2		
porosity, n	0.4387	
saturated conductivity, K_s	0.1452	cm minute^{-1}
Van Genuchten parameter, α	0.056	cm^{-1}
Van Genuchten parameter, β	4.1371	
residual saturation, S_r	0.05699	
Soil layer 3		
porosity, n	0.4764	
saturated conductivity, K_s	0.1296	cm minute^{-1}
Van Genuchten parameter, α	0.0443	cm^{-1}
Van Genuchten parameter, β	4.3565	
residual saturation, S_r	0.05248	
Darcy-Weisbach friction, f_r	0.91	
Equivalent Chezy coefficient, C_c	5569.1	cm$^{1/2}$ minute^{-1}
Equivalent Manning coefficient, n	0.000122	minute cm$^{-1/3}$
Rainfall intensity, i	0.417	cm minute^{-1}
Channel slope	0.01	
Channel length	1220	cm
Channel width	5.1	cm
gravitational acceleration	3.532×10^6	cm minute^2

[†] The soil parameters provide the fit to experimental data of Smith and Woolhiser (1971), as shown in Figures 1.14 and 1.15 for soil layer 1.
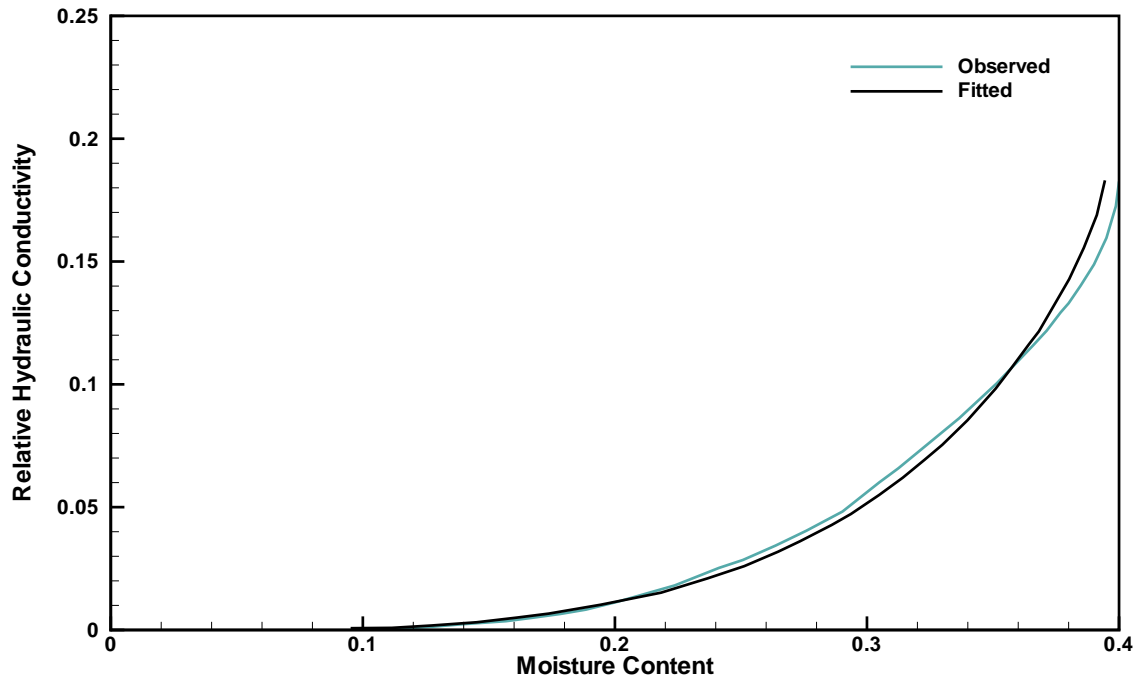
Figure 1.15: Hydraulic Conductivity versus Soil Moisture for Soil Layer 1.

The two-dimensional domain was discretized into 100 columns, 1 row and 40 layers of elements. The top 5 model layers represent soil layer 1, the next 15 model layers represent soil layer 2 and the remaining 20 model layers represent soil layer 3. The length of each element was 12.2 cm with a width of 5.1 cm and a thickness of 1.53 cm in soil layers 1 and 2, and a thickness of 3.805 cm in soil layer 3. The entire rectangular domain is tilted along its length to provide a slope of 0.01 to the model domain. The dual node approach, with a coupling length of 1.35 m and a rill storage height of 0.01 m was used to couple the surface and subsurface flow systems. Rainfall at a rate of 0.416667 cm minute^{-1} is supplied for a duration of 15 minutes followed by 5 minutes with zero recharge. Adaptive time-stepping uses an initial time-step size of 0.01 minutes and a maximum time-step size of 1 minute. Newton iteration considerations include a maximum of 18 iterations an absolute convergence tolerance of 10^{-3} cm. A critical-depth gradient boundary condition is applied at the downstream end of the surface flow nodes, while the lateral and bottom boundaries of the subsurface are provided no flow conditions.

The soil is initially dry at an approximate saturation of 0.2 as shown by Smith and Woolhiser (1971), which is converted to the appropriate head value using the Van Genuchten relation for the appropriate soil layer. The initial water depth for the surface flow nodes was set to 1×10^{-4} m to represent dry starting conditions at the surface. Simulations were performed using the Newton-Raphson scheme, as well as using Manning's equations to represent surface flow conditions.

Figure 1.16 shows the saturation profiles within the soil at a distance of 550 cm from the upstream end at different times, and show that infiltration causes the saturation front to
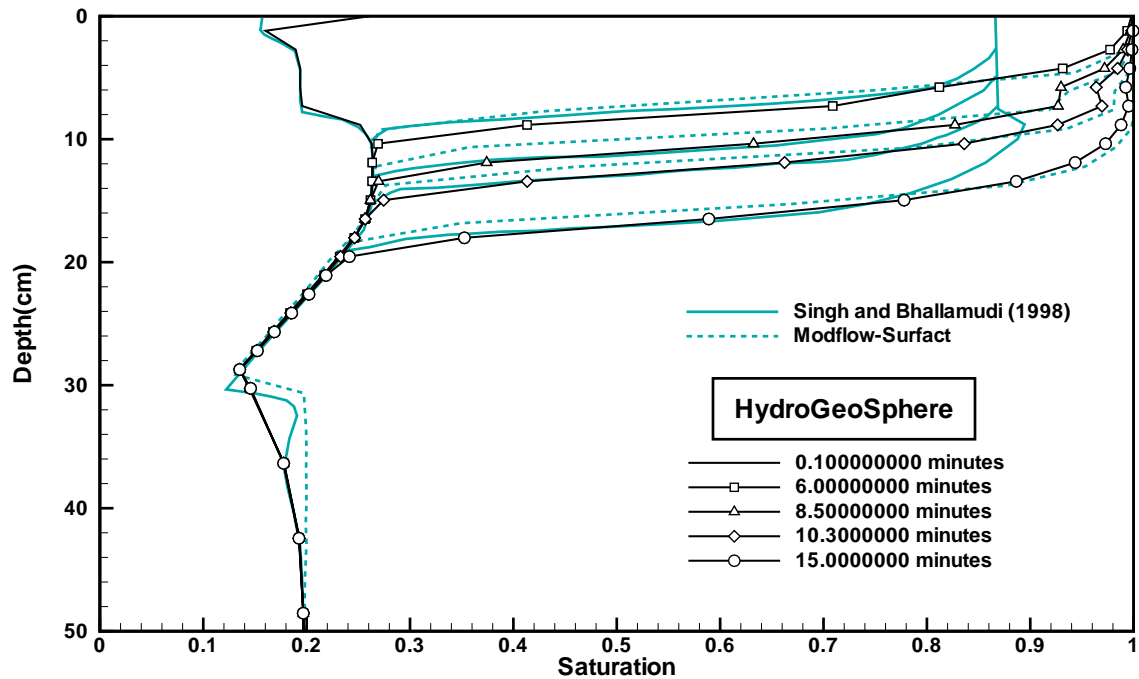
Figure 1.16: Soil Saturation Profile at 550 cm from Upstream End for Simulation of the Smith and Woolhiser (1971) Study.

advance within the soil. The infiltration front predicted by **HydroGeoSphere** compares fairly well with other simulation attempts (Smith and Woolhiser, 1971; Singh and Bhallamudi, 1998) and with available experimental data.

Figure 1.17 shows the outflow hydrograph at the downstream end of the surface flow nodes. This compares well with experimental data, and with other simulation attempts using the kinematic wave equation (Smith and Woolhiser, 1971) or the dynamic wave equation (Singh and Bhallamudi, 1998).

Figure 1.18 shows the surface water depth profiles at 8.3, 15 and 16 minutes of simulation respectively. The depth is noted to increase in time up till the end of the recharge period, and rapidly dissipates thereafter.

Figure 1.19 shows key components of the fluid balance for the simulation. The data are expressed as flow rates in centimetres cubed per minute, so, for example, the rainfall rate shows up as a uniform value of 2592 cm^3 $minute^{-1}$ until a time of 15 minutes, when it drops to zero. Initially, most of the rainfall is taken up by the subsurface, and accumulation in the surface flow domain is negligible before a time of about 3 or 4 minutes. Accumulation in the surface flow domain peaks at about 7 minutes and then declines as water begins discharging at the critical depth boundary. Fluid balance errors, which in this case are the difference between the rainfall plus the critical depth accumulation rates and the subsurface plus the surface domain accumulation rates, were less than a fraction of a percent throughout the simulation.
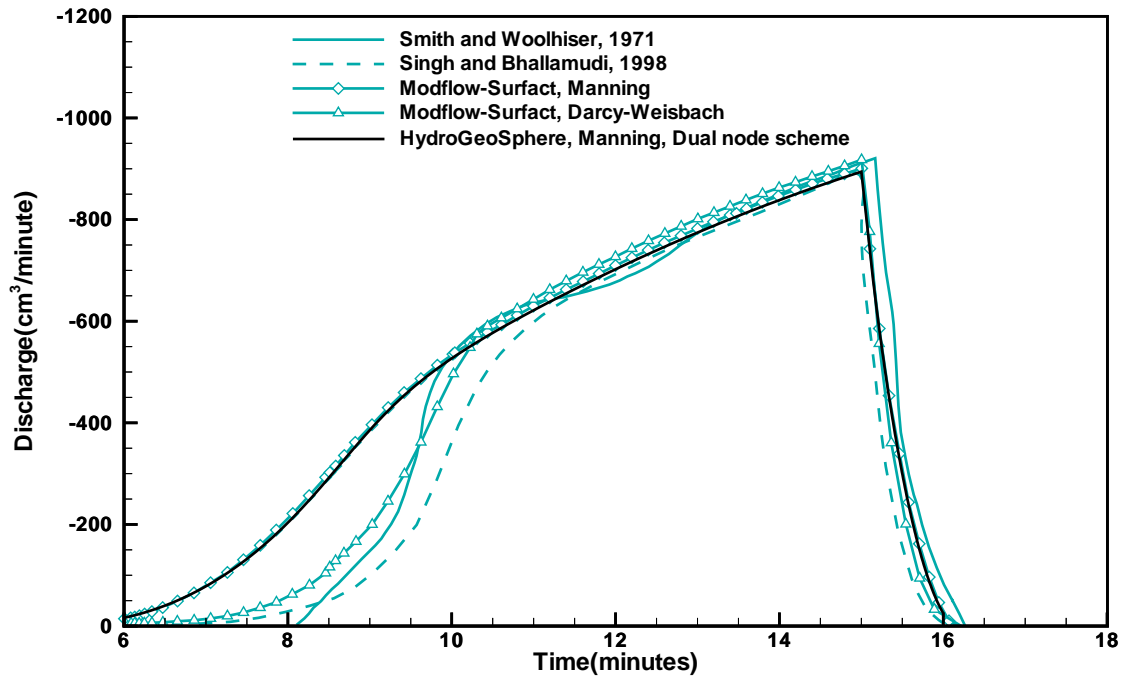
Figure 1.17: Outflow Hydrograph for Simulation of the Smith and Woolhiser (1971) Study.
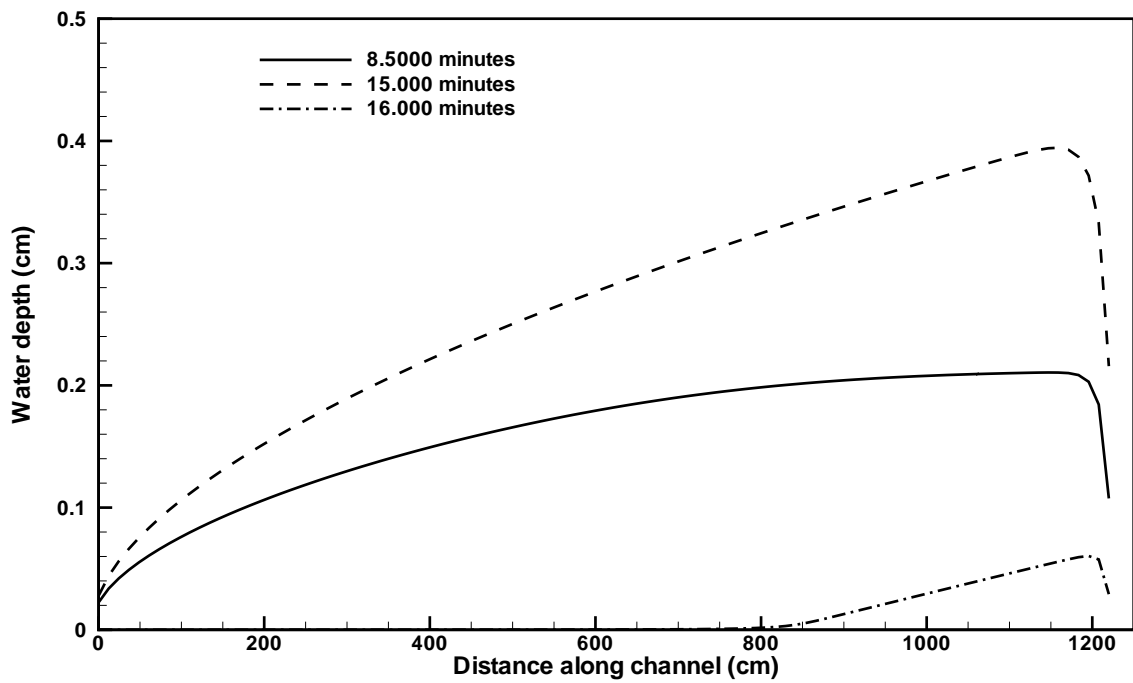
Figure 1.18: Surface Water Depth Profiles at Different Times for the Simulation of the Smith and Woolhiser (1971) Study.
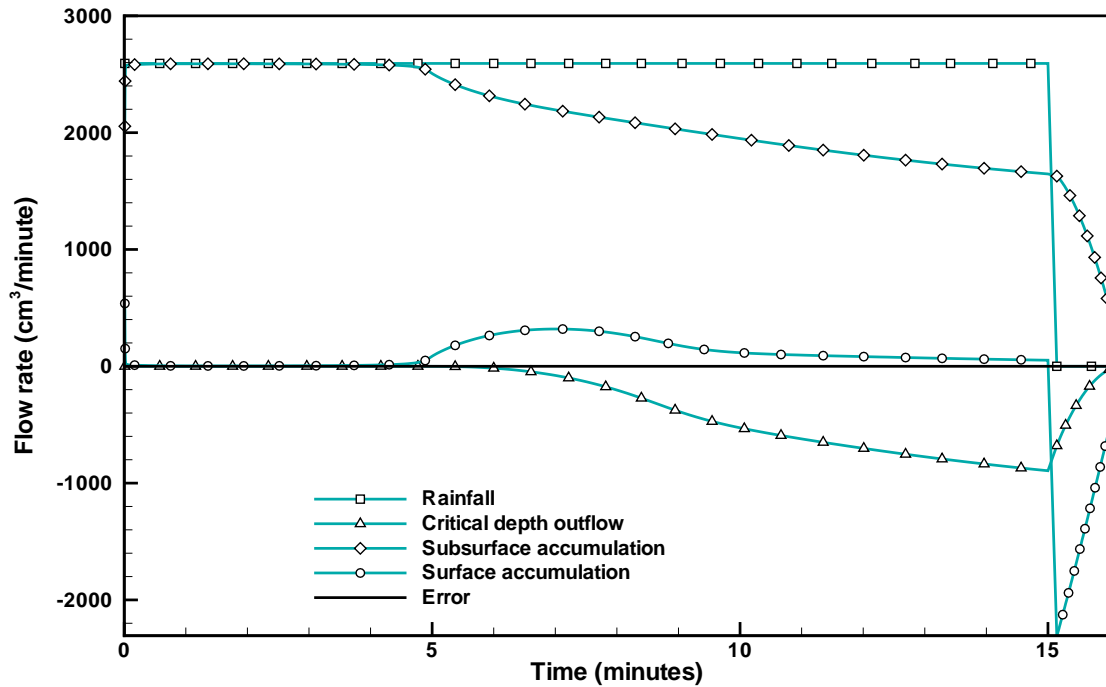
Figure 1.19: Fluid Balance Results for the Simulation of the Smith and Woolhiser (1971) Study.

1.2.3 Level 2: 2-D Surface Flow Study of Di Giammarco

Note: the verification problem described in this section corresponds to the `digiammarco` test case found in the `verification` directory under the **HydroGeoSphere** installation directory.

Two-dimensional areal surface flow is verified using the rainfall-runoff example of Di Giammarco et al. (1996). VanderKwaak (1999) presents details of the simulation, with results from various surface water flow codes benchmarked against this problem. The problem involves two-dimensional surface flow from a tilted V-catchment (Figure 1.20) generated by a 90 minute duration, 3×10^{-6} m s^{-1} intensity rainfall event. Only one half of the domain need be simulated due to symmetry, with published outflow discharge halved, to produce equivalent results. The simulation domain therefore consists of a 1,000 m by 800 m slope connected to 1,000 m length of channel 10 m wide. Surface slopes are 0.05 and 0.02, perpendicular to, and parallel to the channel respectively. Manning's roughness coefficients of 0.15 and 0.015 are applied to the slopes and channel, respectively. A critical depth boundary condition is applied at the downstream end of the channel.

Modeling Approach and Results

The domain was discretized into 10 rows and 9 columns, with the last column representing the 10 m wide channel. The remaining grid blocks are 100 m × 100 m. Only surface flow was simulated, with rainfall applied at the rate of 3×10^{-6} m s^{-1} for 90 minutes, followed

Plan View

Cross Section
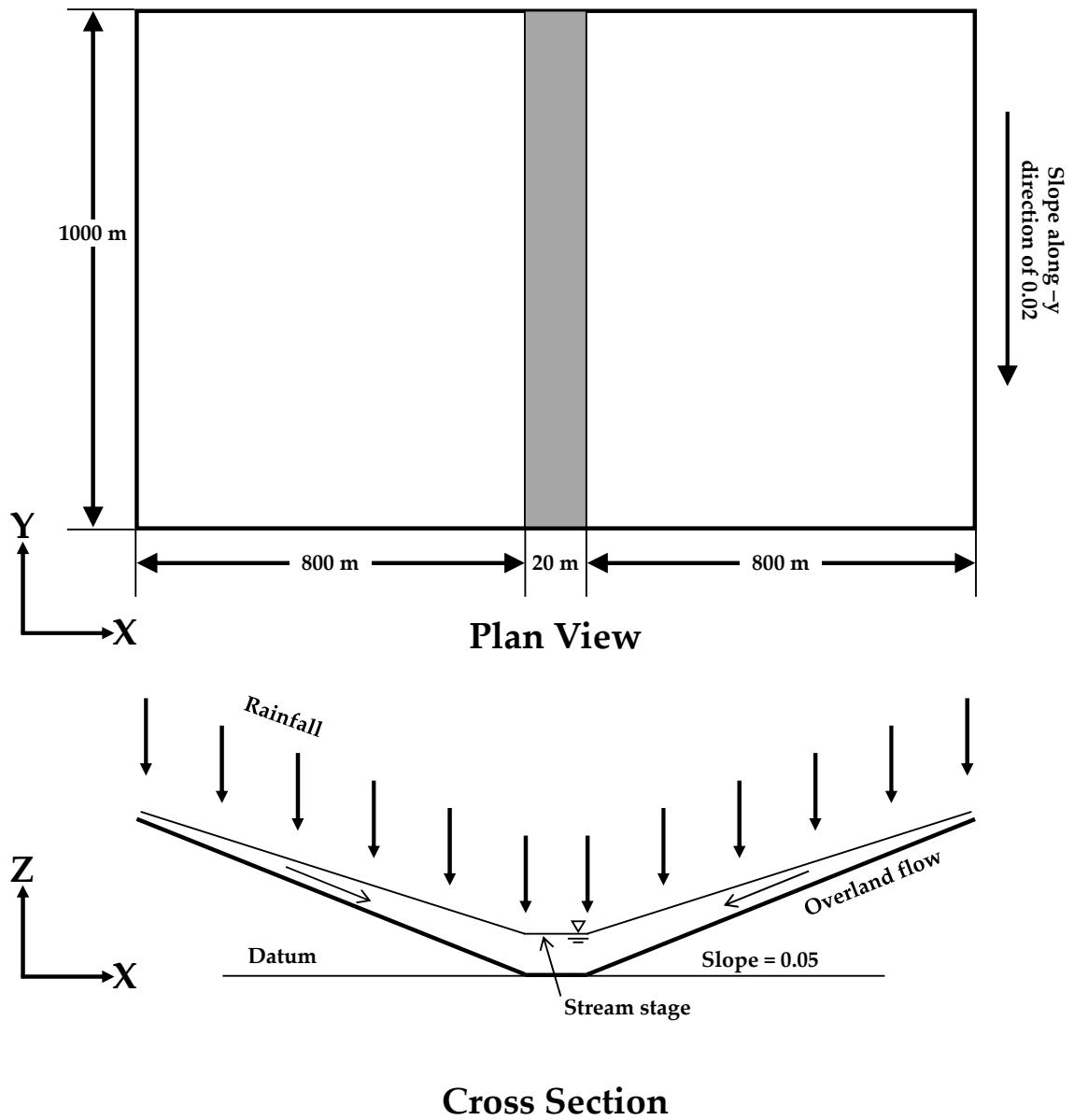
Figure 1.20: Schematic of the 2-D Surface Water Flow Study of Di Giammarco et al. (1996).
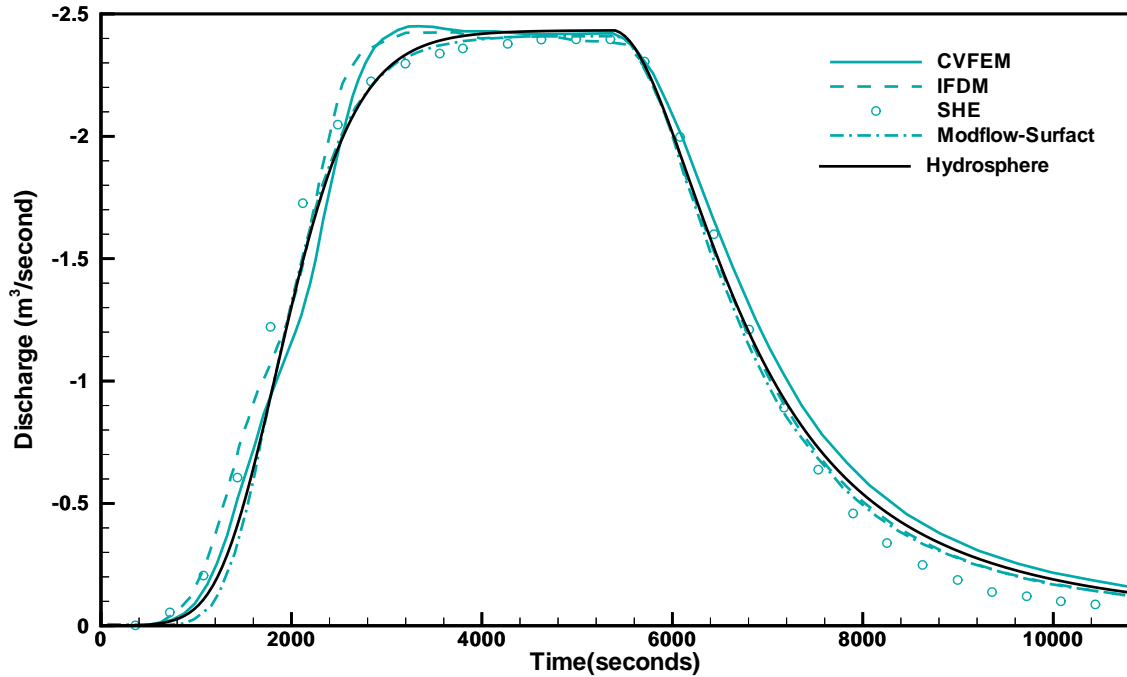
Figure 1.21: Outflow Hydrograph for Simulation of 2-D Surface Water Flow Study of Di Giammarco et al. (1996).

by no rainfall for the second stress period of 90 minutes. Adaptive time stepping with an initial time-step size of 5 s, a maximum time-step size of 100 s and a time-step incrementing factor of 2.0 is used for the simulation. Newton iteration considerations include a maximum of 20 iterations an absolute convergence tolerance of 10^{-4}.

Figure 1.21 compares predicted discharge from **HydroGeoSphere** with predictions from several other codes. Excellent agreement is noted between all results. Figure 1.22 shows the channel stage at two points at the outlet: one near the centre of the channel and one near the edge of the channel. The channel stage from Modflow-Surfact, a cell-centred finite difference model, is seen to fall within the edge and centre channel stages of **HydroGeoSphere**. The stage at the outlet point is noted to increase and dissipate in accordance with the computed discharge fluxes. Most time-steps converged within two iterations, with negligible mass balance errors throughout the simulation.

1.3 One-Dimensional Hydraulic Features

1.3.1 Level 1: Groundwater Pumping and Observation Wells

Note: the verification problem described in this section corresponds to the `1_theis_sat_common`, `2_theis_sat_dual`, `3_theis_unsat_common`, and `4_theis_unsat_dual` (`1D_structures`) test cases found in the `verification` directory under the **HydroGeoSphere**
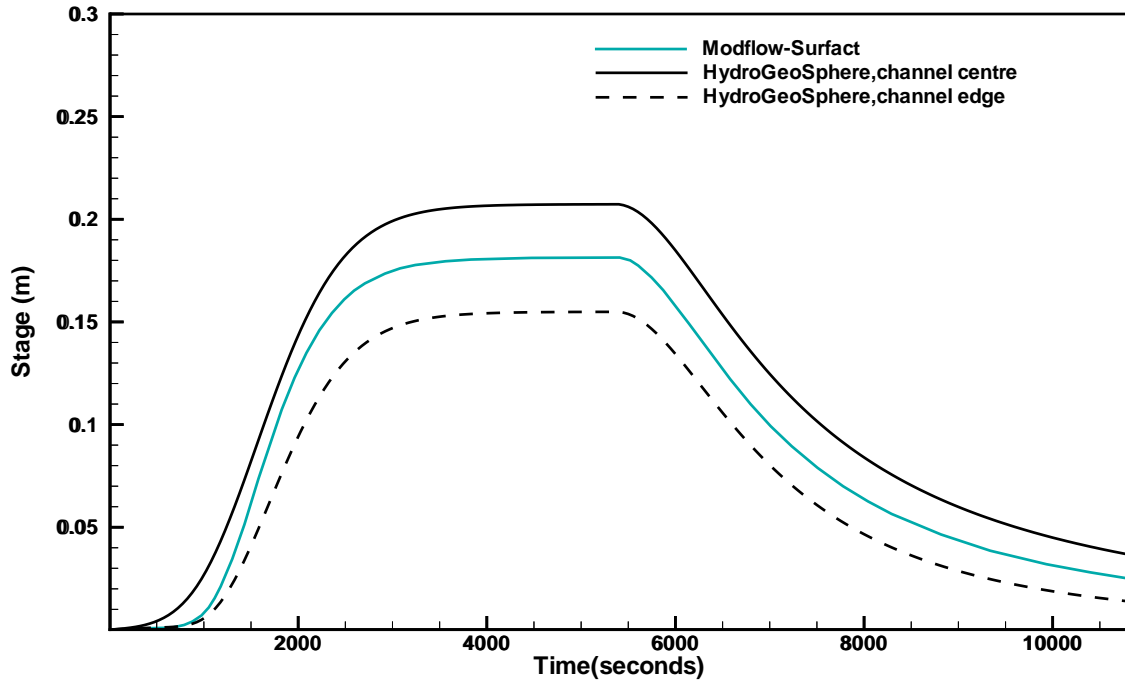
Figure 1.22: Channel Stage at Outlet for Simulation of 2-D Surface Water Flow Study of Di Giammarco et al. (1996).

installation directory.

Groundwater pumping perturbs the hydraulic head distribution and creates a cone of depression around the pumping well. In confined aquifers, water movement is essentially radial or horizontal shown in Figure 1.23 (a). However, unconfined aquifers have vertical flow above the aquifer shown in Figure 1.23 (b). While there are numerous groundwater analytic relations between pumping rates and drawdown, the most common method to evaluate subsurface response is a constant rate pump test in a confined or unconfined aquifer.

For the purpose of testing one-dimensional features, we implemented a simple cylinder-shape aquifer domain with a radius of 5 km and thickness of 20 metres shown in Figure 1.23 (c). A fully-penetrating pumping well is placed in the centre of the domain with a screen radius of 5-cm. The entire porous media domain is set to a homogeneous and isotropic hydraulic conductivity and specific storage of 2.3×10^{-3} m/s and 7.5×10^{-4} m^{-1}. As a means to compare to the analytical solution, the relative permeability and degree of saturation are assumed to be the same and follow a Gardener exponential function in the unsaturated zone.

Twenty 1-m thick layers with triangular prism elements were used to discretize the subsurface domain. The one-dimensional well was discretized with 20 of 1-m long line elements and had a constant pumping rate of 0.08 m^3/s applied to the bottom well node. Two approaches were implemented to couple the porous medium and well domains.The first method used the common node approach that assumes identical hydraulic head values for the well and contacting porous medium. The second method implemented the dual node approach which
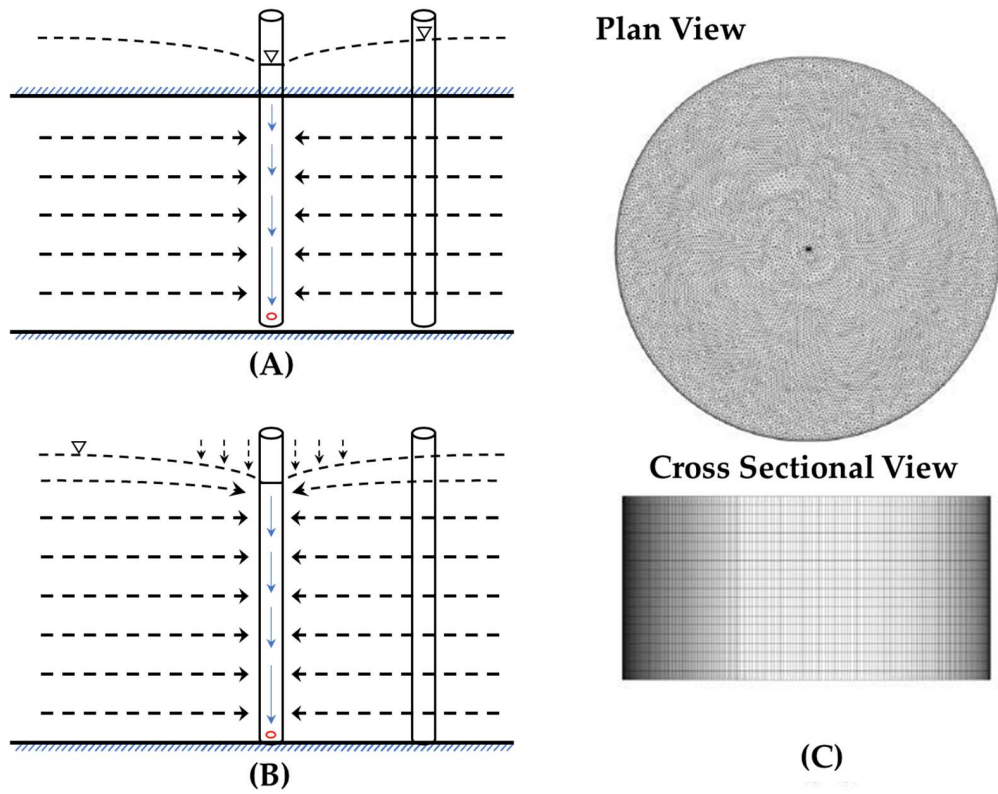
Figure 1.23: Pumping wells create a cone of depression and aquifer properties can be estimated for confined (a) and unconfined (b) aquifers. A 3-D grid system shown in (c) was used to simulate the pumping and drawdown relation in a cylindrical aquifer.
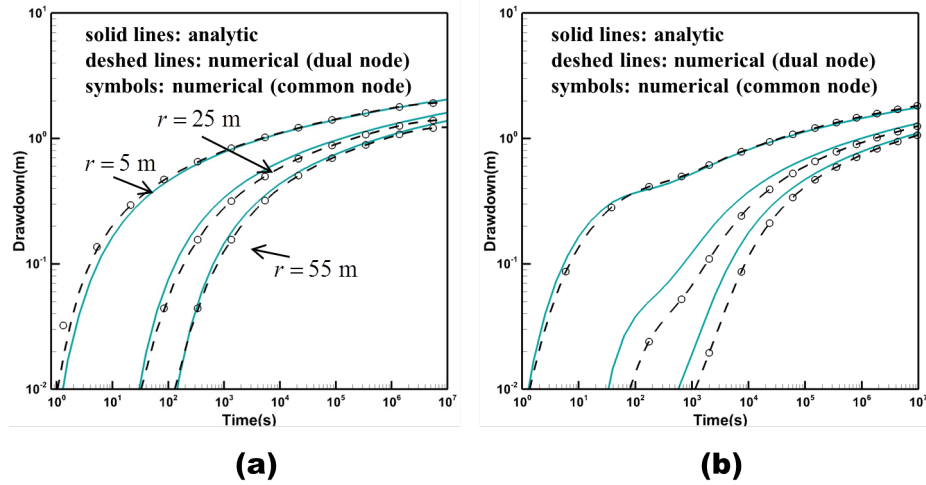
Figure 1.24: The simulated time-drawdown relations for the common and dual node approaches shown by circles and dashed lines. The results are compared to analytical solutions represented by the solid line for confined aquifers (a) and unconfined aquifer (b) systems.

calculates the fluid exchange between the domains via a first-order leakance relationship. The dual node approach used an interface thickness between two domains of 10^{-4} m and a hydraulic conductivity equal to the porous medium.

The analytical solutions for the confined (Theis, 1935) and unconfined aquifers (Mathias and Butler, 2006; Mishra and Neuman, 2010; Barlow and Moench, 2011) were compared to the simulated numerical time-drawdown values for 5 m, 25 m, and 55 m away from the pumping well. The results, shown in Figure 1.24, indicate that the simulated time-drawdown curves can generally replicate the analytical solutions. However for early time observations, there are notable differences between the two solutions for distant unconfined wells and it is not clear whether the discrepancy is due to the assumptions used to derive the analytical solutions (the thickness of the developed unsaturated zone due to pumping is negligible compared to the aquifer thickness) or numerical errors.

The steady-state head, radial flow, and axial flow along the pumping well are illustrated in Figure 1.25. The numerical simulation, shown with circles, used the dual node approach, while the analytical solution with an assumed uniform flow along the saturated portion of the well is shown by the solid lines. The results indicate that the simulated hydraulics in and around the pumping well perfectly match the analytic solutions for the confined aquifer case. The unconfined case has some discrepancies above the water table due to the assumed relations between well conductance and saturation.

1.3.2   Level 1: Subsurface Water Supply Systems

Note: the verification problem described in this section corresponds to the `5_HW_pipe_leaks_uniform` and `6_HW_pipe_leaks` (`1D_structures`) test cases found in the `verification`
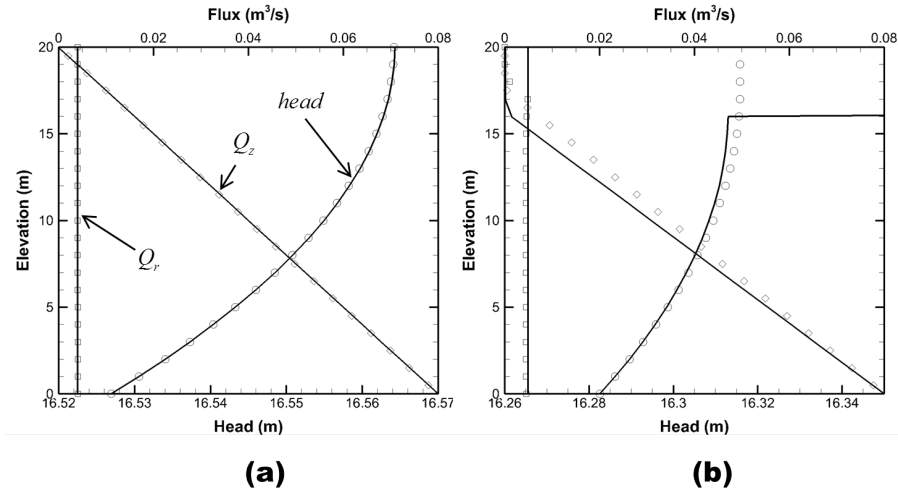
Figure 1.25: Steady state results of the numerical and analytical solutions are shown by circles and solid lines. The hydraulic head, axial flux and radial flux distributions are plotted along the vertical pumping well axis for confined (a) and unconfined (b) aquifer systems.

directory under the **HydroGeoSphere** installation directory.

Urban water supply systems typically distribute potable water from the water treatment facility to an end user through a network of pipes, tanks, pumps and control valves. Water distribution networks always flow from higher head to lower head and the flux and linear head loss inside of the pipes can be determined with an empirical relationship. Larger diameter pipes have lower internal velocities and lose less head per unit length than smaller diameter pipes. Thus, to adjust the tap pressure for the end destination, the pipe diameter can be adjusted to achieve the correct pressure and velocity standards. In order to maintain quality potable water quality throughout the supply system, water mains must maintain a minimum positive pressure to the surroundings so that the outside water cannot enter the pipe system. On the other hand, pipes may break up if the internal pressure exceeds a certain limit.

For verification of the numerical simulation, a one-dimensional pipe flow problem was implemented with the Hazen-Williams equation. The 1-D pipe interacted with the surrounding porous medium and the results were compared to an analytic solutions. The 100-m long 10-cm diameter pipe had a constant pressure head of 30-m at the inlet (x = 100m) and 20-m at the outlet (x = 0m). For illustration and testing purpose, the pipe was assumed to lose 75% of the original water flowing into the pipe inlet due to a uniform leakage for the first case and non-uniform leakage for the second case. The simulated numerical steady-state results predict the same head and flux values as the analytical solutions along the leaking pipes, as shown in Figure 1.26.
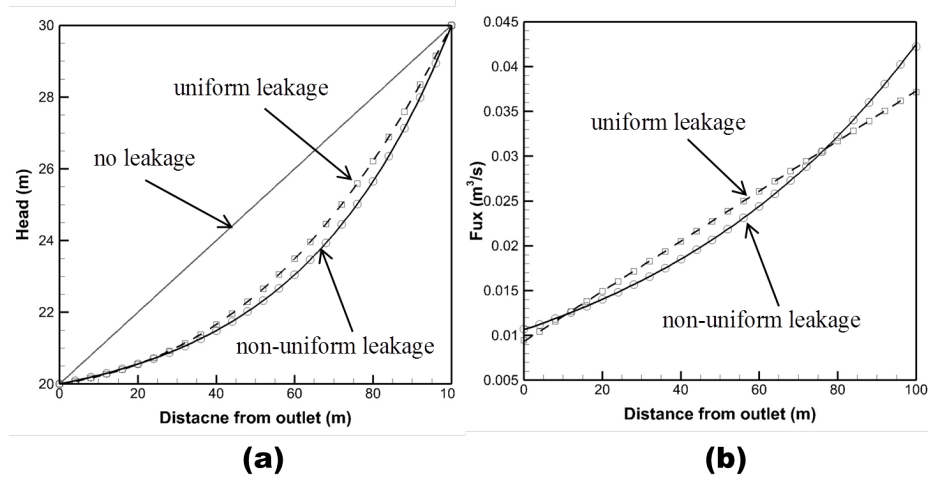
Figure 1.26: Simulated (symbols) and analytic (lines) solutions for hydraulic head, and axial flux distributions along a 100-m long pipe of 10-cm diameter, for a uniform leakage (a: rectangles and dashed lines) and non-uniform leakage (b: circles and solid lines) cases.

1.3.3 Level 2: Subsurface Drain Systems

Note: the verification problem described in this section corresponds to the `7_fipps` and `8_fipps_transient` (`1D_structures`) test cases found in the `verification` directory under the **HydroGeoSphere** installation directory.

MacQuarrie and Sudicky (1996) presented an approach to simulate subsurface rectangular drains by solving a one-dimensional flow equation. The authors demonstrated that the approach was appropriate and efficient by comparing their numerical solutions to the analytic solutions derived by Kirkham (1949) and the two-dimensional numerical solutions provided in Fipps et al. (1986). For the comparison MacQuarrie and Sudicky used a three-dimensional domain that was 3-m deep (z-axis), 30-m long (x-axis), and 30-m wide (y-axis). They used a saturated hydraulic conductivity of 0.0536 m/hr and adapted the Brooks-Corey soil water retention relation parameters from Fipps and Skaggs (1991). The simulated porous media had a horizontal drain pipe extended from 1-m to 29-m in the y-direction and fixed in the x and z directions (x=15-m, z=2-m). The pipe was specified with a flux boundary condition applied at the end of the drain (x=15-m, y=1-m, z=2-m). The steady-state flow case fixed the water-table was to the top of the ground surface and maintained the drain flux rate at 1.7584 m^3/hr.

This study changes the rectangular drain used by MacQuarrie and Sudicky (1996) to a circular drain with an effective radius of 0.0108-m as performed by Fipps et al. (1986). The new steady state simulated solutions were compaered to the Kirkham analytical solutions and MacQuarrie and Sudicky numerical solutions. The steady state vertical pressure head profiles were monitored at two locations, (x=15-m, y=15-m) and (x=22-m, y=15-m), and are shown in Figure 1.27. For the comparison of the transient flow solutions, a no flow condition was applied at the top ground surface. The transient solution was tested for a
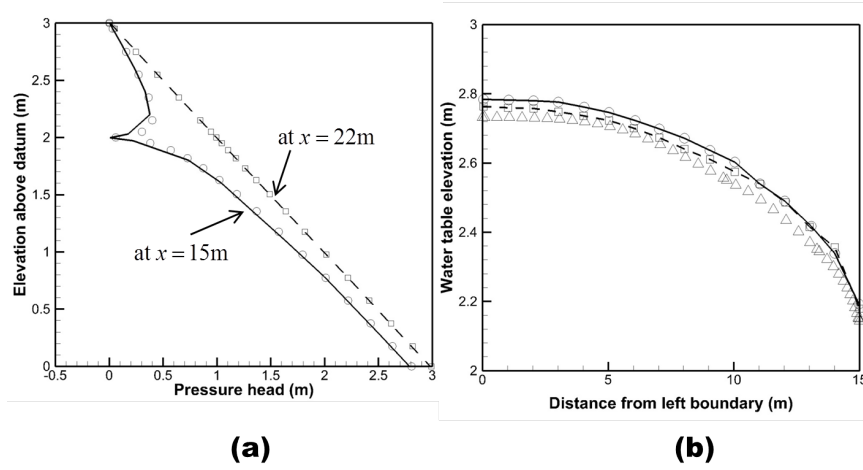
Figure 1.27: The vertical profiles at x=15m and x=22m are shown in (a) for the simulated and the analytical solutions by circles and solid line. The simulated water-table profile, shown in (b), is shown after 15 hours of drainage (triangles) and were compared to the numerical solutions by Fipps et al. (1986) (solid line with circles) and MacQuarrie and Sudicky (1996).

total of 15 hours and the results were compared to the solutions by Fipps et al. (1986) and MacQuarrie and Sudicky (1996) shown in Figure 1.27 (b).

1.3.4 Level 1: Subsurface Sewer Systems and Overland Flow

Note: the verification problem described in this section corresponds to the `9_channel_rect_const_inflow` (`1D_structures`) test case found in the `verification` directory under the **HydroGeoSphere** installation directory.

Sanitary sewer systems, similar to overland flow networks, can be simulated in terms of a series of one-dimensional flow along a drainage network of streams and rivers. The sewers are designed to collect and transport used water to the waste water treatment facilities under gravity driven flow and the water may flow into or out of the collection system depending on the conditions of the pipe hydraulics and the surrounding environment. Partially-saturated flow, as seen in most gravity driven waste water collection systems, is typically described with the Manning's equation.

The implementation of Manning's formula in one-dimensional structures is tested with a 100-m long by 1-m wide rectangular channel. The channel has a constant down stream slope of $\frac{\partial z}{\partial s} = 0.1$ with a constant inflow boundary condition. The inlet surface water depth is specified to a zero-m depth while a critical depth boundary condition is applied at the outlet such that $q_{outlet} = -\sqrt{g \cdot d^3}$. Throughout the channel, a constant influx, $q_r = 6.02 \times 10^{-2}$ m^3/s/m, is applied resulting in a total stream flow of $q(x) = q_0 + q_r \cdot x$. Figure 1.28(a) shows the linear simulated water depth and axial flux distributions results in
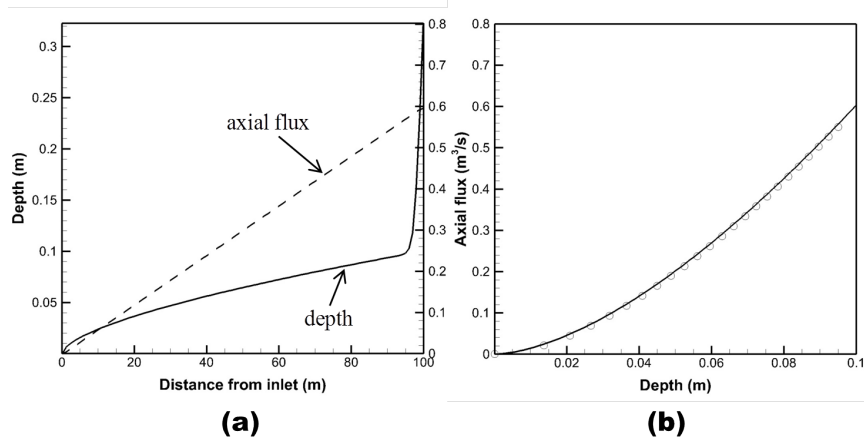
Figure 1.28: Simulated water depth and axial flux distributions along a 100-m long 1-m wide rectangular open channel (a). In (b), the simulated depth-flux relation is compared to the simplified analytic relation when $\partial h/\partial s \approx \partial z/\partial s$ shown by circles and solid lines.

the domain. The simulated depth-flux relation is compared to the Manning's formula where $\frac{\partial z}{\partial s}$ is approximated by bed slope shown in Figure 1.28(b).

1.4 Coupled Surface/Subsurface Flow

1.4.1 Level 3: 3-D Field Scale Study of Abdul

Note: the verification problem described in this section corresponds to the `abdul`, `abdul_snowmelt`, `abdul_thermal`, and `abdul_transport` test cases found in the `verification` directory under the **HydroGeoSphere** installation directory.

A field scale simulation is performed with **HydroGeoSphere** to verify its capabilities for fully three-dimensional surface/subsurface flow modeling. Experiments conducted at Canadian Forces Base Borden, in Ontario, Canada, by Abdul (1985) are selected for this simulation. VanderKwaak (1999) presents details of the site, its characteristics, the experimental setup and the results. Figure 1.29 shows the experimental plot, approximately 80 m × 16 m areally and up to 4 m deep. A man-made stream channel lies approximately 1.2 m below the surrounding grassy land. The channel is initially dry prior to the application of the artificial rainfall via irrigation sprinklers. The initial water table lies around 22 cm below the streambed with the artificial recharge applied at a rate of 2 cm hour^{-1} for 50 minutes. Infiltration in upland regions, discharge in lower regions and runoff, all govern the behavior of the system. Soil properties and roughness coefficients are provided in Table 1.11.

Modeling Approach and Results

The domain was discretized areally into 1372 nodes and 2651 triangular elements. Vertically, the grid is distorted to conform with the topographic elevation as shown in Figure 1.30.
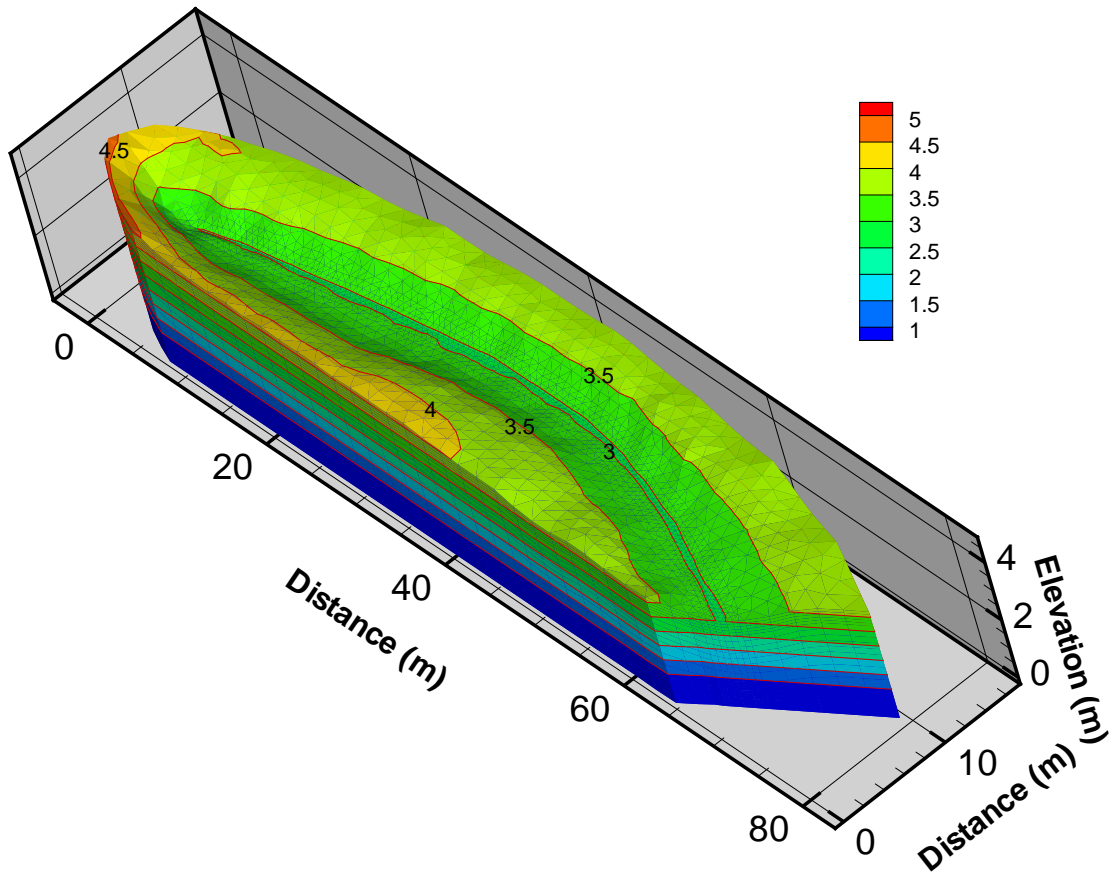
Figure 1.29: Site Description for Rainfall-Runoff Field Experiment of Abdul (1985) from (VanderKwaak, 1999).

Table 1.11: Parameter Values for Simulation of the 3-D Field Scale Study of Abdul (1985).

Parameter	Value	Unit
porosity, Θ	0.37	
hydraulic conductivity, K	1×10^{-5}	m s^{-1}
storage coefficient, S_s,	1.2×10^{-7}	m^{-1}
Van Genuchten parameter, α	1.9	m^{-1}
Van Genuchten parameter, β	6	
residual saturation, S_r	0.18	
Brooks-Corey coefficient, n	3.4	
Manning coefficient for plot	0.3	s m$^{-1/3}$
Manning coefficient for channel	0.03	s m$^{-1/3}$
Initial water table elevation	2.78	m
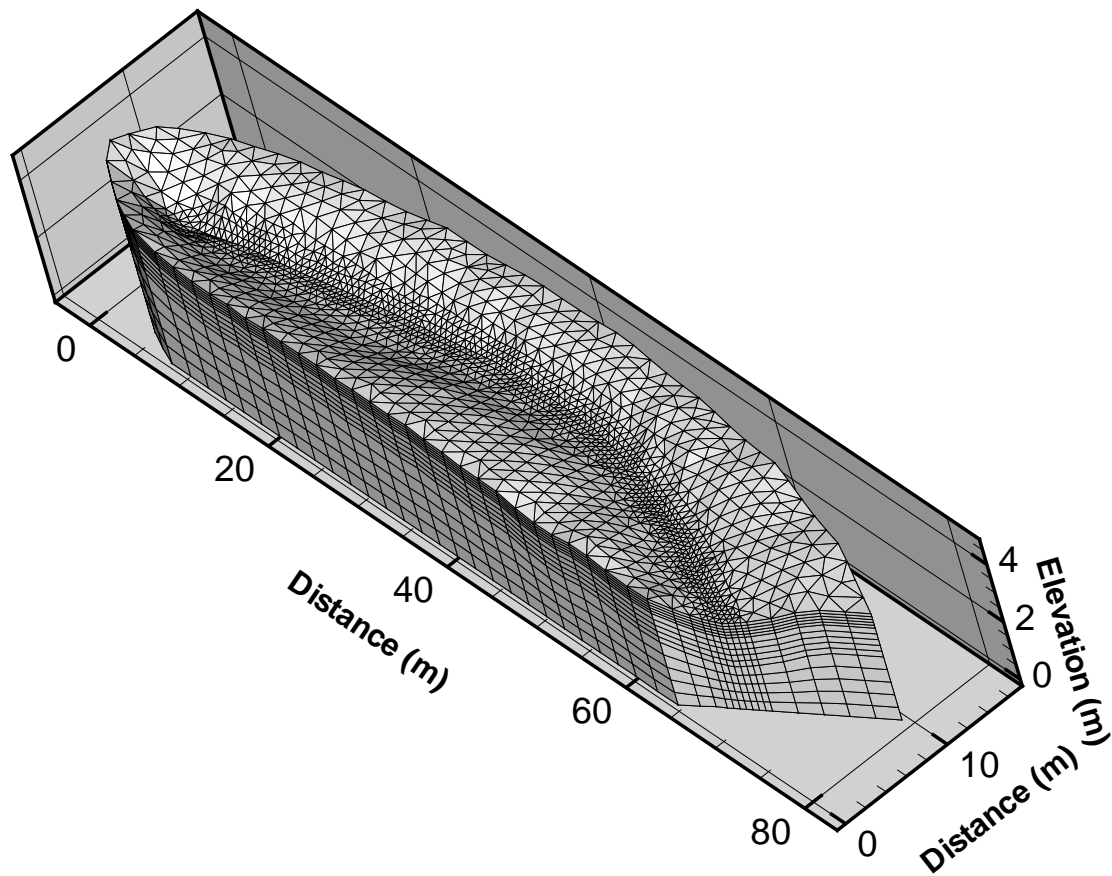
Figure 1.30: Three-dimensional View of Topography and Finite element Grid, for Simulation of the Abdul (1985) Rainfall-Runoff Field Experiment.

Fifteen layers of elements were used with a fine discretization of 0.1 m near the surface which was enlarged to 1 m near the bottom. The dual node approach was used to simulate surface flow. The resulting 3-D finite element mesh is identical to the one used by VanderKwaak (1999). Recharge is provided at the rate of 5.56×10^{-6} m s^{-1} for a first stress period of 50 minutes, with zero recharge for the second 50 minute stress period. A critical depth boundary condition is applied all around the upper surface of the domain, and the simulation is performed for 100 minutes, with no recharge occurring for the second 50 minute stress period. Adaptive time-stepping is used with an initial time-step size of 5s, a maximum time-step size of 100s, and time-step incrementing and decrementing factor limits of 2.0 and 0.5, respectively. Iteration parameters include 100 and 15 inner and outer iterations respectively, and a convergence tolerance of 1×10^{-4} m. Figure 1.31 shows the outflow hydrograph to be close to the experimental values, and to the simulation of VanderKwaak (1999). As noted by VanderKwaak (1999), this system's outflow hydrograph is extremely sensitive to channel elevations, initial water-table levels, and side-slopes of the plot.

The spatial distribution of water depth within the domain at time 50 minutes is shown in Figure 1.32 for both VanderKwaak (1999) and **HydroGeoSphere**. These compare well for
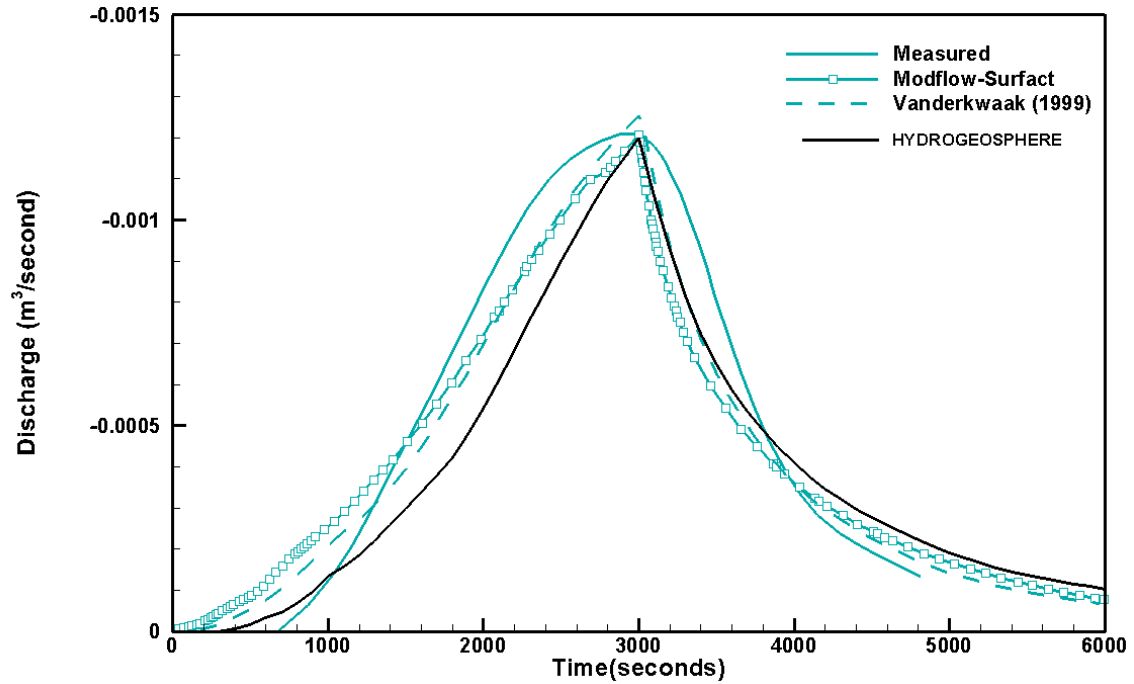
Figure 1.31: Outflow Hydrograph for Simulation of the Abdul (1985) study.

regions of maximum water depth around the channel but differ elsewhere.

These small differences between the outflow hydrograph and surface water depth between the two simulations may be due to the different approaches used to define the flow coupling term between the surface and subsurface meshes in the dual node approach. VanderKwaak (1999) used a flow coupling length (in this case 1×10^{-4} m), height of microtopography (1 $\times10^{-2}$ m) and mobile water depth (1×10^{-4} m) to define the coupling term while **Hydro-GeoSphere** uses a coupling length of 1×10^{-1} m and a rill storage height of 2×10^{-3} m. Also, VanderKwaak (1999) assigned critical depth boundary conditions to a few nodes at the outflow end of the channel, while in **HydroGeoSphere**, the critical depth boundary was assigned all around the outside of the domain, which would account for the depressions in the water depth surface observed for **HydroGeoSphere** in Figure 1.32.

1.4.2   Level 2: 3-D Surface/Subsurface Flow and Evapotranspiration

Note: the verification problem described in this section corresponds to the `panday` test case found in the `verification` directory under the **HydroGeoSphere** installation directory.

Evapotranspiration is verified using the example of Panday and Huyakorn (2004), who extended the 2-D V-catchment surface flow problem described in Section 1.2.3 to include the subsurface domain, which extends to a depth of 20 m below the channel outlet. The domain is discretized into 11 subsurface layers with areal gridding mirroring the grid of the overland flow domain. The top ten subsurface layers each have a thickness of 1 m and the bottom of
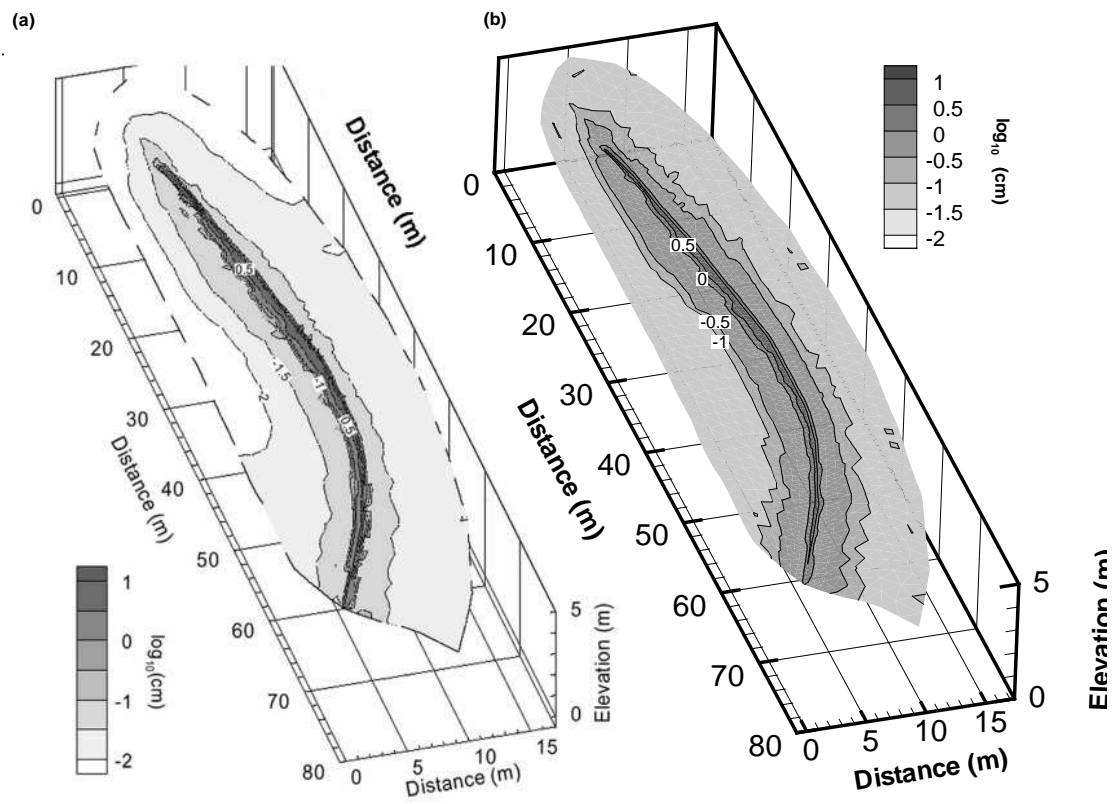
Figure 1.32: Spatial Distribution of Water Depth after 50 Minutes of Field Experiment for (a) VanderKwaak (1999) and (b) **HydroGeoSphere**.

Table 1.12: Parameter Values for the Simulation of the Panday and Huyakorn (2004) Study.

Parameter	Value	Unit
Reference evapotranspiration	3×10^{-7}	m
Leaf area index	2.08	
Saturation at field capacity	0.32	
Saturation at wilting point	0.2	
Saturation at oxic limit	0.76	
Saturation at anoxic limit	0.9	
Energy limiting stage saturation	0.32	
Evaporation limiting stage saturation	0.2	
Transpiration constants		
C_1	0.3	
C_2	0.2	
C_3	3×10^{-6}	m s^{-1}
Soil evaporation distribution function		
Depth = 0.0	0.703	
Depth = 1.0	0.259	
Depth = 2.0	0.037	
Depth = 3.0	0.0	
Root zone distribution function		
Depth = 0.0	0.703	
Depth = 1.0	0.259	
Depth = 2.0	0.037	
Depth = 3.0	0.0	

the last layer is at $z = -20$ m. Again, only one half of the domain need be simulated due to symmetry, with published outflow discharge halved, to produce equivalent results. The subsurface domain has horizontal and vertical hydraulic conductivity values of 5×10^{-5} and 5×10^{-6} m s^{-1} respectively, a porosity value of 0.1, and Van Genuchten parameters α, β, and S_{wr} equal to 2.25 m^{-1}, 1.89, and 0.16, respectively.

The same rainfall intensity of 3×10^{-6} m s^{-1} as for the previous case is applied for a period of 35 days, followed by no rainfall for the second stress period of 15 days.

In order to gauge the performance of the evapotranspiration formulation, evapotranspiration losses, as parameterized in Table 1.12 were applied. Because Modflow-Surfact uses a block-centred approach while **HydroGeoSphere** uses a node-centred approach, the evaporation and root zone distribution functions are similar, but not identical.

Adaptive time stepping with an initial time-step size of 5s, a maximum time-step size of 10000s and a time-step incrementing factor of 2.0 is used for the simulation. Newton iteration considerations include a maximum of 15 iterations and an absolute convergence tolerance of 10^{-3}.

Figure 1.33 compares predicted fluid fluxes from **HydroGeoSphere** with predictions from
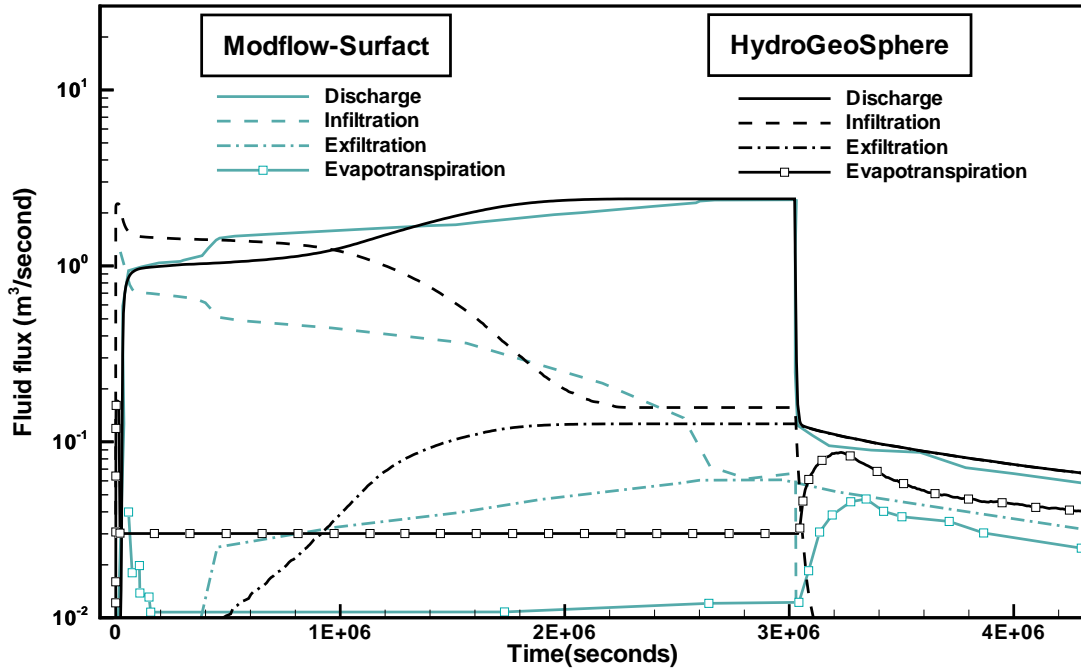
Figure 1.33: Water Budget Components for the Simulation of the Panday and Huyakorn (2004) Study.

Modflow-Surfact. The responses of the two models are somewhat similar. The disparity is attributed to differences in the formulation of the surface/subsurface flux coupling term between the block-centred and node-centred approaches.

1.5 Subsurface Transport

1.5.1 Level 1: Chain Decay Transport in a Porous Medium

Note: the verification problem described in this section corresponds to the `pm_cd` test case found in the `verification` directory under the **HydroGeoSphere** installation directory.

In order to verify the accuracy of **HydroGeoSphere** in simulating the movement of a multi-component decay chain in a porous medium it was compared with the exact analytical solution CMM (Sudicky, 1991; Sudicky et al., 2013).

The problem was set up for the three-member decay chain:

$$\text{Uranium}^{234} \rightarrow \text{Thorium}^{230} \rightarrow \text{Radium}^{226}$$

The input parameters and values for the analytical solution are shown in Table 1.13:

The analytical solution can simulate 1-D, 2-D or 3-D behavior with respect to plume development. In this case, it was set up to simulate 1-D behavior.

Table 1.13: Parameter Values for Chain-decay Transport in a Porous Medium.

Parameter	Value	Unit
Velocity	100.0	m yr^{-1}
Dispersivity	10.0	m
Diffusion coefficient	0.0	m^2 yr^{-1}
Retardation factor		
$\quad$ Uranium^{234}	1.43×10^4	
$\quad$ Thorium^{230}	5.0×10^4	
$\quad$ Radium^{226}	5.0×10^2	
Decay coefficient		
$\quad$ Uranium^{234}	2.83×10^{-6}	yr^{-1}
$\quad$ Thorium^{230}	9.0×10^{-6}	yr^{-1}
$\quad$ Radium^{226}	4.33×10^{-6}	yr^{-1}
Initial source concentration		
$\quad$ Uranium^{234}	1.0	
$\quad$ Thorium^{230}	0.0	
$\quad$ Radium^{226}	0.0	

In the numerical model, a grid which was 500 m long in the x-direction and 1 m in the y and z directions was generated. A uniform nodal spacing of 5 m was used in the x-direction. Medium properties and flow boundary conditions were assigned such that a uniform linear flow velocity equal to 100 m yr^{-1} parallel to the x-axis was produced. A constant concentration of 1.0 was specified for Uranium^{234} at the upstream x-face.

Figure 1.34 shows concentration profiles for the three members of the decay chain at a time of 10000 years for both CMM and **HydroGeoSphere**. It can be seen that the results are almost identical.

1.5.2 Level 1: Chain Decay Transport in a Single Fracture

Note: the verification problem described in this section corresponds to the `f_cd` test case found in the `verification` directory under the **HydroGeoSphere** installation directory.

In order to verify the accuracy of **HydroGeoSphere** in simulating the movement of a multi-component decay chain in a fractured media it was compared with the exact analytical solution DKCRACK (Sudicky, 1994).

The problem involves the same three-member decay chain used in the porous media example described above. The input parameters and values for the analytical solution are shown in Table 1.14.

Note that subsurface water velocity in the matrix is 0.0, an assumption made in the analytical solution. Movement of contaminant into the matrix blocks is solely by molecular diffusion.

In the numerical model, a grid which was 200 m long in the x-direction and 1 m in the y

Table 1.14: Parameter Values for Chain-decay Transport in a Fracture.

Parameter	Value	Unit
Velocity in fracture	100.0	m yr^{-1}
Longitudinal dispersivity in fracture	1.0	m
Fracture aperture	1.0×10^{-4}	m
Fracture separation	0.1	m
Matrix porosity	0.01	
Matrix tortuosity	0.1	
Inlet velocity [†]	100.0	m yr^{-1}
Inlet dispersion	0.0	m yr^{-1}
Diffusion coefficient [‡]		
Uranium^{234}	3.1536×10^{-2}	m^2 yr^{-1}
Thorium^{230}	3.1536×10^{-2}	m^2 yr^{-1}
Radium^{226}	3.1536×10^{-2}	m^2 yr^{-1}
Fracture retardation factor		
Uranium^{234}	1.0	
Thorium^{230}	1.0	
Radium^{226}	1.0	
Matrix retardation factor		
Uranium^{234}	1.43×10^4	
Thorium^{230}	5.0×10^4	
Radium^{226}	5.0×10^2	
Decay coefficient		
Uranium^{234}	2.83×10^{-6}	yr^{-1}
Thorium^{230}	9.0×10^{-6}	yr^{-1}
Radium^{226}	4.33×10^{-6}	yr^{-1}
Initial source concentration		
Uranium^{234}	1.0	
Thorium^{230}	0.0	
Radium^{226}	0.0	

[†] An inlet velocity equal to the velocity in the fracture and an inlet dispersion of 0 is equivalent to a first-type source
[‡] Free solution diffusion coefficient
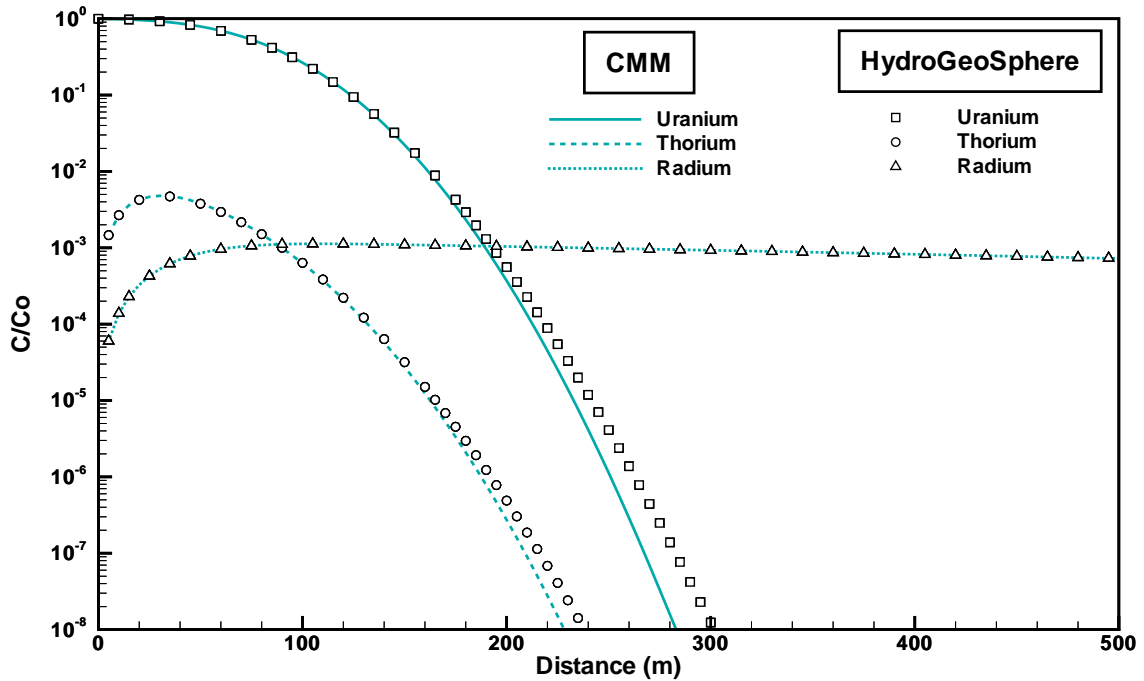
Figure 1.34: Results for a 3-member Decay Chain in a Porous Medium at 10000 Years.

and 0.1 m in the z directions was generated. A uniform nodal spacing of 5 m was used in the x-direction. Medium properties and flow boundary conditions were set up such that a uniform fracture flow velocity of 100 m yr^{-1} parallel to the x-axis was produced. A constant concentration of 1.0 was specified for Uranium^{234} at the upstream end of the fracture.

Figure 1.35 shows the concentration profiles of Uranium, Thorium and Radium at 10000 years for both DKCRACK and **HydroGeoSphere** simulations. The results are nearly identical.

1.5.3 Level 1: Time-variable Source Condition

Note: the verification problem described in this section corresponds to the `pm_tvs` test case found in the `verification` directory under the **HydroGeoSphere** installation directory.

In order to verify the accuracy of **HydroGeoSphere** in simulating a time-variable source condition, it was compared with an exact analytical solution SUPER1D (Sudicky, 1986) for a uniform vertical, one-dimensional flow field. A time-variable Tritium source is applied with an with an input function for Tritium Units (TU) as shown in Figure 1.36. Radioactive decay is neglected in the simulation. Other input parameters for the analytical solution are shown in Table 1.15.

In the numerical model, a grid which was 100 m long in the x-direction and 10 m in the y and z directions was generated. A uniform nodal spacing of 5 m was used in the x-direction.
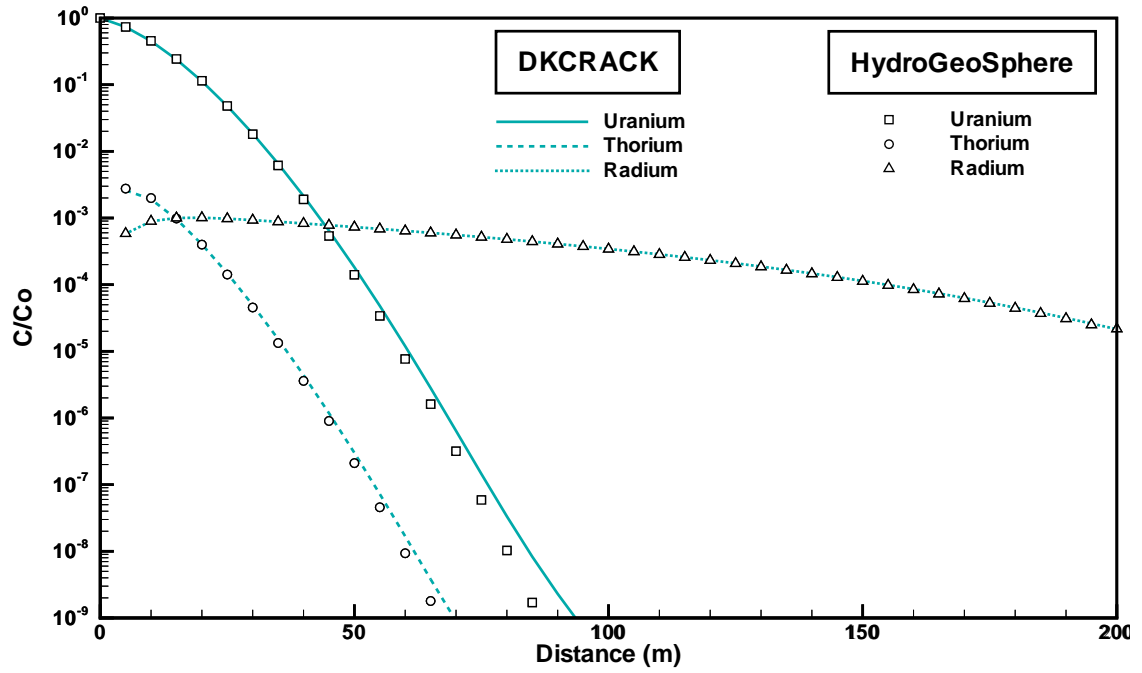
Figure 1.35: Results for a 3-member Decay Chain in a Fractured Medium at 10000 Years.
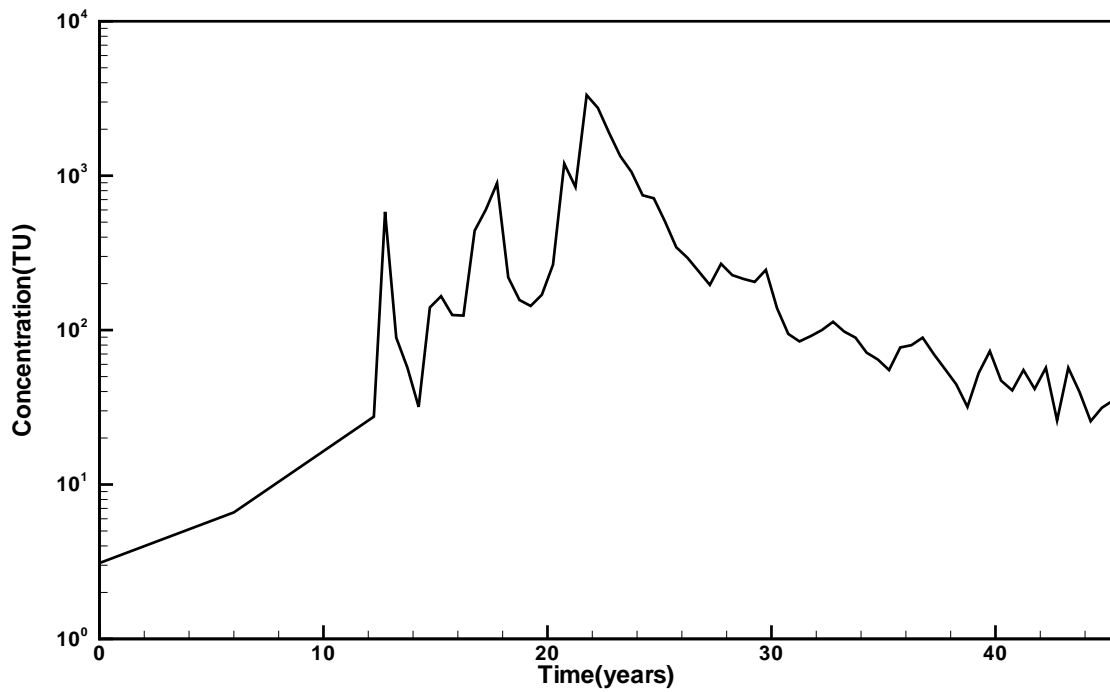
Figure 1.36: Input Function for Time-variable Source Transport.

Table 1.15: Parameter Values for Time-varying Source Transport Simulation.

Parameter	Value	Unit
Velocity	1.0	m yr^{-1}
Dispersivity	1.0	m
Diffusion coefficient	0.0	m^2 yr^{-1}
Retardation factor	1.0	
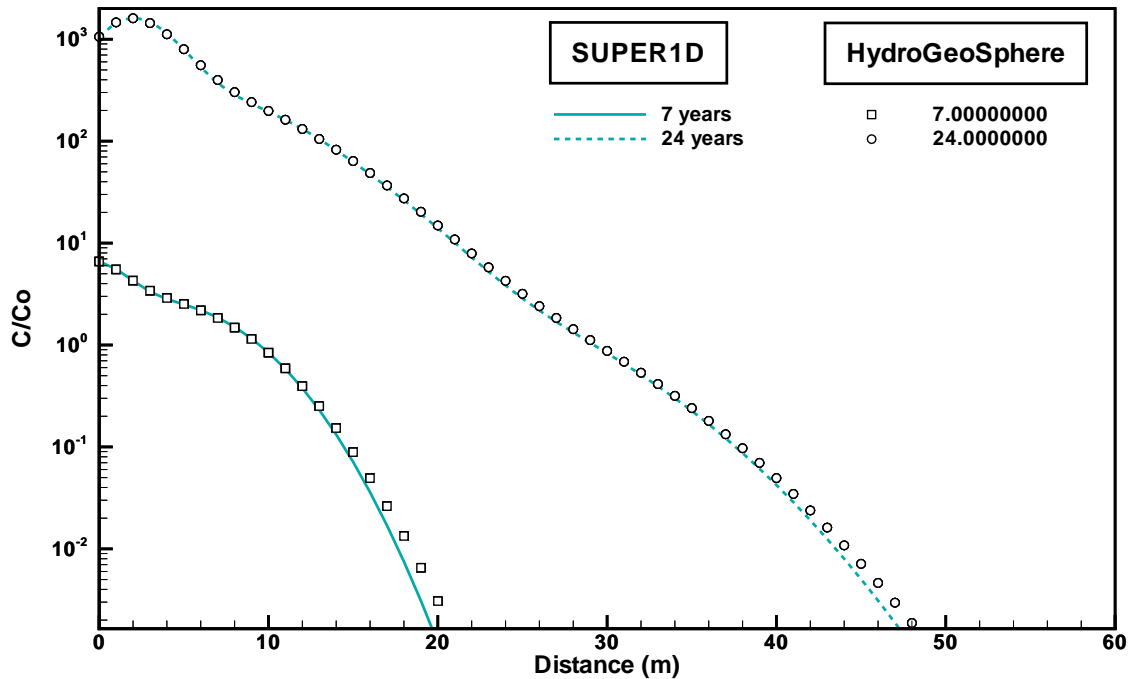
Figure 1.37: Results for a Time-variable Source Function.

Medium properties and flow boundary conditions were set up such that a uniform average linear subsurface water flow velocity of 1.0 m yr^{-1} parallel to the x-axis was produced. The time-variable source function given above was specified at the upstream x-face.

Concentration profiles for the contaminant at times equal to 7 and 24 years are shown in Figure 1.37. Results from **HydroGeoSphere** are nearly identical to the analytical solutions.

In the numerical model, the adaptive timestepping routine was used and the maximum percent concentration change allowed was 10%. The results are very close to those obtained from the analytical solution.

Table 1.16: Parameter Values for Dual-porosity Transport Simulation.

Parameter	Value	Unit
Darcy velocity	2.5	cm day^{-1}
Total porosity	0.5	
Mobile fraction	0.5	
Dispersion coefficient	10.0	cm^2 day^{-1}
Retardation factor	1.0	
Mass transfer coefficient	0.1	day^{-1}

1.5.4   Level 1: Transport in a Dual-Porosity Medium

Note: the verification problem described in this section corresponds to the `dual` test case found in the `verification` directory under the **HydroGeoSphere** installation directory.

In order to verify the accuracy of **HydroGeoSphere** in simulating transport in a dual-porosity medium, it was compared with the analytical solution MPNE (Neville). The input parameters for the analytical solution are shown in Table 1.16.

In the numerical model, a grid which was 60 cm long in the x-direction and 1 cm in the y and z directions was generated. A uniform nodal spacing of 1 cm was used in the x-direction. Medium properties and flow boundary conditions were set up such that a uniform average linear flow velocity of 10 cm day^{-1} parallel to the x-axis resulted. A constant concentration of 1.0 was specified at the upstream end of the system. The porosity of both the mobile and immobile zones was set to 0.25, which gives a total porosity of 0.5 with the mobile fraction being equal to 0.5, which is equivalent to the analytical solution input parameters. The dispersivity was set to 1.0 cm, which is equivalent to a dispersion coefficient of 10 cm^2 day^{-1} when multiplied by the average linear subsurface water velocity.

Figure 1.38 shows a concentration profile at a time of 2.5 days for both MPNE and **HydroGeoSphere**. It can be seen that the results are almost identical.

1.5.5   Level 2:   Coupled Flow and Transport in a Dual-Permeability Medium

Note: the verification problem described in this section corresponds to the `gerke` test case found in the `verification` directory under the **HydroGeoSphere** installation directory.

The capability of **HydroGeoSphere** to simulate transient flow and solute transport in a coupled porous medium-dual continuum system was tested by comparing it to results obtained by Gerke and van Genuchten (1993). The problem consists of a one-dimensional column 40 cm in length, in which the macropores are assumed to be planes with a spacing of 2 cm that subdivide the porous medium into uniform blocks. Similar to Gerke and van Genuchten (1993), the domain was finely discretized in the vertical direction, using elements which were 0.1 m in length. The initial pressure head in the domain was set to -1000 cm. A
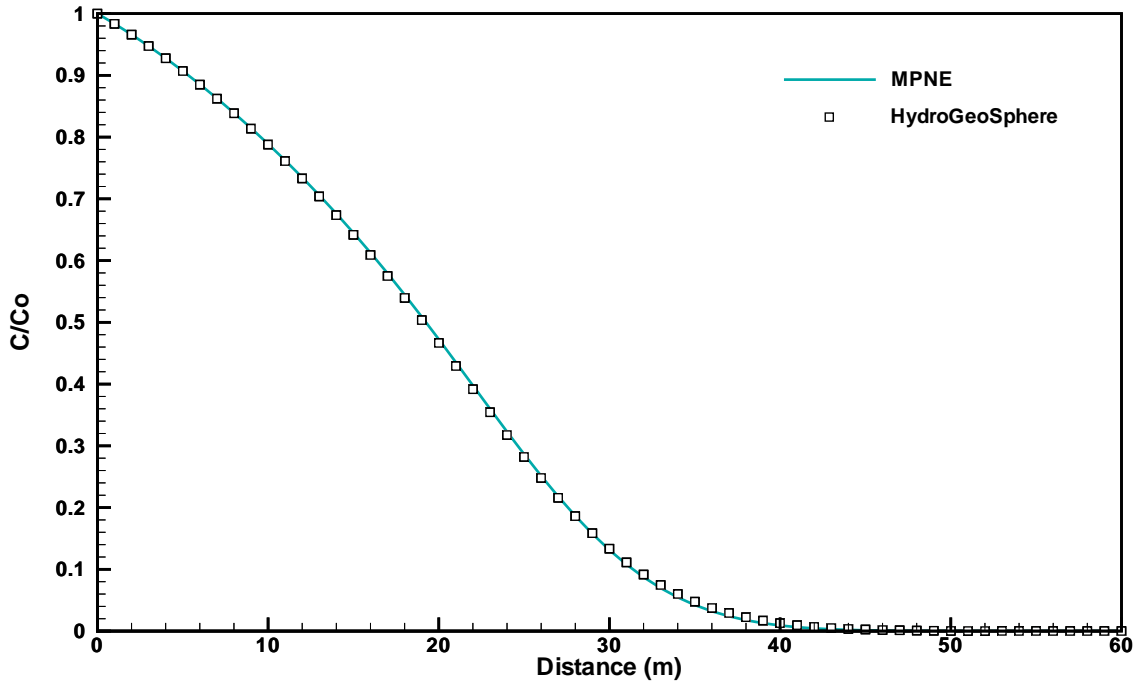
Figure 1.38: Results for Transport in a Dual-porosity Medium.

uniform rainfall of 50 cm day^{-1} was applied to the dual continuum, and water was allowed to drain freely from the base of the system in both the porous medium and dual-continuum. The initial solute concentration in the domain was set to 1.0. The hydraulic and transport parameters of the system are presented in Table 1.17. The fluid exchange term α_{wd} is 0.6 cm^{-1} day^{-1}, which is half that used by Gerke and van Genuchten (1993). This is a way of reconciling the results of the two codes, as Gerke and van Genuchten (1993) use central weighting of relative permeability for computing the exchange fluxes between the two continua, while **HydroGeoSphere** uses upstream weighting.

Figure 1.39 shows pressure head profiles versus depth at 0.01, 0.04 and 0.08 days for both the porous medium and dual continuum.

Figure 1.40 shows concentration profiles versus depth at 0.01, 0.04 and 0.08 days for both the porous medium and dual continuum.

1.5.6 Level 2: Transport Due to an Injection/Withdrawal Well

Note: the verification problem described in this section corresponds to the `one_well_pumping` and `one_well_injection` test cases found in the `verification` directory under the **HydroGeoSphere** installation directory.

This verification problem considers an injection/pumping cycle for a fully penetrating well in a confined aquifer (Figure 1.41). Water with a constant concentration Co is injected

Table 1.17: Parameters for the Gerke and van Genuchten (1993) study.

Parameter	Value	Unit
Porous medium		
Saturated hydraulic conductivity, $\mathbf{K}$	1.0526	cm day^{-1}
Porosity, θ_s	0.5	
Specific storage, S_s	1×10^{-7}	cm^{-1}
Volume fraction, w_m	0.95	
Van Genuchten α	0.005	cm^{-1}
Van Genuchten β	1.5	
Residual water saturation S_{wr}	0.10526	
Dispersivity α_l, α_t	2.0	cm
Dual continuum		
Saturated hydraulic conductivity, $\mathbf{K_d}$	2000	cm day^{-1}
Porosity, θ_{sd}	0.5	
Specific storage, S_{sd}	1×10^{-7}	cm^{-1}
Volume fraction, w_d	0.05	
Van Genuchten α	0.01	cm^{-1}
Van Genuchten β	2.0	
Residual water saturation S_{wrd}	0.0	
Dispersivity α_{ld}, α_{td}	2.0	cm
Interface		
Saturated hydraulic conductivity, K_a	0.01	cm day^{-1}
Geometrical shape factor β_d	3	
Van Genuchten α	0.005	cm^{-1}
Van Genuchten β	1.5	
Residual water saturation S_{wr}	0.10526	
Fluid exchange term α_{wd}	0.6	cm^{-1} day^{-1}
Mass exchange term α_s	0.15	day^{-1}
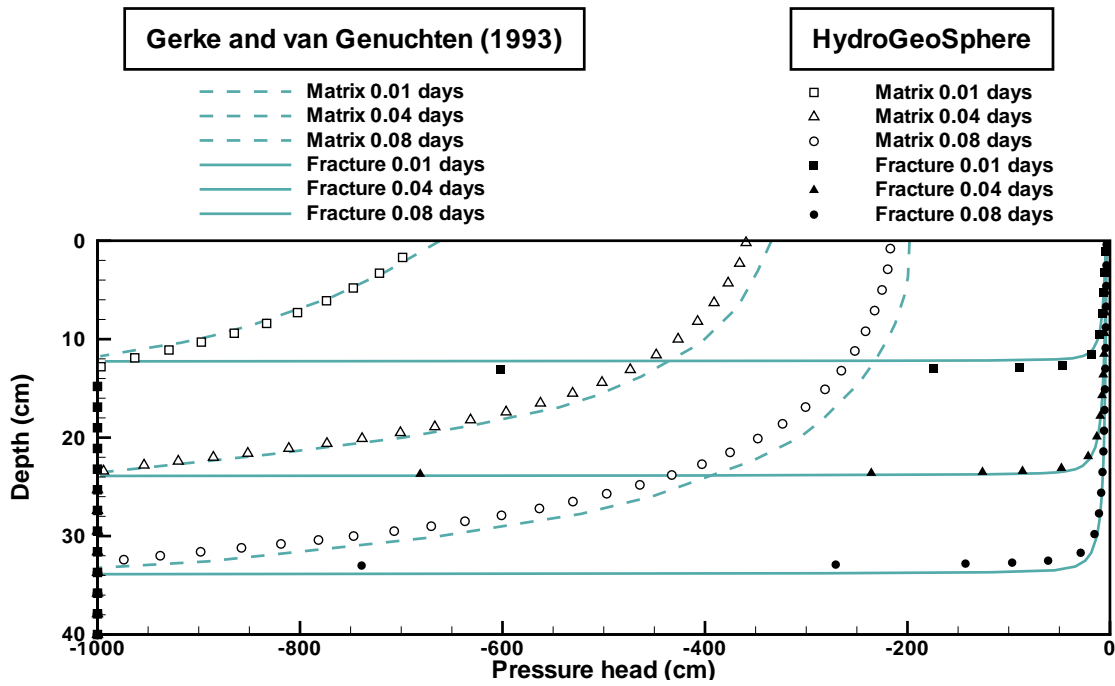
Figure 1.39: Pressure head profiles of the Gerke and van Genuchten (1993) study.
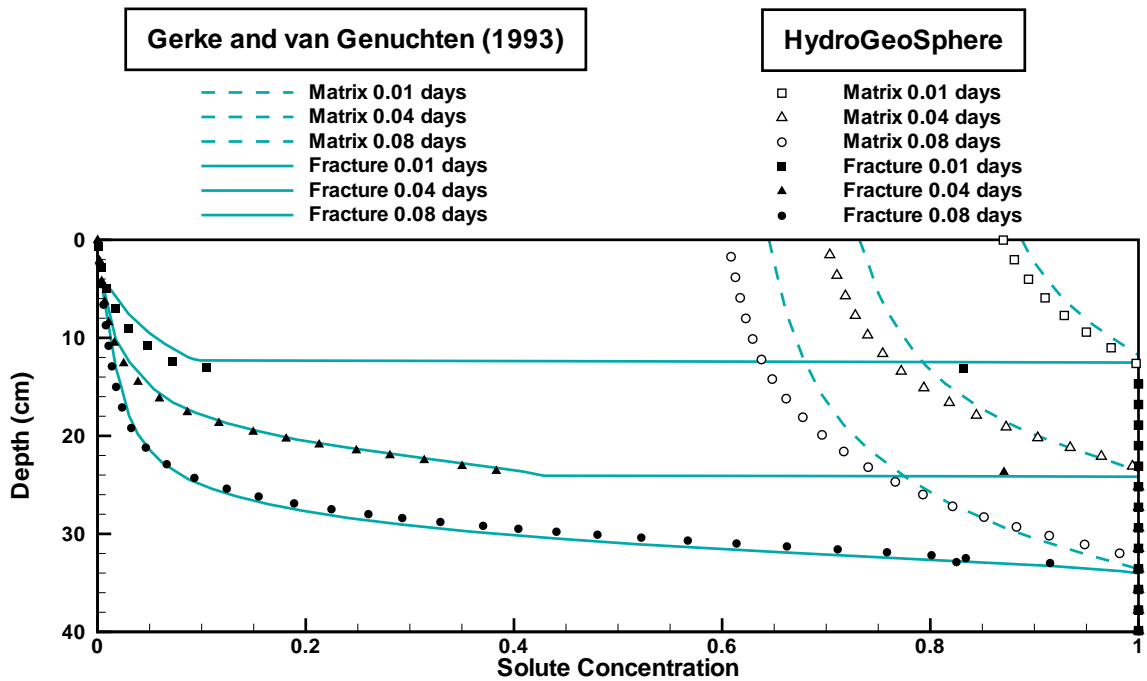
Figure 1.40: Concentration profiles of the Gerke and van Genuchten (1993) study.
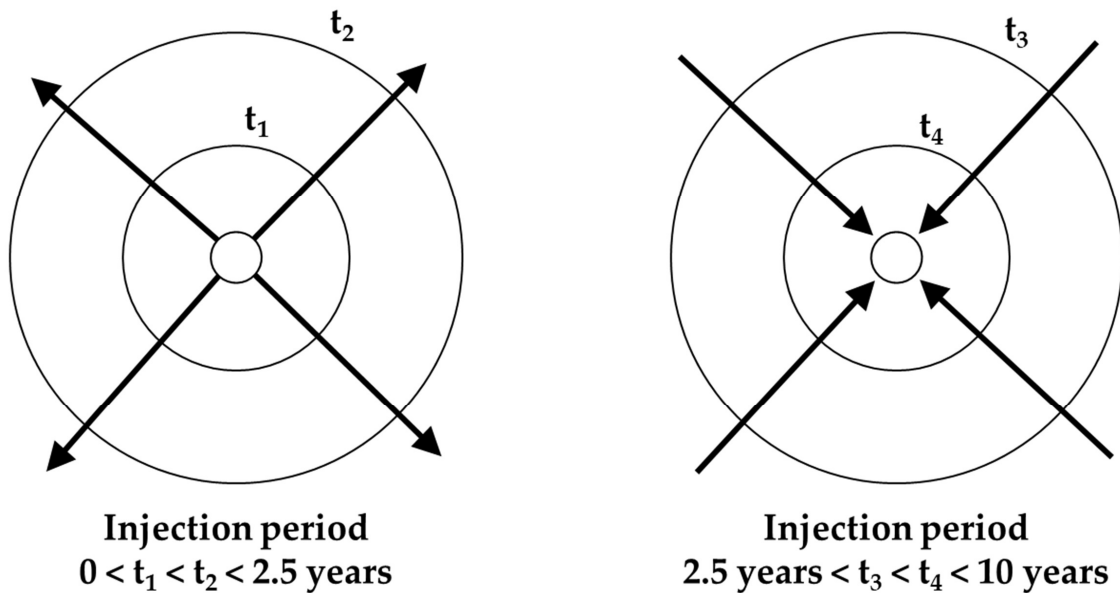
Figure 1.41: Injection/Withdrawal Well System.

into the well in the center of the domain for the first stress period. For the second stress period, the flow is reversed and the contaminated water is pumped out. The system reaches a steady state instantaneously for each stress period. An approximate analytical solution for this problem is given by Gelhar and Collins (1971).

The numerical model consist of 100 columns, 100 rows, and one layer. All parameters are presented in Table 1.18. A constant head of 50 feet was applied on the outer boundary of the domain to produce a steady state flow-field. The simulation was done in two periods: the first stress period is an injection for 2.5 years and the second stress period is a pumping for a period of 7.5 years. The simulation with **HydroGeoSphere** is compared with the analytical solution in Figure 1.42. The breakthrough curve obtained from **HydroGeoSphere** is comparable to the analytical solution.

1.5.7 Level 1: Two-Dimensional Transport from a Point Source in a Steady State Uniform Flow Field

Note: the verification problem described in this section corresponds to the `point_source_case1` and `point_source_case2` test cases found in the `verification` directory under the **HydroGeoSphere** installation directory.

This problem concerns two-dimensional dispersion of solute in a uniform and steady subsurface water flow field as depicted in Figure 1.43. It assumes a small injected rate to avoid disturbance of the natural subsurface water flow field. An analytical solution for such a situation can be found in Wilson and Miller (1978).

Table 1.18: Model Parameters for the Simulation of Transport From an Injection/extraction Well.

Parameter	Value	Unit
Cell width along rows Δx	328.1	ft
Cell width along columns Δy	328.1	ft
Thickness	20	ft
Hydraulic conductivity of the aquifer	0.005	ft s^{-1}
Porosity	0.3	
Longitudinal dispersivity α_L	100	ft
Transverse dispersivity α_T	100	ft
Volumetric injection (+)/extraction(-) rate for first/second stress periods	1	ft^3 s^{-1}
Concentration during the first stress period	1	
Length of the injection period	2.5	yr
Length of the extraction period	7.5	yr
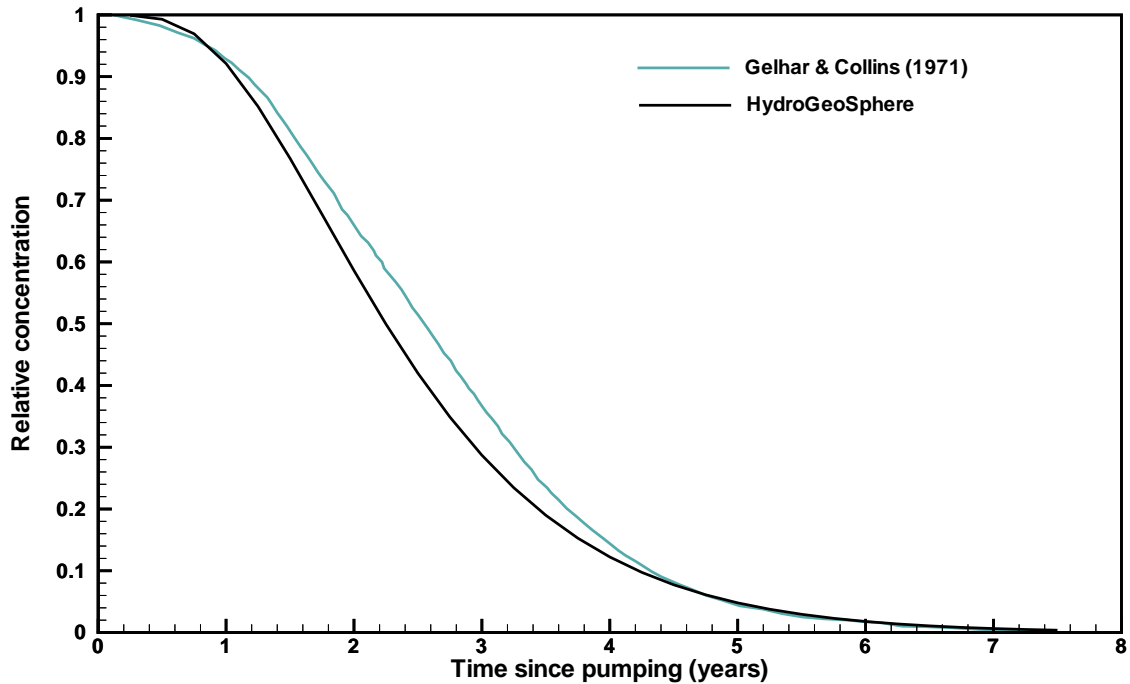
Figure 1.42: Breakthrough Curve from Simulation of Transport Due to an Injection/withdrawal Well.
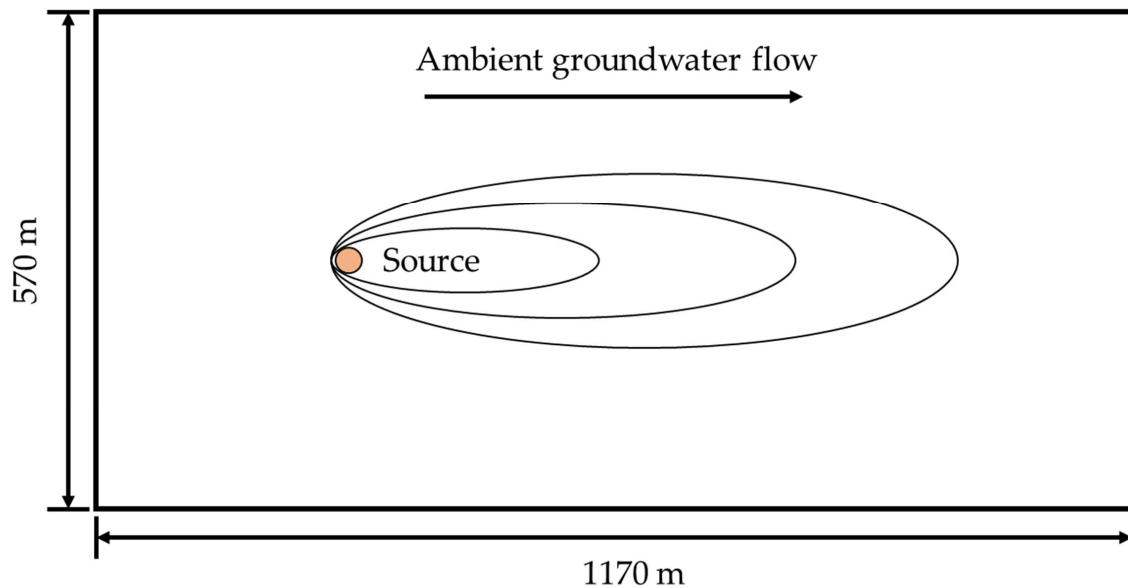
Figure 1.43: Two-Dimensional Transport from a Point Source.

Two cases involving conservative and non-conservative species were simulated using **Hydro-GeoSphere**. The model parameters, shown in Table 1.19, are taken from Huyakorn et al. (1984). The selected parameter values for Case 1 were based on data from the field study of hexavalent chromium contamination reported by Perlmutter and Lieber (1970). For Case 2, the values of retardation and decay constant were chosen arbitrarily to test the performance of **HydroGeoSphere** for a non-conservative species.

Both simulations were performed using a rectangular domain containing 741 30 m × 30 m elements and 14 equal time steps of 100 days each. Concentration profiles along the x-axis at time equal to 1400 days are plotted in Figure 1.44. Numerical results from **HydroGeoSphere** are compared with the analytical solution, the finite-difference model MODFLOW-SURFACT (HydroGeoLogic, Inc., 1996), and the finite-difference solution of FTWORK (Faust et al., 1990). In each case **HydroGeoSphere** produces solutions which are of comparable accuracy with respect to the other models.

1.5.8   Level 1: Transport Due to an Injection-Withdrawal Well Pair

Note: the verification problem described in this section corresponds to the `two_well` test case found in the `verification` directory under the **HydroGeoSphere** installation directory.

This problem concerns solute transport between a pair of discharging and recharging wells operating at a constant flow rate. Both wells fully penetrate a constant-thickness confined aquifer that is assumed to be homogeneous, isotropic and of infinite areal extent. The flow field is assumed to be in steady-state with typical flow lines and solute fronts depicted in Figure 1.45.

Table 1.19: Parameters for Simulation of 2-D Transport from a Point Source

Parameter	Value	Unit
Darcy velocity q	0.161	m day^{-1}
Porosity θ	0.35	
Longitudinal dispersivity α_L	21.3	m
Transverse dispersivity α_T	4.3	m
Thickness of the saturated aquifer b	33.5	m
Contaminant Mass flux per unit thickness of aquifer Qc_o	704	g m^{-1} day^{-1}
CASE 1:		
Linear adsorption coefficient, K_d	0	m^3 kg^{-1}
Retardation coefficient, $R = \rho_b K_d / \varphi$	1	
Decay constant, λ	0	day^{-1}
CASE 2:		
Linear adsorption coefficient, K_d	0.14	m^3 kg^{-1}
Retardation coefficient $R = \rho_b K_d / \varphi$	2	
Decay constant λ	0.00019	day^{-1}
Bulk density ρ_b	2.5	kg m^{-3}
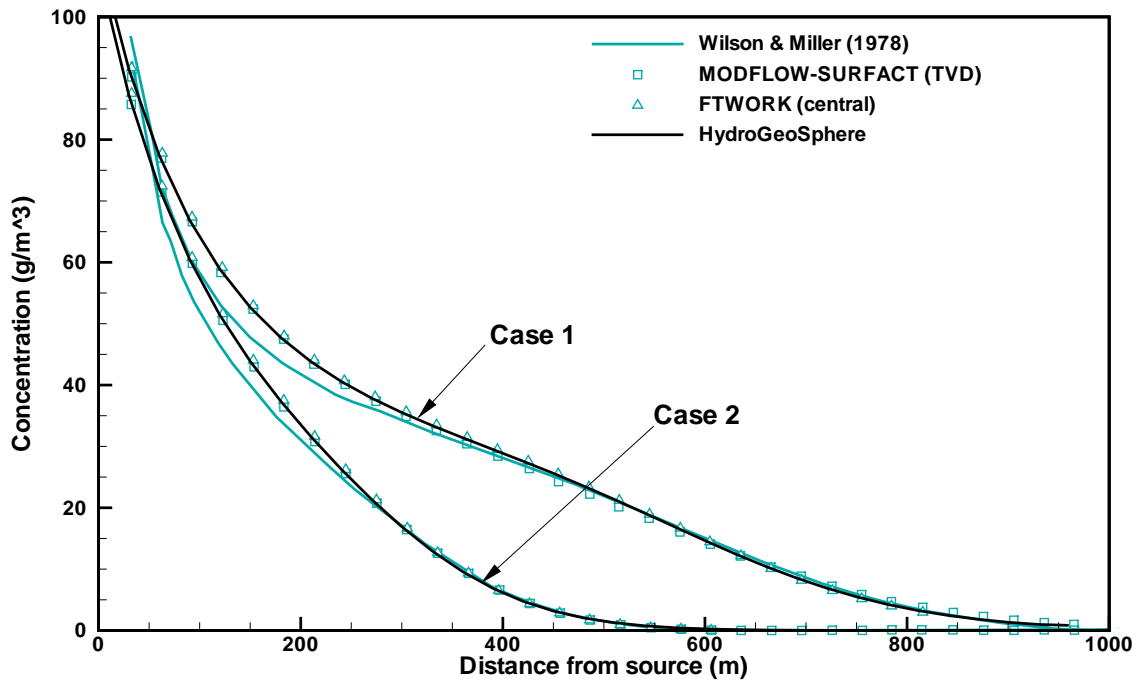
Figure 1.44: Concentration Profiles Along the Center Line for $t = 1400$ days.
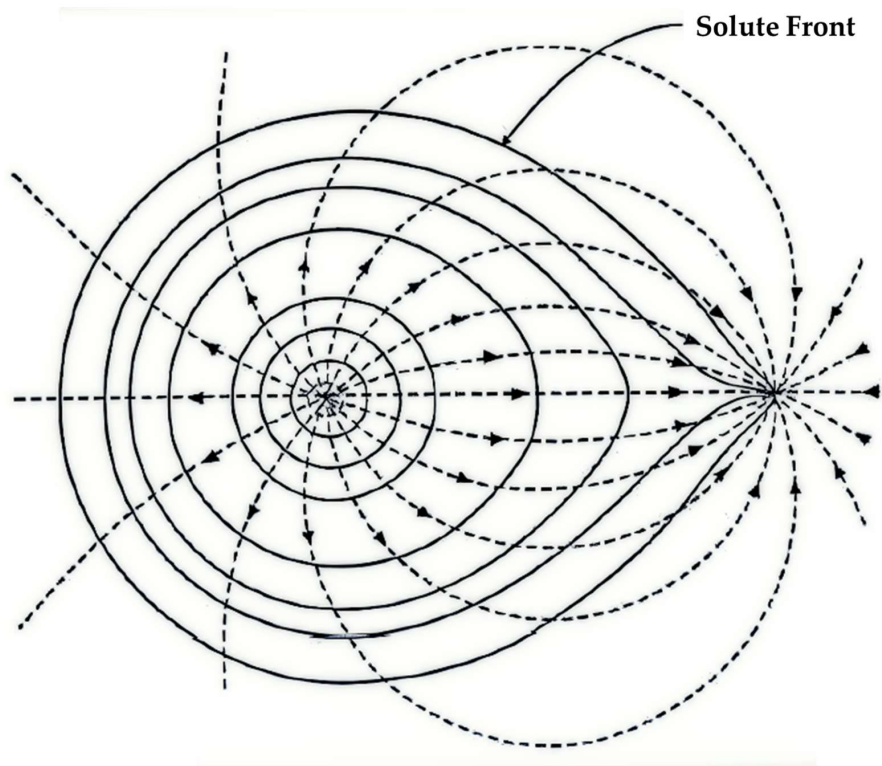
Figure 1.45: Injection/Withdrawal Well Pair.

Table 1.20: Parameters for Simulations of Transport Due to an Injection-withdrawal Pair.

Parameter	Value	Unit
Well flow rate, Q_{inj}=Q_{pump}	2.339	$cm^3\ s^{-1}$
Well spacing	61.0	cm
Thickness of aquifer, b	8.9	cm
Porosity,	0.374	
Retardation coefficient, R	1	
Decay constant, λ	0	
Longitudinal dispersivity α_L	0.294	cm
Transverse dispersivity α_T	0	
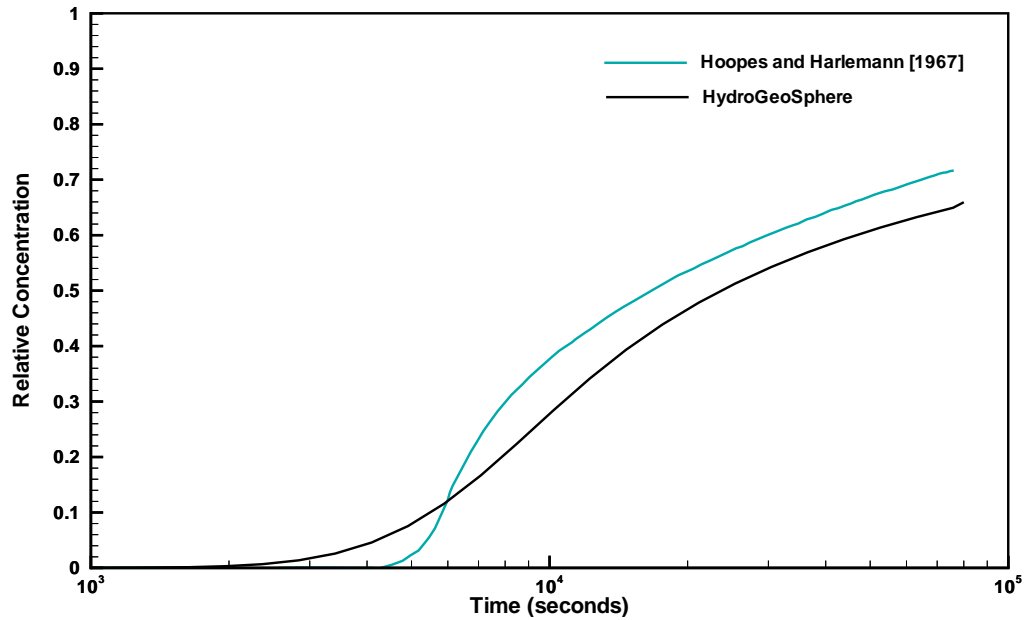
Figure 1.46: Breakthrough Curve of Concentration Solute at the Pumping Well.

The analytical solution which represents this case was developed by Hoopes and Harleman (1967). The numerical model consist of 31 columns, 33 rows and one layer. Model parameters are presented in Table 1.20. The hydraulic conductivity used is 0.005 cm s^{-1}.

The simulation was done with fifty time steps for a total simulation of 8×10^4 s. The initial time step size is 2 s and increases by a factor of 1.2 thorough the simulation. The initial concentration in the domain is equal to zero and a unit concentration is prescribed at the injection well. Figure 1.46 presents the results obtained from **HydroGeoSphere** which compares well with the analytical solution. Breakthrough is however diffused in the numerical solution resulting from the coarse discretization used in a complex flow field.
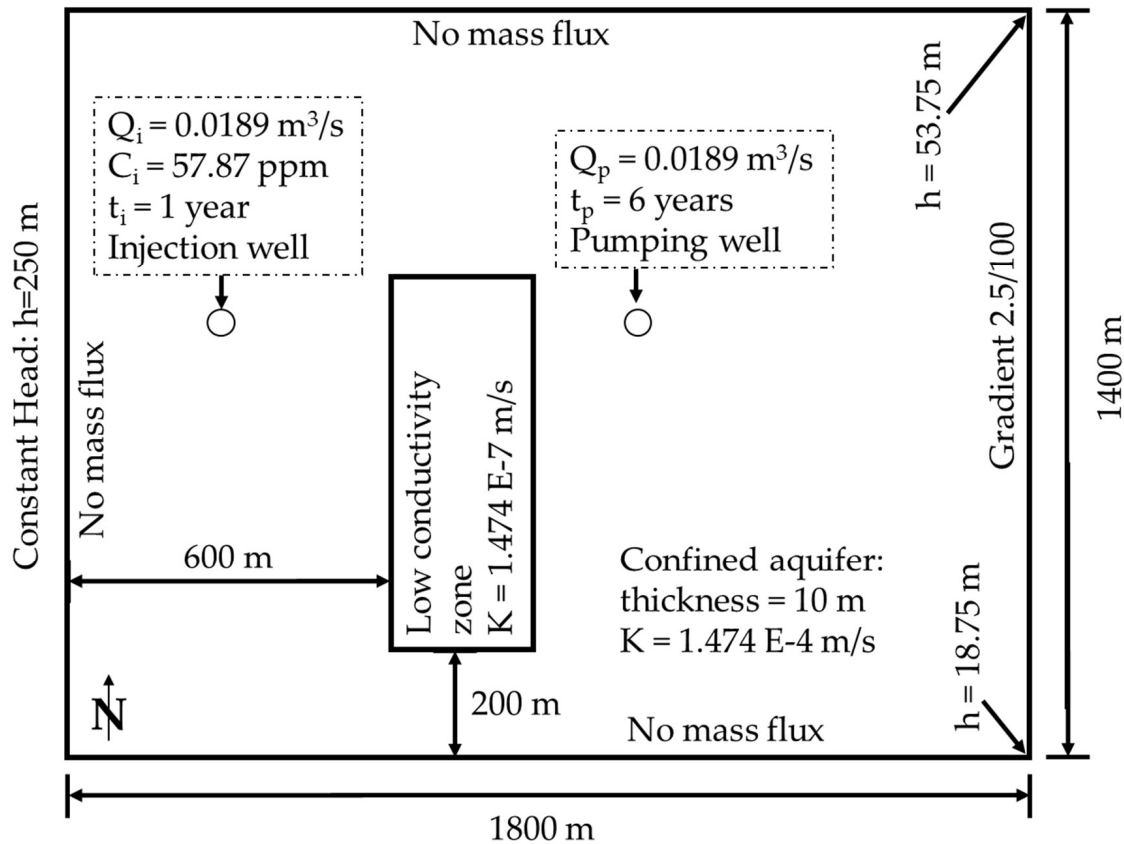
Figure 1.47: Problem Description for 2-D Transport in a Heterogeneous Confined Aquifer.

1.5.9 Level 2: Two-Dimensional (Areal) Transport of a Contaminant Plume in a Heterogeneous Confined Aquifer with a Pair of Injection And Withdrawal Wells And Strong Ambient Subsurface Flow

Note: the verification problem described in this section corresponds to the `two_well_het_ss` test case found in the `verification` directory under the **HydroGeoSphere** installation directory.

This problem taken from Zheng (1990) is shown in Figure 1.47. It concerns contaminant transport in a heterogeneous aquifer under a strong ambient steady-state subsurface water flow field. North and South boundaries represent zero flux conditions while East and West boundaries represent constant-head conditions whereby the East boundary has also an imposed gradient. Contaminant is injected into the aquifer for a period of one year and is subsequently allowed to distribute for another five years. The total mass injected is 1825 kg ($M_i = Q_i C_i t_i$). One well located downstream pumps 0.0189 m$^3/s$ throughout the simulation period. A low conductivity zone is located between the two wells (200 m × 600 m). For both zones, longitudinal and transverse dispersivities are respectively equal to 20 et 4 m. The effective porosity is equal to 0.3.
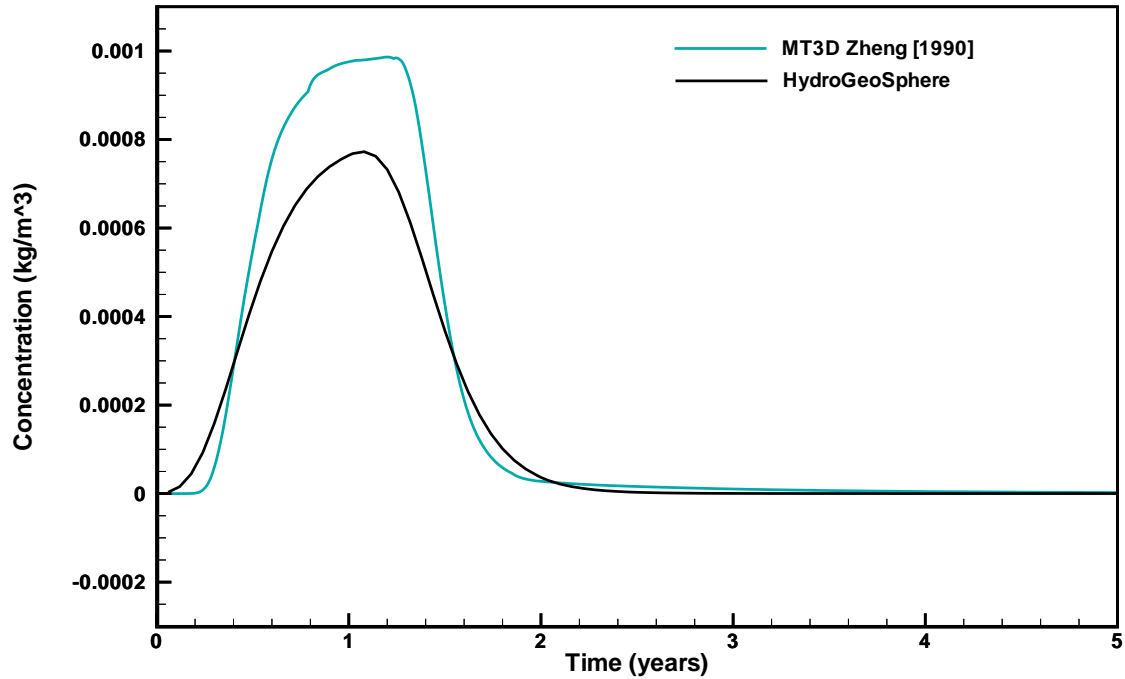
Figure 1.48: Concentrations Observed at the Pumping Well.

The grid used for **HydroGeoSphere** simulations contains 18 columns, 14 rows and one layer of cells of uniform dimensions of 100 m × 100 m. The simulation was done with 100 equal time steps for a total time of 6 years. Results show a good correlation between the **HydroGeoSphere** simulation and MT3D results (see Figure 1.48) with negligible mass balance error as shown in Figure 1.49.

1.5.10   Level 2: Two-Dimensional Transport of a Contaminant Plume in a Heterogeneous Confined Aquifer

Note: the verification problem described in this section corresponds to the `two_well_het_trans` test case found in the `verification` directory under the **HydroGeoSphere** installation directory.

This problem has the same setting as the one presented in Section 1.5.9 except that the simulation is done within a transient flow field. The total thickness of the aquifer is 25 m. The set-up is shown in Figure 1.50. The total mass injected is 473.05 kg. The specific storage is estimated to be 0.01. For both zones, the porosity, the longitudinal and transverse dispersivities are equal to 0.25, 20 m, and 4 m, respectively.

The simulation was done in transient flow for a period of 7 years. The grid used is the same as the one in the example shown in Section 1.5.9. The pumping rate is 0.24 m^3 s^{-1} for a one year period separated by one year without pumping. Pumping begins after one year and the total duration of simulation is seven years which includes three pumping stages. The
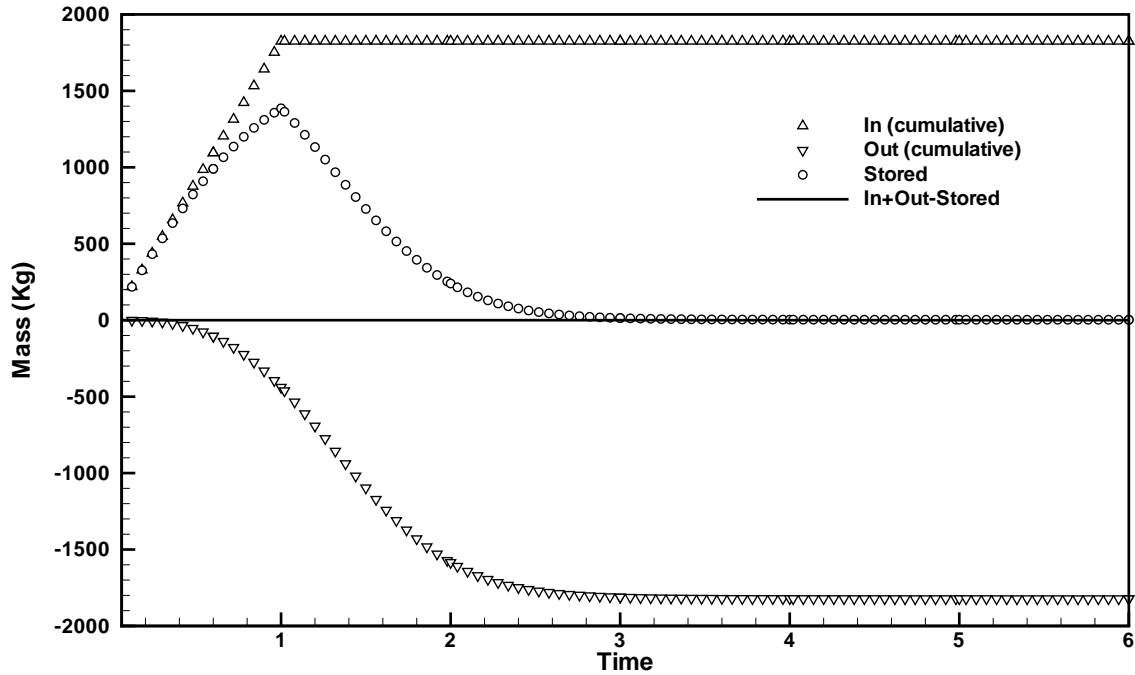
Figure 1.49: Mass Budget for the 2-D Transport Simulation.

initial time step size is 1.2 days which is incremented by a factor of 1.5 up to a maximum time step size of 12 days. Hydraulic heads observed at the pumping well are presented in Figure 1.51. The comparison is made with MODFLOW.

Solute concentrations at the pumping well were evaluated during the simulation and are presented in Figure 1.52. **HydroGeoSphere** results compare fairly well with the breakthrough obtained from MT3D. The solute mass balance evaluated in Figure 1.53 shows negligible mass balance errors throughout the simulation. The total mass OUT is about 474 g, a little more than the total mass IN which is 473.05g.

1.5.11   Level 2: Two-Dimensional Transport of Contaminant in the Water Phase of an Unsaturated Rectangular Soil Slab

Note: the verification problem described in this section corresponds to the `unsat_slab` test case found in the `verification` directory under the **HydroGeoSphere** installation directory.

This problem concerns transport of a non-conservative solute in a transient 2-D unsaturated flow field. The system is initially dry and free of solutes and water with dissolved solute is allowed to enter the system at the upper portion of the left hand boundary as shown in Figure 1.54. Inflow head is 6 cm with a prescribed solute concentration of 1 ppm. Outflow occurs along the entire right hand side boundary under initial pressure conditions of -90 cm. The remaining boundaries are under no-flow, zero concentration gradient conditions.
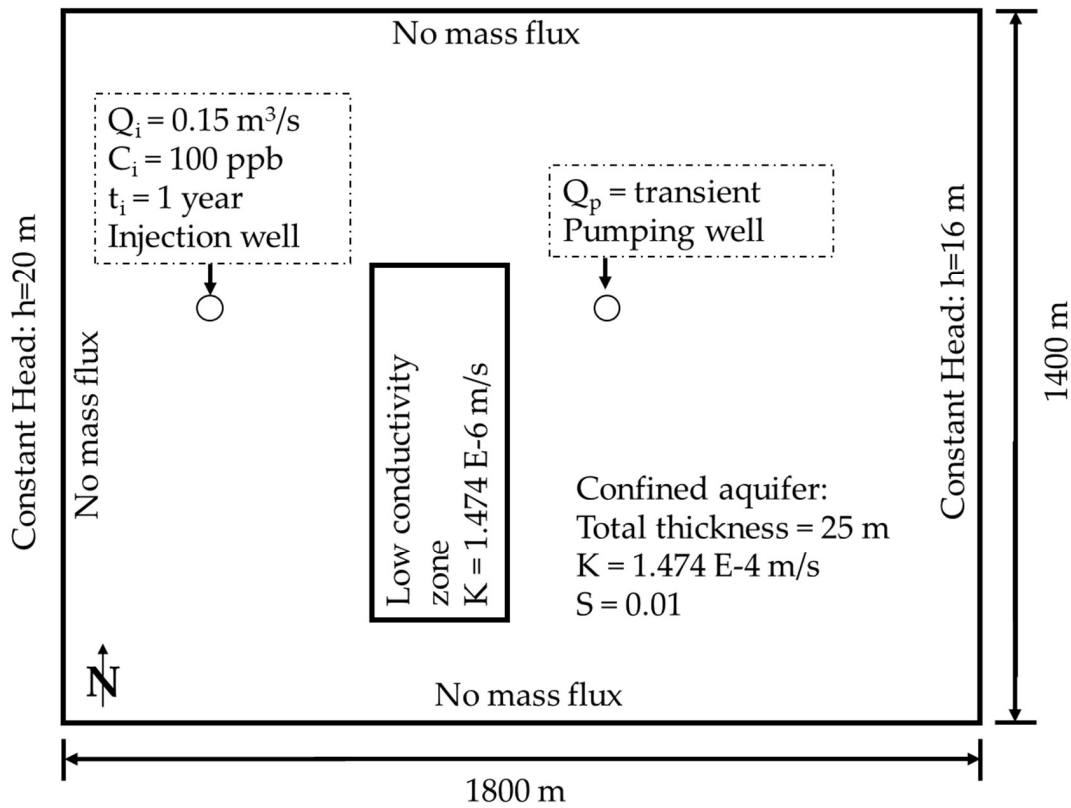
Figure 1.50: Problem Description for 2-D Transport.
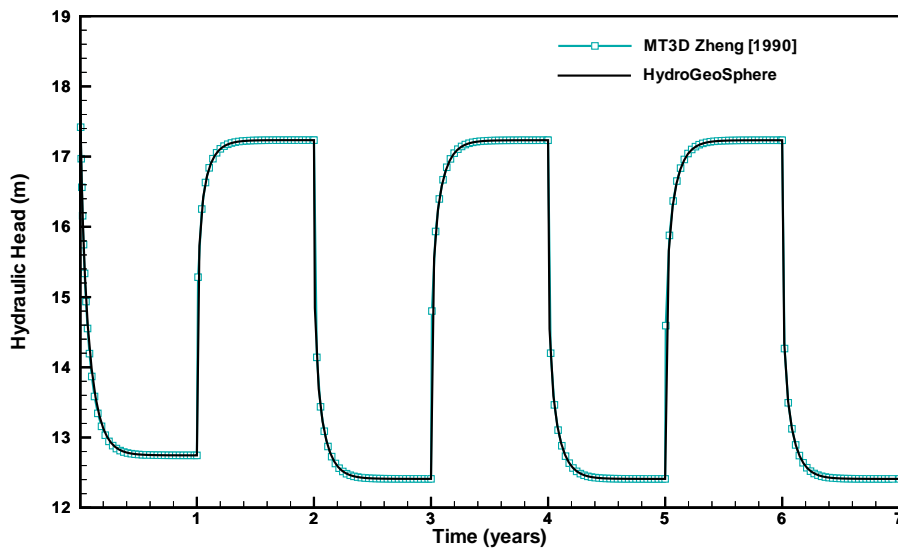
Figure 1.51: Hydraulic Head Distribution at the Pumping Well During the Simulation.
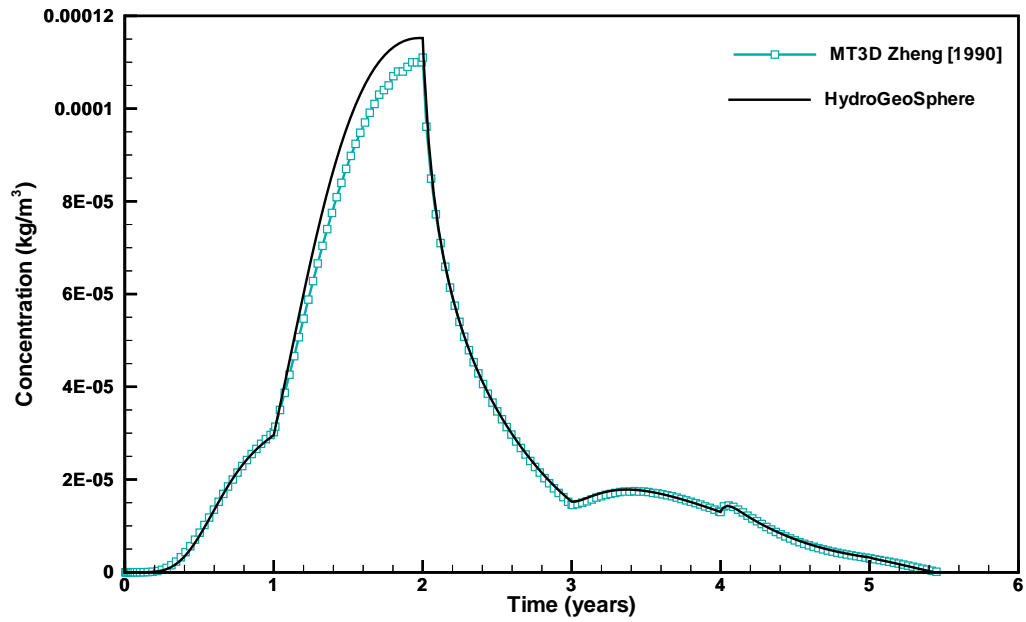
Figure 1.52: Breakthrough Curve Observed at the Pumping Well for 2-D Transport Simulation.
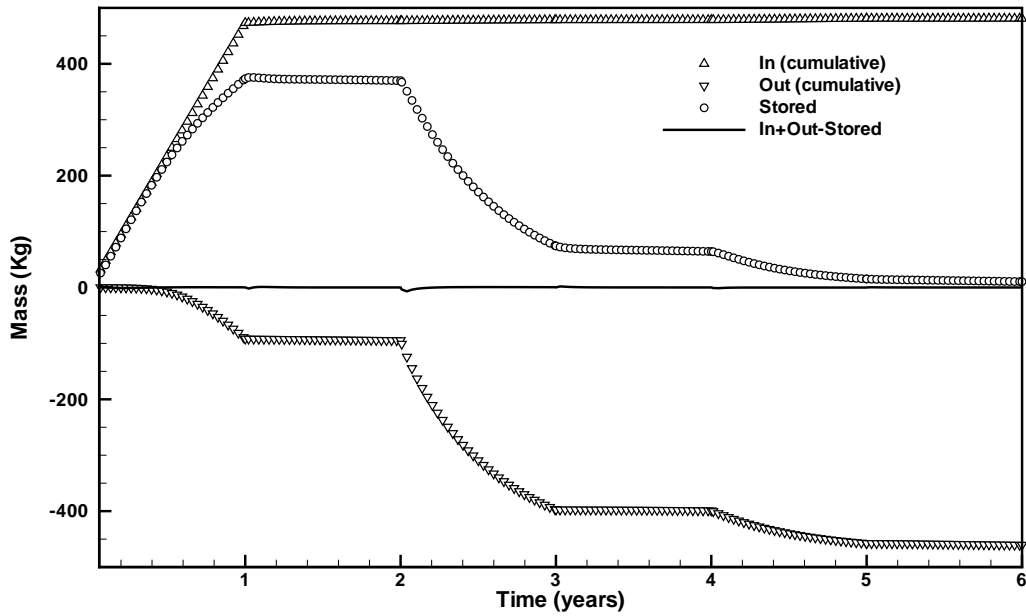
Figure 1.53: Solute Mass Balance for 2-D Transport Simulation in Transient Flow Field.
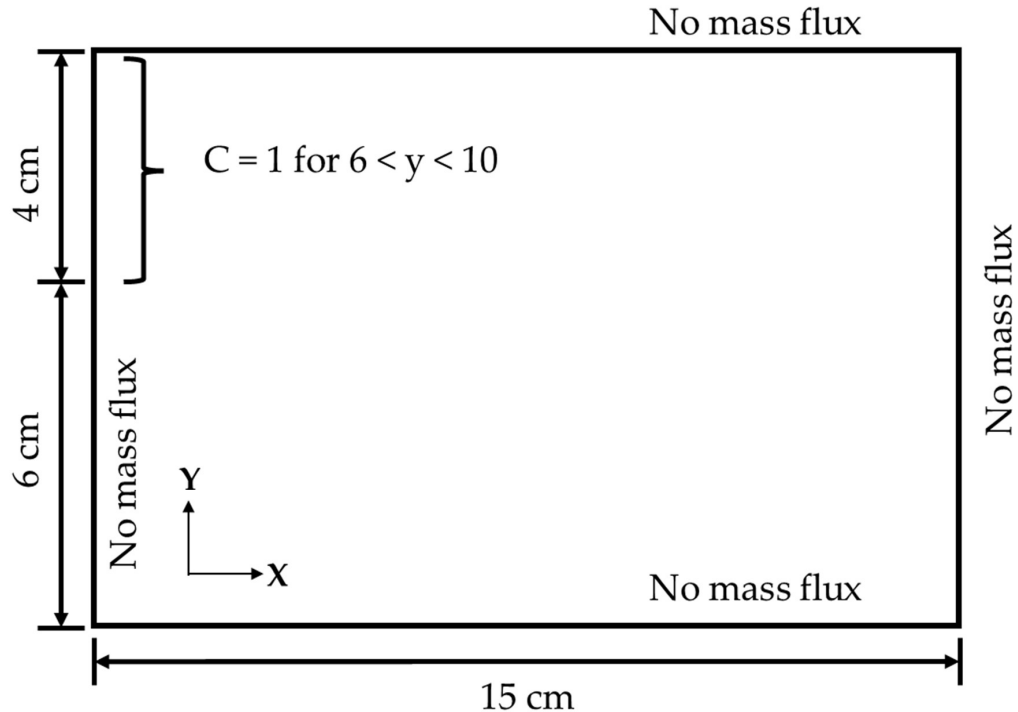
Figure 1.54: Problem Description for 2-D Transport in an Unsaturated Rectangular Soil Slab.

The domain dimension is 15 cm horizontally and 10 cm vertically, discretized using a grid with constant cell spacing of 1 cm. The soil is assumed to be homogeneous and isotropic. Table 1.21 presents the hydraulic properties of the soil. The simulation was done with an initial time step size of 0.01 days which is enlarged with a factor of 1.2 up to a maximum time step size of 0.05 days. The physical transport parameters are shown in Table 1.22. The total duration of the simulation is 0.508 days. The values of concentration in the rectangular soil slab are computed for time equal to 0.508 days and are presented in Figure 1.55.

1.6 Variable-Density Flow

1.6.1 Level 2: Variable-Density Flow in Porous Media, Elder's Problem

Note: the verification problem described in this section corresponds to the `elder` test case found in the `verification` directory under the **HydroGeoSphere** installation directory.

Variable-density flow and transport in porous media was verified in two dimensions using the Elder (1967) salt convection problem. The results presented by Frolkovič and De Schepper (2001) were chosen to be compared to those of **HydroGeoSphere**, and are considered more trustworthy since both numerical models use the control volume finite element method as

Table 1.21: Hydraulic Properties of the Rectangular Soil Slab.

Parameter	Value	Unit
Saturated hydraulic conductivity, K	1	cm day^{-1}
Specific storage, S_s	1×10^{-14}	
Van Genuchten α	0.005	cm^{-1}
Van Genuchten β	2	
Brooks Corey parameter, n	2	
Residual water saturation S_{wr}	0.3333	

Table 1.22: Physical Parameters Values for Simulation of Transport in an Unsaturated Rectangular Soil Slab.

Parameter	Value	Unit
Porosity	0.45	
Initial concentration C_o	0	
Longitudinal dispersivity α_L	1	cm
Transverse dispersivity α_T	0	
Molecular diffusion D_o	0.01	cm^2 day^{-1}
Decay constant	0.001	day^{-1}
Bulk density	1.46	g cm^{-3}
Distribution coefficient K_d	0.308	cm^3 g^{-1}
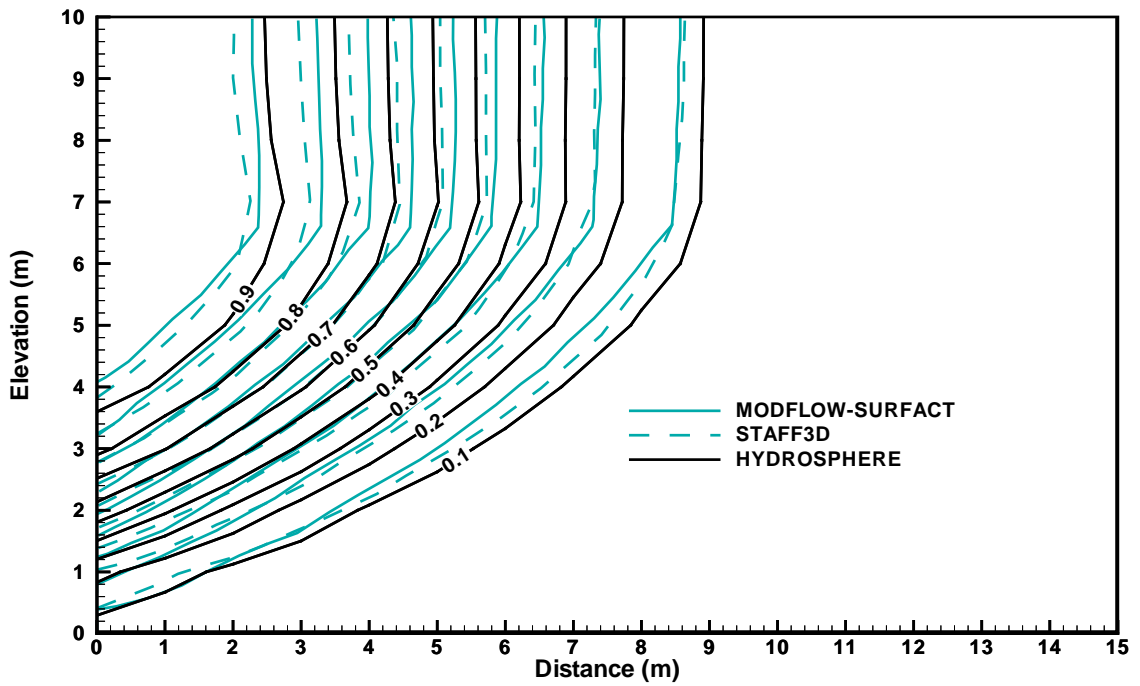
Figure 1.55: Simulated Contaminant Concentrations in an Unsaturated Rectangular Soil Slab at 0.508 days.

Table 1.23: Parameters used for the Saltpool_1 Simulation

Parameter	Value	Unit
Free-solution diffusion coefficient (D_d)	3.56×10^{-6}	$m^2 \ s^{-1}$
Brine density (ρ_{max})	1200	$kg \ m^{-3}$
Reference density (ρ_0)	1000	$kg \ m^{-3}$
Fluid dynamic viscosity (μ)	1.124×10^{-3}	$kg \ m^{-1} \ s^{-1}$
Hydraulic conductivity (K)	150	$m \ yr^{-}1$
Porosity (n)	0.1	
Longitudinal dispersivity (α_L)	0.0	m
Transverse dispersivity (α_T)	0.0	m

well as the same flow variable (fluid pressure, P).

Frolkovič and De Schepper (2001) carried out their numerical simulations in the half domain of the symmetric Elder problem, using an extremely fine grid consisting of 32,768 nodes. All simulations used implicit transport time weighting, as is common in other variable-density simulations, and full upstream weighting as proposed by Frolkovič and De Schepper (2001).

The physical parameters given by Oswald and Kinzelbach (2004) were used and are shown in Table 1.23.

Their results are in very good visual agreement with those from the **HydroGeoSphere** model (Figure 1.56).

1.6.2 Level 3: Variable-Density Flow in Porous Media, Saltpool Experiment

Note: the verification problem described in this section corresponds to the `saltpool1` test case found in the `verification` directory under the **HydroGeoSphere** installation directory.

A new benchmark problem for variable-density transport in 3D has been presented by Oswald and Kinzelbach (2004). This problem is based on the three-dimensional variable-density flow and solute transport experiments in porous media conducted by Oswald (1999). In these experiments, a 0.2 m × 0.2 m × 0.2 m closed box initially contained saltwater from the bottom up to 6 cm, with the rest of the box filled with freshwater. A constant freshwater recharge through one upper corner of the box disturbed this stable layering of two miscible fluids. The concentration of the mixed fluid versus time was measured at the discharging open hole on the opposite side of the input location. Oswald (1999) used two different initial concentrations $c_{01} = 0.01$ (case 1) and $c_{02} = 0.1$ (case 2). The experimental results were numerically reproduced by Johannsen et al. (2002), who also present tabular data of the measured concentrations versus time.

The **HydroGeoSphere** model output was compared in three dimensions with experimental results of Oswald (1999), given in Johannsen et al. (2002). The physical parameters given
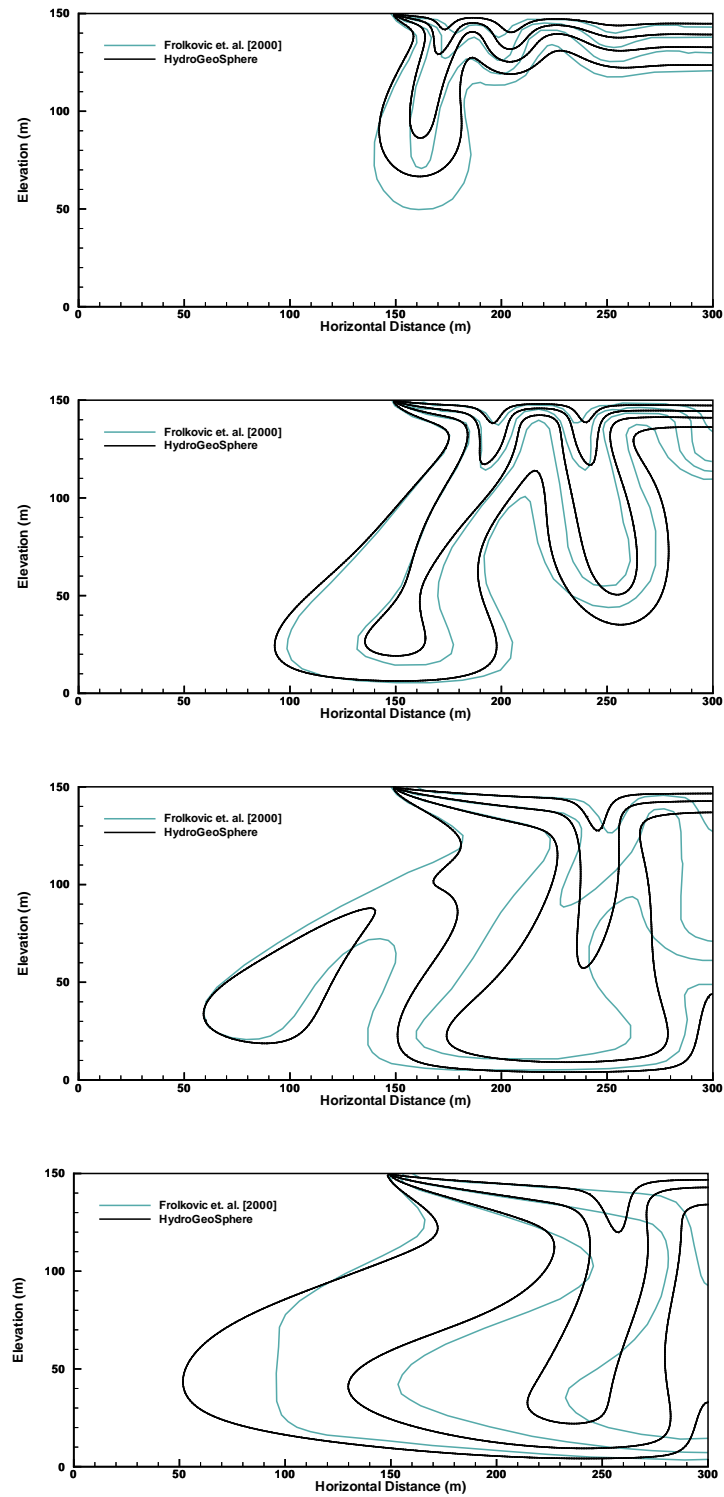
Figure 1.56: Results of the Elder problem for an extremely fine grid (256 × 128 elements in the half domain) at 2.5, 5, 10 and 20 years simulation time. Shown are the 20%, 40%, 60% and 80% contours.

Table 1.24: Parameters used for the Saltpool_1 Simulation

Parameter	Value	Unit
Free-solution diffusion coefficient (D_d)	8.7×10^{-10}	m^2 s^{-1}
Brine density (ρ_{max})	1005.9	kg m^{-3}
Reference density (ρ_0)	998.23	kg m^{-3}
Fluid dynamic viscosity (μ)	1.002×10^{-3}	kg m^{-1} s^{-1}
Hydraulic conductivity (K)	9.325×10^{-3}	m s^{-1}
Porosity (n)	0.372	
Longitudinal dispersivity (α_L)	0.0012	m
Transverse dispersivity (α_T)	0.00012	m

by Oswald and Kinzelbach (2004) were used and are shown in Table 1.24.

The first problem of the lower initial concentration 0.01 (case 1) was used because Johannsen et al. (2002) showed that, in this case, grid convergence is achieved with a relatively coarse grid, whereas for case 2, the solution converged only for a very fine grid, consisting of at least 274,625 grid points (Johannsen et al., 2002). Good agreement between the experimental results from Oswald (1999), the numerical results from Diersch and Kolditz (2002) and the **HydroGeoSphere** model was obtained (Figure 1.57). The long-term results of this low density case more closely resemble the experimental data than in Diersch and Kolditz (2002); however, differences remain.

1.6.3 Level 2: Variable-Density Flow in Fractured Porous Media

Note: the verification problem described in this section corresponds to the `shikaze` test case found in the `verification` directory under the **HydroGeoSphere** installation directory.

Variable-density flow in vertical fractures was verified by reproducing the results presented by Shikaze et al. (1998). The trial which includes only vertical fractures was used as a test case. The external hydraulic heads on both aquifer top and bottom were set to zero because Shikaze et al. (1998) showed that density effects are best accounted for if the imposed head gradient vanishes. Otherwise, the effect of forced convection may suppress free convection. In the numerical simulations, the left and right boundaries were assumed to be impermeable for flow. The top of the domain is assumed to be a salt lake with a constant concentration equal to 1.0. All other boundaries for transport are zero dispersive-flux boundaries. The physical parameters used are identical to those presented by Shikaze et al. (1998) and summarized in Table 1.25. The 3D domain is of size $\ell_x = 10$ m, $\ell_y = 1$ m and $\ell_z = 10$ m. The spatial discretization used was 0.025 m in both the x- and the z-direction and unity in the y-direction. Fracture spacings are nonuniform as shown in Figure 1.58. The Figure shows excellent agreement between the concentration distributions calculated by the two numerical models.
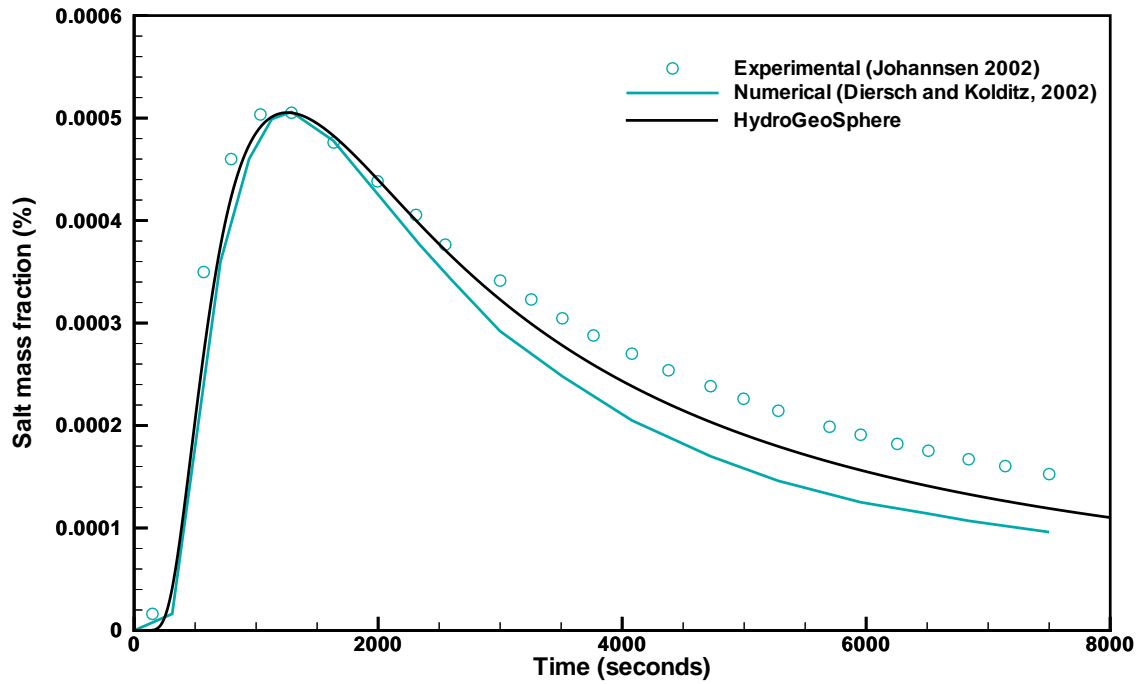
Figure 1.57: Results of three-dimensional variable-density transport simulations in porous media.

Table 1.25: Model parameters used in fractured media studies. All parameters are identical to those used by Shikaze et al. (1998).

Parameter	Value	Unit
Free-solution diffusion coefficient (D_d)	5×10^{-9}	$m^2 \ s^{-1}$
Brine density (ρ_{max})	1200	$kg \ m^{-3}$
Reference density (ρ_0)	1000	$kg \ m^{-3}$
Fluid compressibility (α_{fl})	4.4×10^{-10}	$kg^{-1} \ m \ s^2$
Matrix compressibility (α_m)	1.0×10^{-8}	$kg^{-1} \ m \ s^2$
Fluid dynamic viscosity (μ)	1.1×10^{-3}	$kg \ m^{-1} \ s^{-1}$
Matrix permeability (κ_{ij})	10^{-15}	m^2
Matrix longitudinal dispersivity (α_l)	0.1	m
Matrix transverse dispersivity (α_t)	0.005	m
Matrix porosity (ϕ)	0.35	
Tortuosity (τ)	0.1	
Fracture dispersivity (α^{fr})	0.1	m
Fracture aperture $(2b)$	50	μm
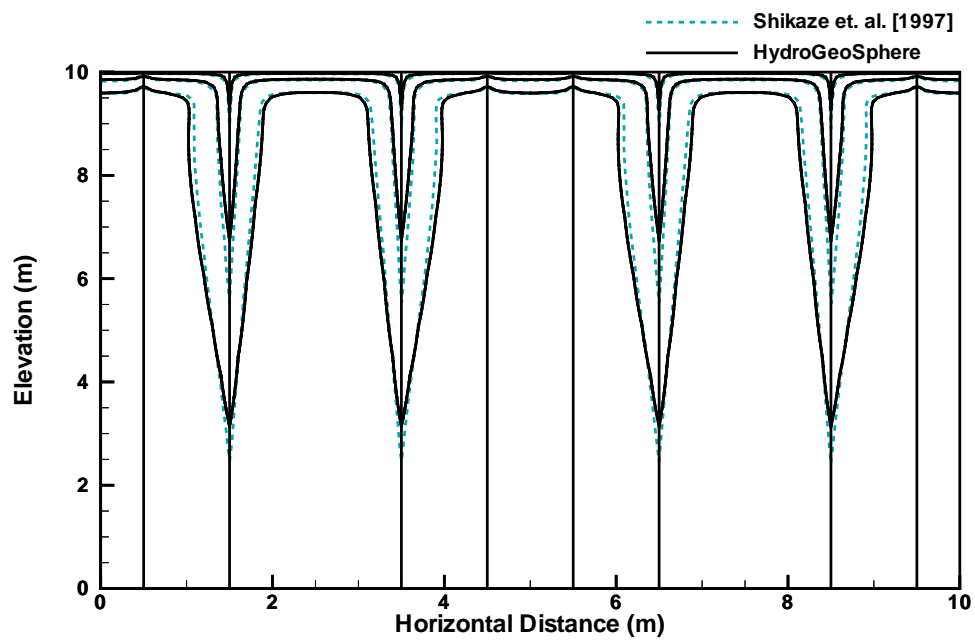
Figure 1.58: Variable-density flow in a set vertical fractures embedded in a porous matrix. Shown are the concentration contours 0.1 to 0.9 with a contour interval of 0.4 at 2 years simulation time.

1.7 Heat Transfer

1.7.1 Level 1, 2: Heat Transfer in Porous Media

Note: the verification problem described in this section corresponds to the `ward` test case found in the `verification` directory under the **HydroGeoSphere** installation directory.

The first test case verifies 1D heat transfer in an unfractured porous matrix. A constant velocity along the flow axis is imposed. The impact of temperature on fluid properties is ignored, which linearizes the problem. Thermal energy is transported by way of conduction, advection and mechanical dispersion. In this case, the governing equation can be written in the form:

$$D_{th}\frac{\partial^2 T}{\partial x^2} - v_{th}\frac{\partial T}{\partial x} = \frac{\partial T}{\partial t} \tag{1.7}$$

where D_{th} [L^2 T^{-1}] is the thermal dispersion coefficient:

$$D_{th} = \frac{k_b + \phi D_{xx}\rho_l\tilde{c}_l}{\rho_b\tilde{c}_b} \tag{1.8}$$

and v_{th} [L T^{-1}] is the retarded velocity:

$$v_{th} = q \cdot \frac{\rho_l\tilde{c}_l}{\rho_b\tilde{c}_b} = q \cdot \frac{1}{\phi R_{th}} \tag{1.9}$$

with the thermal retardation coefficient R_{th} [-] (Molson et al., 1992):

$$R_{th} = 1 + \frac{(1 - \phi)\rho_s\tilde{c}_s}{\phi\rho_l\tilde{c}_l} \tag{1.10}$$

Equation (1.7) has the standard parabolic-hyperbolic form of a 1D partial differential equation. Therefore, if (1.7) is subject to the Dirichlet boundary condition, $T = T_1$, the solution is the Ogata-Banks analytical solution (Ogata and Banks, 1961):

$$\frac{T - T_0}{T_1 - T_0} = \frac{1}{2}\left[\text{erfc}\left(\frac{x - v_{th}t}{2\sqrt{D_{th}t}}\right) + \exp\left(\frac{v_{th}x}{D_{th}}\right)\text{erfc}\left(\frac{x + v_{th}t}{2\sqrt{D_{th}t}}\right)\right] \tag{1.11}$$

where T_0 is the initial temperature in the domain.

In the numerical simulation, the finite element domain was spatially discretized by using 20 uniform blocks in the flow direction. All simulation parameters are given by Table 1.26. The developed numerical model is compared with the analytical solution (1.11) as well as with numerical results presented by Ward et al. (1984) who used the code SWIFT. The results are depicted in Figure 1.59.

1.7.2 Level 1: Heat Transfer in Fractured Media

Note: the verification problem described in this section corresponds to the `tempf` test case found in the `verification` directory under the **HydroGeoSphere** installation directory.
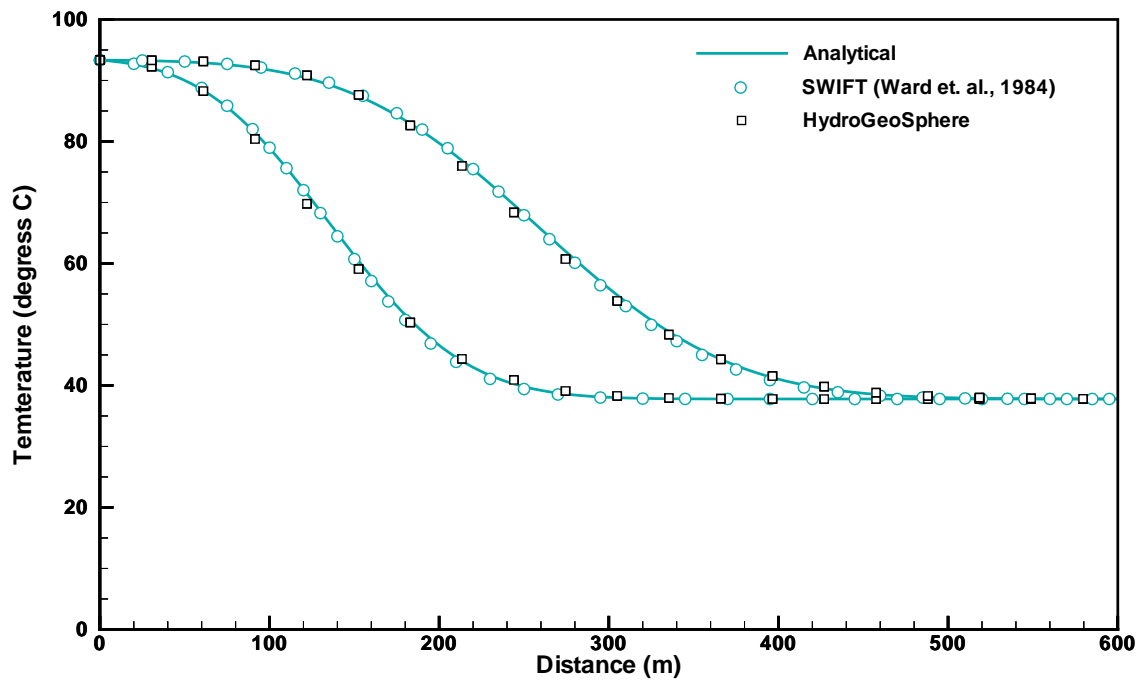
Figure 1.59: Temperature profiles of 1D heat transfer in an unfractured porous matrix (example 1). Shown are the temperatures in the matrix at 2,148 (left) and 4,262 (right) days.

Table 1.26: Model parameters used in the verification example for 1D heat transfer in an unfractured porous matrix. All parameters are identical to those used by Ward et al. (1984).

Parameter	Value	Unit
Bulk thermal conductivity (k_b)	2.16	kg m s^{-3} K^{-1}
Heat capacity of solid ($\tilde{c}_s$)	1254.682	m^2 s^{-2} K^{-1}
Solid density (ρ_s)	1602	kg m^{-3}
Heat capacity of water ($\tilde{c}_l$)	4185	m^2 s^{-2} K^{-1}
Fluid density (ρ_l)	1000	kg m^{-3}
Matrix porosity (ϕ)	0.1	
Longitudinal dispersivity (α_l)	14.4	m
Heat dispersion coefficient[a] (D_{th})	1.15×10^{-5}	m^2 s^{-1}
Thermal retardation coefficient[b] (R_{th})	5.323	
Darcy flux (q)	3.53×10^{-7}	m s^{-1}
Retarded velocity[c] (v_{th})	6.63×10^{-7}	m s^{-1}
Initial temperature (T_0)	37.78	°C
Boundary temperature (T_1)	93.33	°C
Domain size (ℓ_x)	600	m
Output times (t_1, t_2)	2148, 4262	days

[a] from relation (1.8)
[b] from relation (1.10)
[c] $q/(\phi R^{th})$

The second test case verifies advective-conductive-dispersive 1D heat transfer in a single fracture embedded in an impermeable matrix. As in the previous case, a constant flow velocity along the axis is imposed and fluid properties are kept constant in order to linearize the problem. Hence, the governing equation simplifies to:

$$D_{th}^{fr} \frac{\partial^2 T^{fr}}{\partial z^2} - v^{fr} \frac{\partial T^{fr}}{\partial z} = \frac{\partial T^{fr}}{\partial t} \tag{1.12}$$

where D_{th}^{fr} [L^2 T^{-1}] is the fracture thermal dispersion coefficient, given by:

$$D_{th}^{fr} = \frac{k_l}{\rho_l \tilde{c}_l} + D_{zz}^{fr} \tag{1.13}$$

and where v^{fr} is the constant groundwater flow velocity along the fracture. Equation (1.12) is a standard 1D parabolic-hyperbolic partial differential equation. If the Dirichlet boundary condition $T^{fr} = T_1^{fr}$ is imposed on the fracture inlet, the Ogata-Banks analytical solution (Ogata and Banks, 1961) is now:

$$\frac{T^{fr} - T_0^{fr}}{T_1^{fr} - T_0^{fr}} = \frac{1}{2} \left[\text{erfc} \left(\frac{z - v^{fr}t}{2\sqrt{D_{th}^{fr}t}} \right) + \exp \left(\frac{v^{fr}z}{D_{th}^{fr}} \right) \text{erfc} \left(\frac{z + v^{fr}t}{2\sqrt{D_{th}^{fr}t}} \right) \right] \tag{1.14}$$

where T_0^{fr} is the initial temperature in the fracture.

In the numerical simulation, the finite element domain was spatially discretized along the fracture by using element sizes that gradually increase by the factor 1.1 from $\Delta z = 0.1$ m
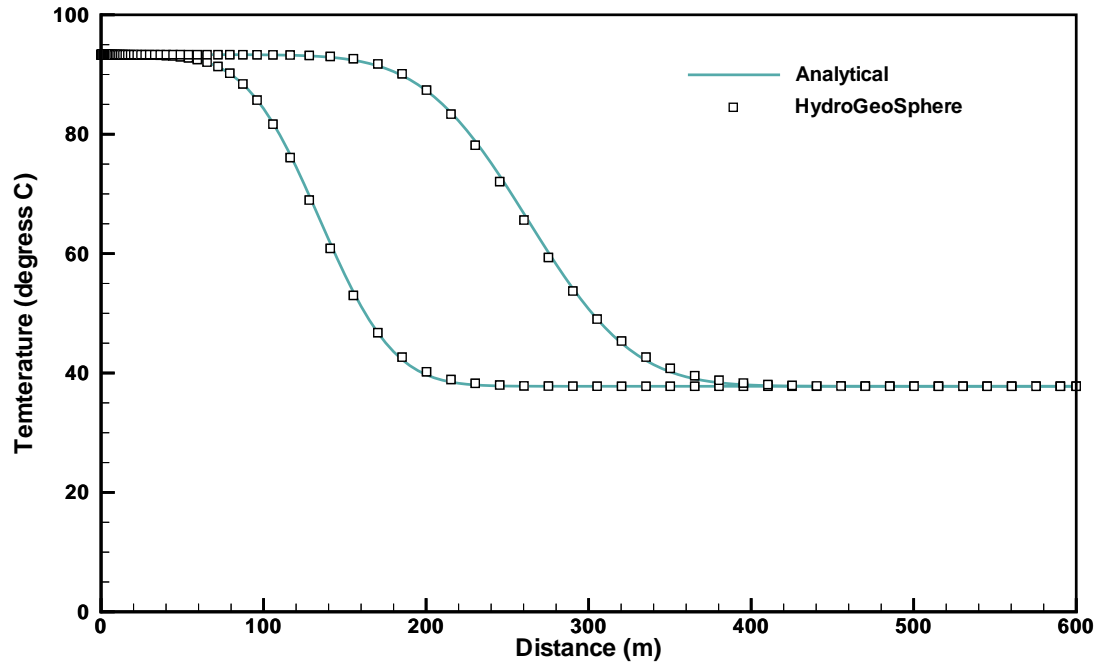
Figure 1.60: Temperature profiles of 1D heat transfer in a single fracture within an impermeable matrix (example 2). Shown are the temperatures in the fracture at 2,148 (left) and 4,262 (right) days.

near the elevated temperature to $\Delta z = 15$ m at the domain boundary. The groundwater velocity in the fracture was set to 7.0×10^{-7} m s^{-1} and the fracture dispersivity used was 5.0 m, giving the fracture thermal dispersion coefficient as 3.62×10^{-6} m^2 s^{-1}. All other parameters are identical to those used in the previous example and given in Table 1.26. The simulation results are depicted in Figure 1.60.

1.7.3 Level 1: Heat Transfer in Fractured Porous Media

Note: the verification problem described in this section corresponds to the `meyer` test case found in the `verification` directory under the **HydroGeoSphere** installation directory.

The third test case verifies 2D heat transfer in a single fracture embedded in a porous matrix. This verification example is based on analytical results presented by Meyer (2004), who investigated advective transient heat transfer in a fracture while in the porous matrix, heat is transported due to conduction alone. Mechanical heat dispersion as well as conduction within the fracture are not considered, making numerical integration unnecessary. The groundwater flow velocity in the fracture is constant. Under these assumptions, the governing

equations of this problem simplify to:

$$\rho_b \tilde{c}_b \; \frac{\partial T}{\partial t} - k_b \; \frac{\partial^2 T}{\partial x^2} = 0 \qquad\qquad b \leq x \leq \infty \qquad\qquad (1.15)$$

and

$$\rho_l \tilde{c}_l \; \frac{\partial T^{fr}}{\partial t} + \rho_l \tilde{c}_l \; v^{fr} \; \frac{\partial T^{fr}}{\partial z} - \frac{k_b}{b} \; \frac{\partial T^{fr}}{\partial x}\bigg|_{x=b} = 0 \qquad 0 \leq z \leq \infty \qquad (1.16)$$

for heat transport in the matrix and in the discrete fracture, respectively. The last term in (1.16) expresses conductive loss of heat from the fracture into the matrix on the fracture-matrix interface. Initially, the entire system has the uniform temperature, T_0. The fluid entering the fracture has the constant temperature, T_1. All boundaries, except the fracture inlet and outlet, are impermeable for groundwater flow and for heat exchange. According to Meyer (2004), the transient solution along the fracture is:

$$\frac{T^{fr} - T_0}{T_1 - T_0} = \text{erfc} \left(\frac{z \; \sqrt{k_b \; \rho_b \tilde{c}_b}}{2 v^{fr} \rho_l \tilde{c}_l b \; \sqrt{(t - z/v^{fr})}} \right) \qquad (1.17)$$

Using the analytical results presented by Tang et al. (1981), it can be shown that the transient solution along a cross-section from the fracture into the porous matrix is given by

$$\frac{T - T_0}{T_1 - T_0} = \text{erfc} \left(\frac{z \; \sqrt{k_b \; \rho_b \tilde{c}_b}}{2 v^{fr} \rho_l \tilde{c}_l b \; \sqrt{(t - z/v^{fr})}} + \frac{\sqrt{\rho_b \tilde{c}_b} \; (x - b)}{2 \sqrt{k_b} \; \sqrt{(t - z/v^{fr})}} \right) \qquad (1.18)$$

The fracture-matrix system used is identical to that shown in Figure 1.61. The finite element domain was spatially discretized in the x-direction by gradually increasing Δx with constant factor 1.1 from $\Delta x = 0.01$ m near the fracture to $\Delta x = 0.1$ m at the domain boundary. In the flow direction, Δz also increases gradually from $\Delta z = 0.1$ m near the elevated temperature to $\Delta z = 0.5$ m at the domain boundary. All other parameters are presented in Table 1.27 and the simulation results are exhibited in the Figures 1.62 and 1.63.

1.7.4 Level 2: Heat Transfer in Anisotropic Porous Media

Note: the verification problem described in this section corresponds to the `yang` test case found in the `verification` directory under the **HydroGeoSphere** installation directory.

The last verification problem for heat transfer is the 2D field scale example presented by Yang and Edwards (2000), and includes all heat transfer mechanisms in both continua with variable fluid properties. This test case represents a realistic scenario of radioactive waste disposal in the low-permeability anisotropic granitic rock of the Canadian Shield (Davison et al., 1994). Figure 1.64 shows the conceptual model, a vertical slice of dimensions 2,000 m × 1,000 m with a unit thickness. Radionuclides are disposed of in a 1,300 m long horizontal
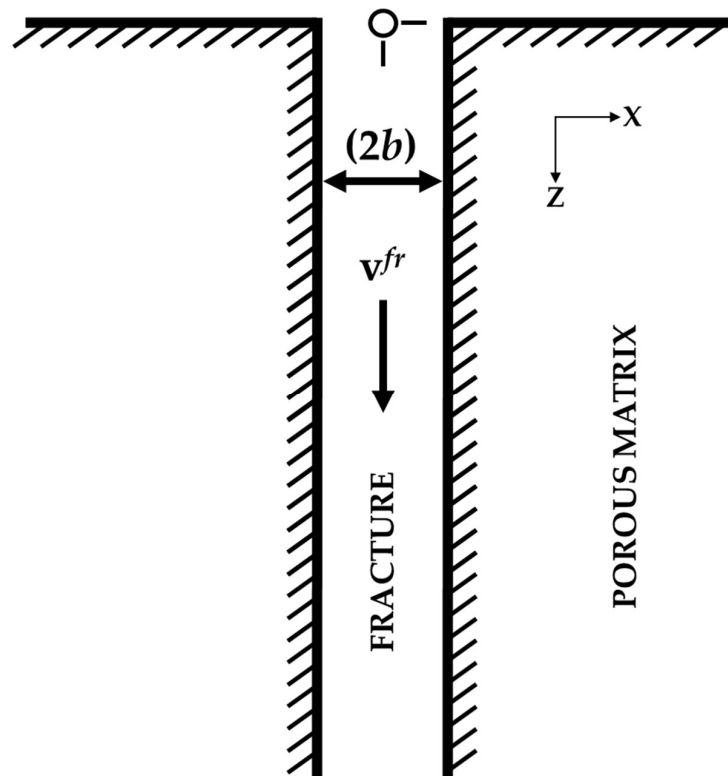
Figure 1.61: Fracture-matrix system used for model verification (Tang et al., 1981).
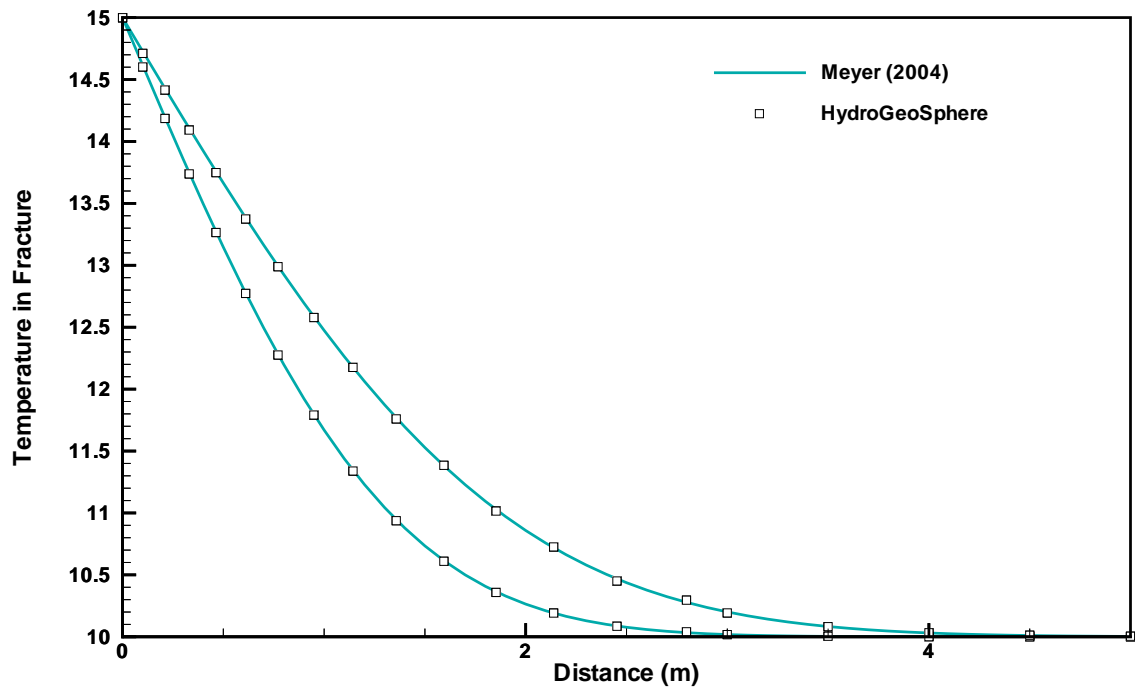
Figure 1.62: Temperature profiles of 1D heat transfer in discretely-fractured porous media. Shown are the temperatures in the fracture at 5,000 (left) and 10,000 (right) seconds.
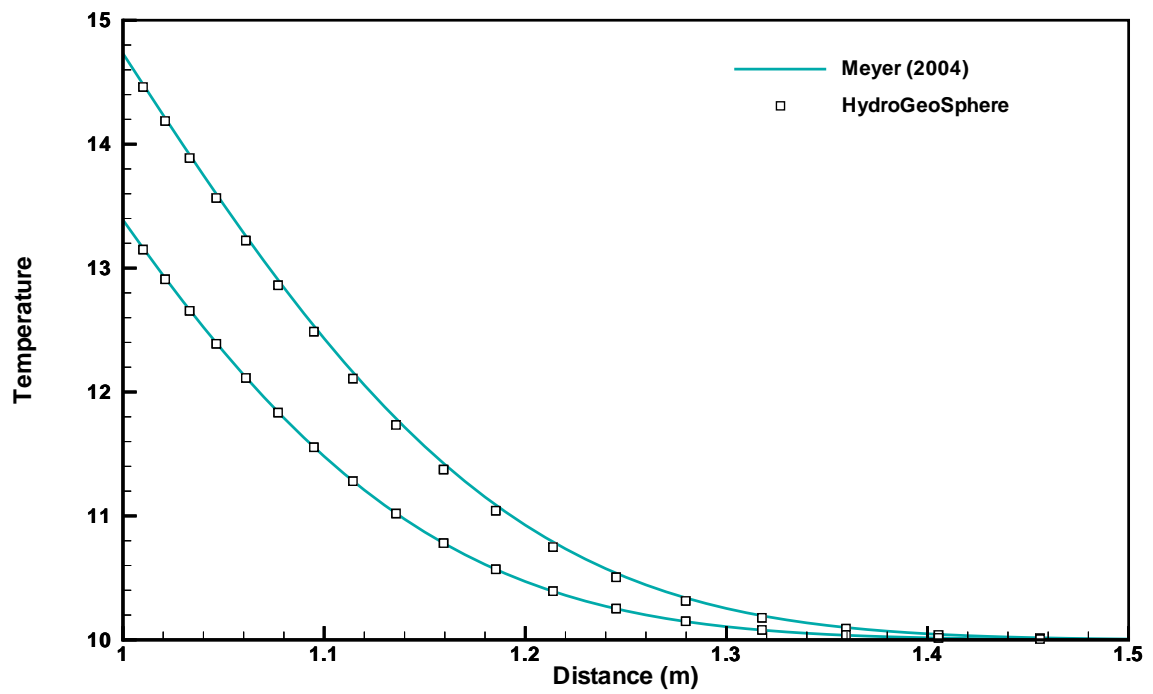
Figure 1.63: Temperature profiles of 1D heat transfer in discretely-fractured porous media. Shown are the temperatures in the matrix at 10,000 seconds simulation time at the distances 0.1 (left) and 0.61 (right) m from the fracture.
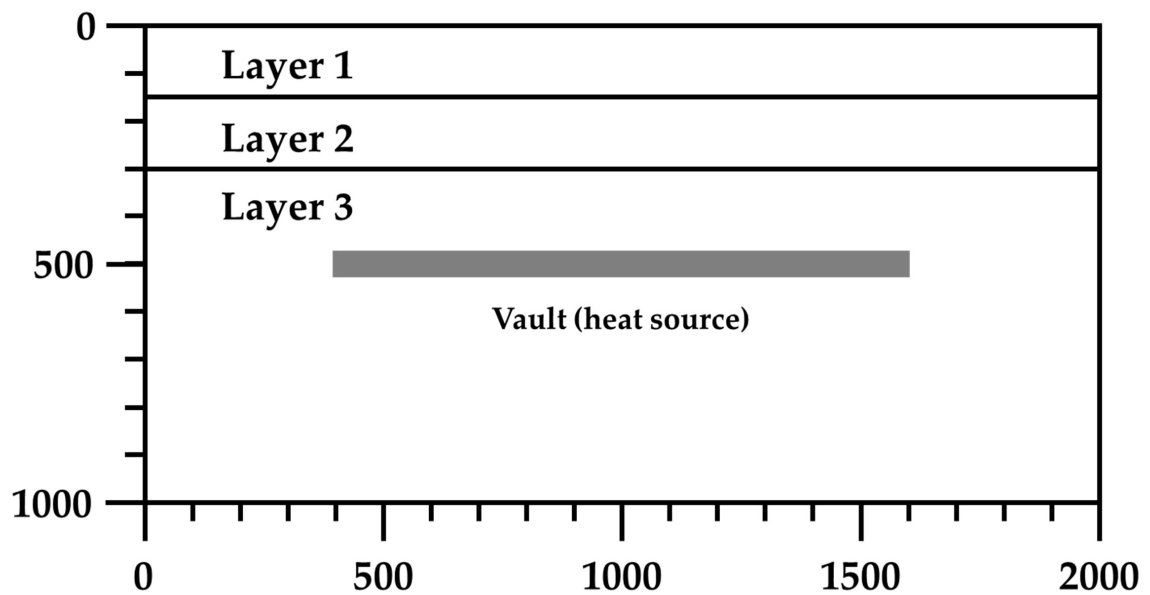
Figure 1.64: The conceptual model for variable-density heat transfer in anisotropic porous media (Yang and Edwards, 2000, Example 4). The heat source in the vault is due to the remaining radioactivity of the stored waste. Top and bottom boundaries are assigned the constant temperatures 6°C and 17.5°C, respectively, with the corresponding geothermal gradient 11.5 K km^{-1}.

Table 1.27: Model parameters used in the verification example for 2D heat transfer in a single fracture embedded in a porous matrix. All parameters are identical to those used by Meyer (2004).

Parameter	Value	Unit
Bulk thermal conductivity (k_b)	3.4	kg m s^{-3} K^{-1}
Heat capacity of solid $(\tilde{c}_s)$	908	m^2 s^{-2} K^{-1}
Solid density (ρ_s)	2550	kg m^{-3}
Heat capacity of water $(\tilde{c}_l)$	4192	m^2 s^{-2} K^{-1}
Fluid density (ρ_l)	997	kg m^{-3}
Matrix porosity (ϕ)	0.2	
Groundwater flow velocity in the fracture (v^{fr})	0.05	m s^{-1}
Initial temperature (T_0)	10	°C
Boundary temperature (T_1)	15	°C
Domain size (ℓ_x, ℓ_z)	2, 10	m
Location of cross-sections (z_1, z_2)	0.1, 0.61	m
Output times (t_1, t_2)	5000, 10000	s

vault at a depth of 500 m below surface. The simulation domain consists of three anisotropic porous layers. The radioactive waste represents an exponentially decreasing heat source due to remaining radioactivity (Davison et al., 1994). Thus, the term $\Gamma = 11.59$ kg m^{-1} s^{-3} · exp(-5.5×10^{-10} s^{-1} · t), as given by Yang and Edwards (2000), was added as a heat sink term to the left hand side of the governing equation. All boundaries are impermeable for flow. Top and bottom boundaries have constant temperatures to mimic a geothermal gradient of 11.5 K km^{-1}, which is natural in the study area. All other boundaries are impermeable for heat transfer. Initially, the geothermal field is undisturbed with horizontal isotherms.

In the numerical simulations carried out with **HydroGeoSphere**, the temperature is assumed to have an impact on both fluid properties density and viscosity. This conforms with the assumption made by Yang and Edwards (2000). Chemical reactions are not considered. All model parameters are summarized in Table 1.28. The variable-density, variable-viscosity flow and heat transfer results are exhibited in Figure 1.65, which shows excellent agreement between the two numerical models.

1.7.5   Level 2: Borden thermal injection experiment

Note: the verification problem described in this section corresponds to the `thermal_molson` test case found in the `verification` directory under the **HydroGeoSphere** installation directory.

Subsurface thermal energy transport is verified by comparing results from HydroGeoSphere with the model verification example used by Molson et al. (1992). This verification example involves a simulation of the Borden thermal injection experiment. A description of the experiment and the observed data are presented by Palmer et al. (1992). Unless otherwise
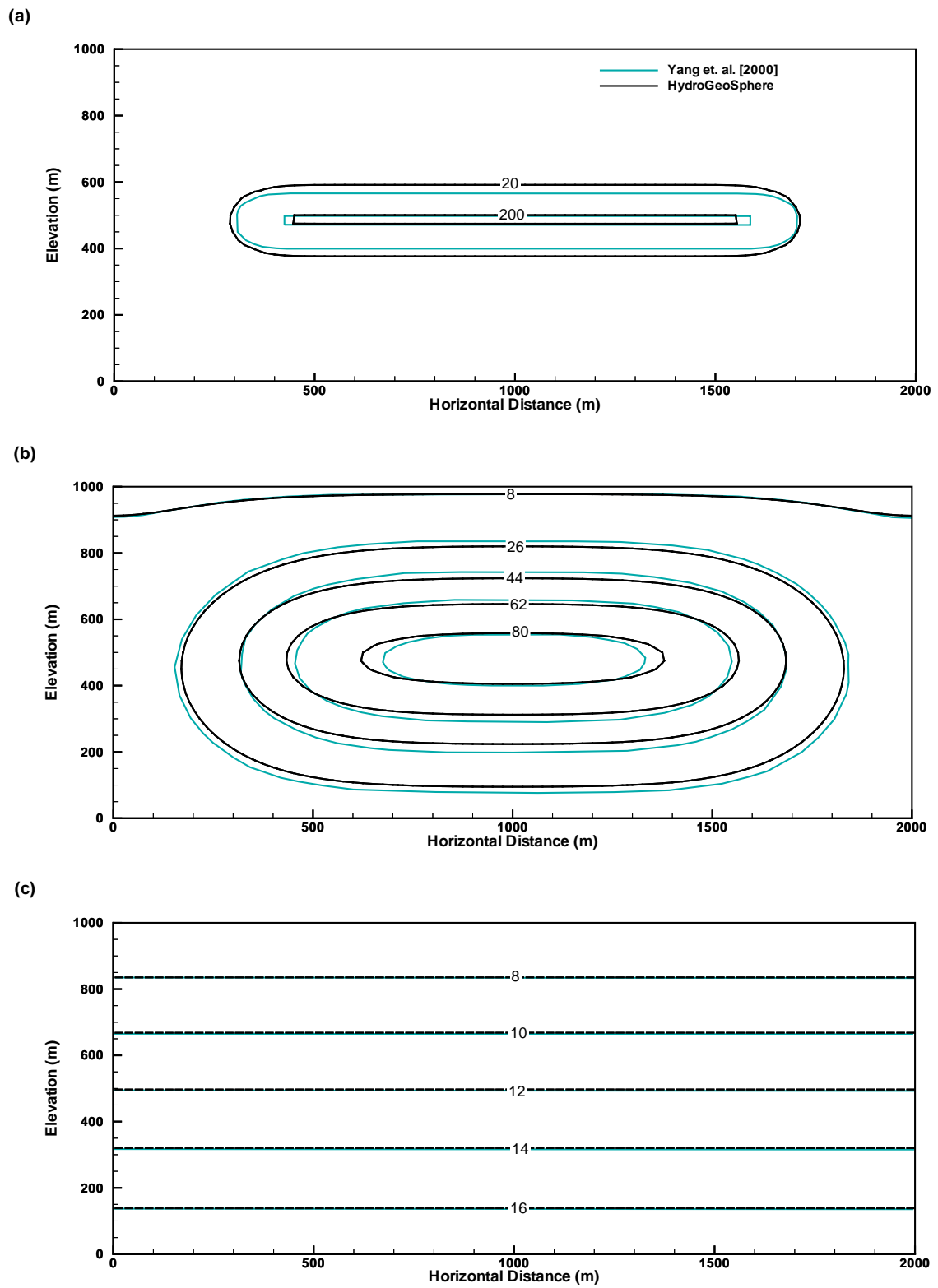
Figure 1.65: Evolution of temperature in anisotropic porous media with an exponentially decreasing heat source. Simulation times are (a) 10^4 days, (b) 3×10^5 days, (c) 7×10^6 days. Shown are isotherms in degrees Celsius.

Table 1.28: Model parameters used in the verification example for 2D variable-density thermal flow and heat transfer in anisotropic porous media. All parameters are identical to those used by Yang and Edwards (2000).

Parameter	Value	Unit
Bulk thermal conductivity (k_b)	2.0	kg m s^{-3} K^{-1}
Heat capacity of solid $(\tilde{c}_s)$	800	m^2 s^{-2} K^{-1}
Heat capacity of water $(\tilde{c}_l)$	4174	m^2 s^{-2} K^{-1}
Solid density (ρ_s)	2630	kg m^{-3}
Matrix permeability $(\kappa_{xx}, \kappa_{zz})$	Layer 1: 1.0×10^{-15}, 5.0×10^{-15}	m^2
	Layer 2: 1.0×10^{-17}, 5.0×10^{-17}	m^2
	Layer 3: 1.0×10^{-19}, 1.0×10^{-19}	m^2
Matrix porosity (ϕ)	0.004	
Domain size (ℓ_x, ℓ_z)	2000, 1000	m
Spatial discretization $(\Delta x, \Delta z)$	25, 25	m

stated, all parameters used in the HydroGeoSphere simulation are identical to those used by Molson et al. (1992). The domain size was $40 \times 30 \times 20$ m, and was discretized in all directions using 0.5 m block elements. The initial temperature of the domain varied from 15 ^oC at ground surface to 9 ^oC 6 m below the surface. The injection well was located at x = 12 m, y = 15 m, z = 16 m and water was injected at a temperature of 37 ^oC for the first 6 days. The flow and transport parameters are given in Table I. The aquifer thermal parameters are listed in Table II. The simulation was run for 76 days, and the results are presented at 9 days, 27 days and 76 days for a 2-D longitudinal cross-section through the injection well (Figure 1). The results from the HydroGeoSphere simulation are compared to those presented by Molson et al. (1992). Figure 1 shows that the temperature results from both models agree. The minor differences that do occur are due to the different treatment of the temperature boundary condition at the surface of the domain. In addition, Molson et al. (1992) used temperature-dependent density and viscosity terms, whereas the HydroGeoSphere simulation treated these parameters as constant under the given range in subsurface temperatures.

1.8 Travel Time Probability

1.8.1 1D travel time PDF

Note: the verification problem described in this section corresponds to the `1D_backwards_transport` test case found in the `verification` directory under the **HydroGeoSphere** installation directory.

The travel time PDF for a semi-infinite domain is the flux concentration solution of Eq. (2.183a), which is obtained by applying the boundary conditions $g_t(t, 0) = \delta(t)$ and $D\frac{\partial g_t(t,x)}{\partial x}|_{x=\infty} = 0$, with $D = \alpha_L v + D_m$. This solution reads:

$$g_t(t,x) = \frac{x}{\sqrt{4\pi Dt}\, t} \exp\left(-\frac{(x-vt)^2}{4Dt}\right) \tag{1.19}$$

Considering a 1D domain with outlet position at $x = L$, the backward travel time PDF is deduced by replacing x by $L - x$, to give:

$$g_t(t,x) = \frac{L-x}{\sqrt{4\pi Dt}\, t} \exp\left(-\frac{(L-x-vt)^2}{4Dt}\right) \tag{1.20}$$

In Figure 1.66, the numerical forward and backward travel time PDF's are compared to this analytical solution.
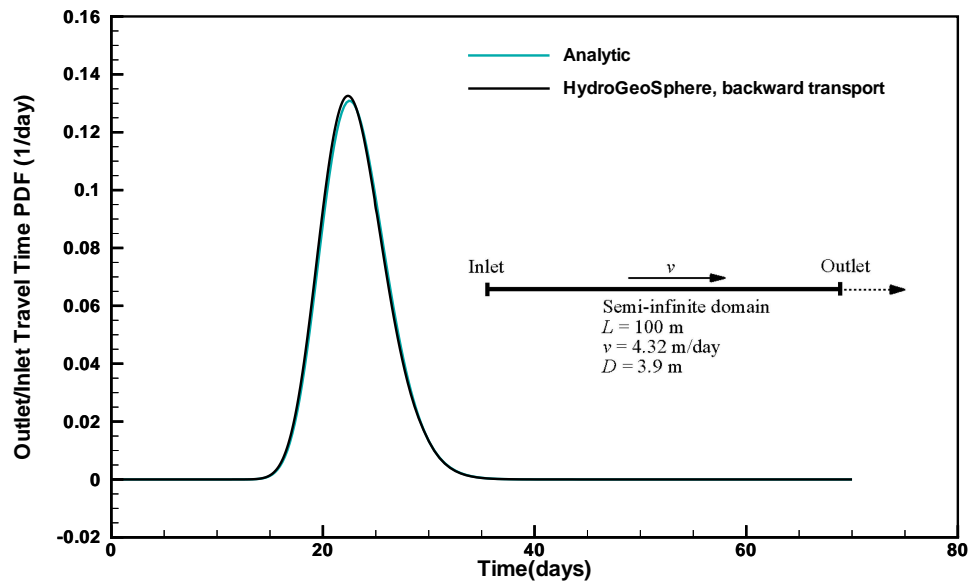

Figure 1.66: Forward and backward travel time PDF's versus analytical solution for a 1D semi-infinite domain.

Chapter 2

Illustrative Examples

2.1 Travel Time Probability

2.1.1 Capture zone probability of a pumping-well

In this section, an illustration of the capture zone probability definition by using the boundary value problem (2.203) is given. The theoretical system corresponds to a uniformly recharged aquifer (rainfall infiltration of 0.432 m/year), containing a single extraction well (extraction rate of 300 m^3/year), and with a natural outlet to which a uniform hydraulic head of 32 m is prescribed (see Fig. 2.1). The aquifer is homogeneous with respect to hydraulic conductivity, porosity and dispersivity. Flow is at steady-state. Figure 2.1 shows the well capture zone probability at time $t = 1, 5$ and 50 days, the date 50 days providing a probability field close to steady-state (absolute capture zone).

Figure 2.2 shows the solution of Eqs. (2.195) and (2.197). Figure 2.2a provides the average time a water particle will take prior to exiting at the pumping-well, exclusively. To do so, Eq. (2.197) has been solved by assigning $\langle E \rangle = 0$ at the well and a zero flux at the natural outlet. This solution can be combined with the capture zone probability distribution, for well protection zone definition purposes.

Figure 2.2b shows the mean age distribution at aquifer scale, figure 2.2c the mean life expectancy distribution, and figure 2.2d gives the mean total transit time (from inlet to outlets) distribution ($\langle T \rangle = \langle A \rangle + \langle E \rangle$).

2.2 Simulating Tidal Fluctuation

This example shows the use of historical tide data as a boundary condition on a simple sloping surface water domain.

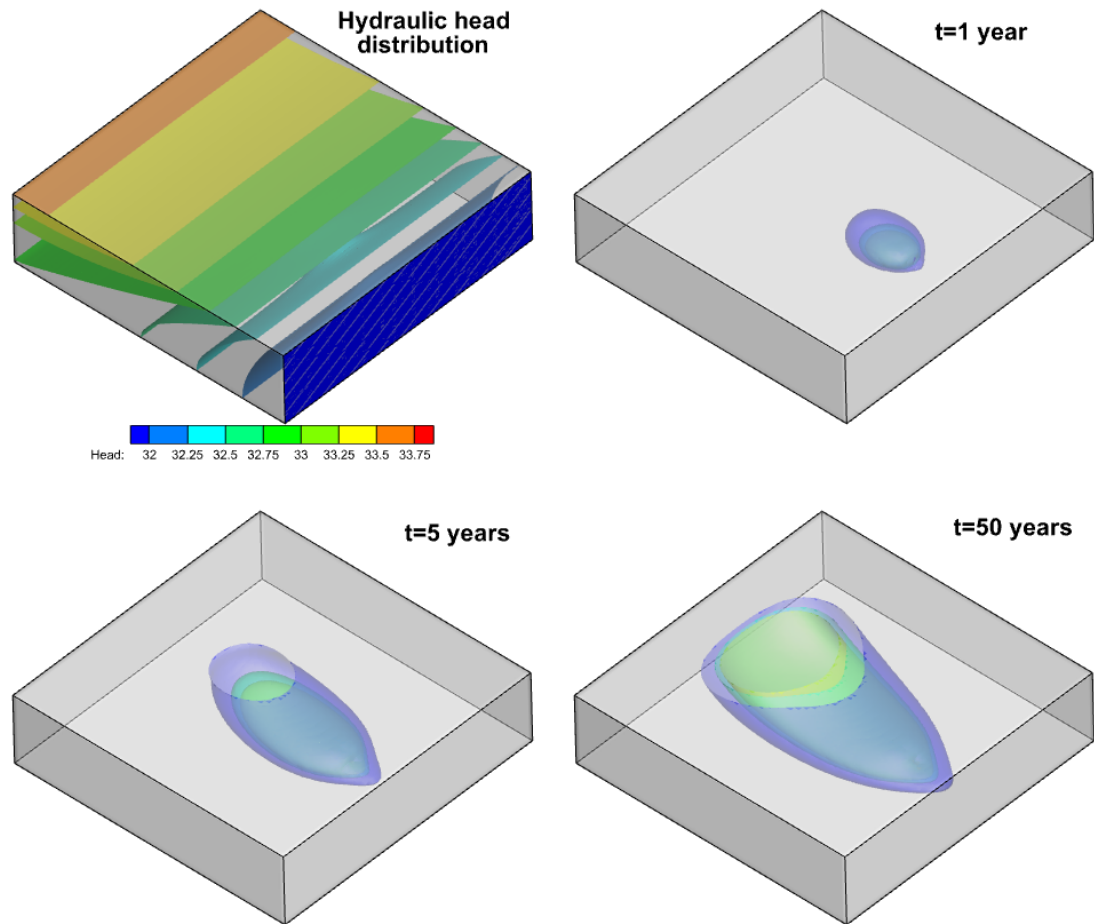This data was obtained from the Center for Operational Oceanographic Products and

Figure 2.1: Pumping-well temporal capture zone probability. The aquifer size is $128 \times 128 \times 32$ m. Iso-probability surfaces 0.1-0.5-0.9.
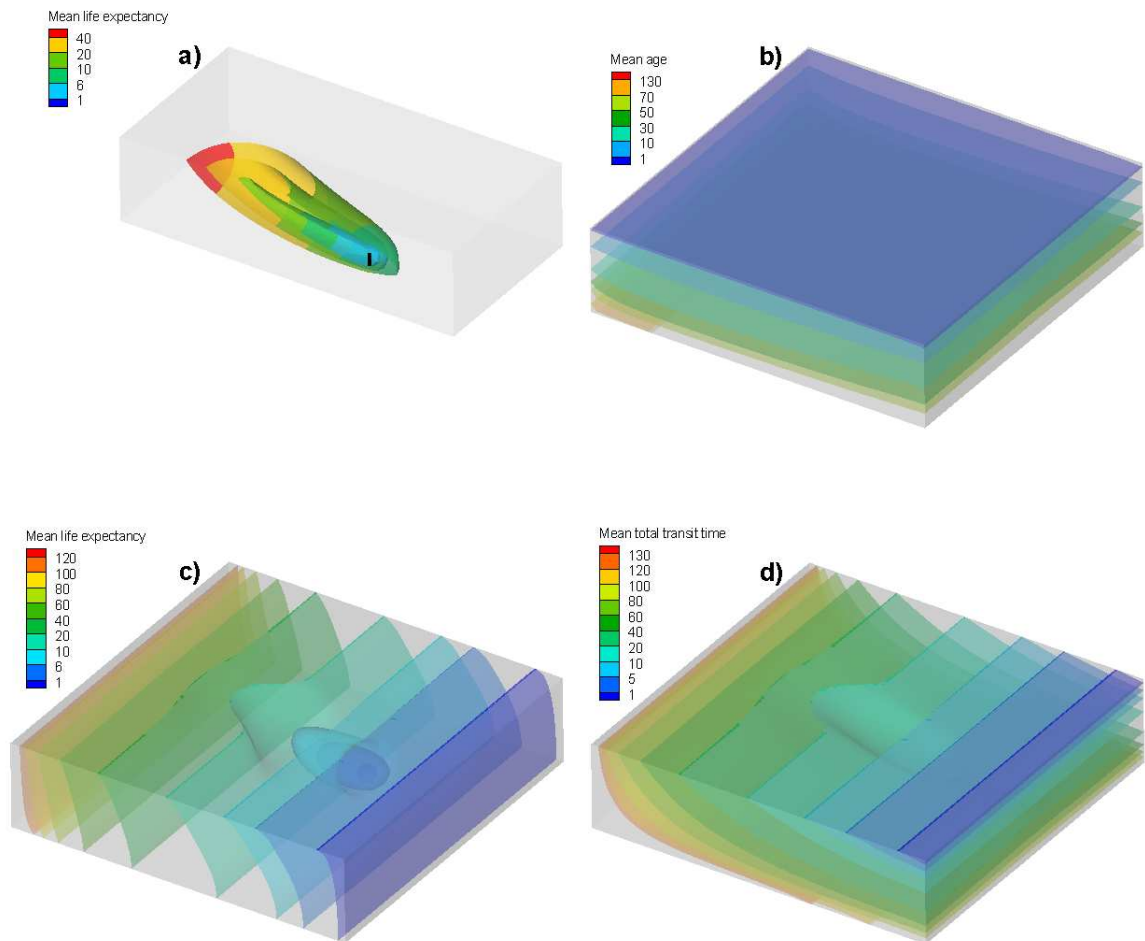
Figure 2.2: Temporal moment solutions in days: (a) Mean life-expectancy-to-well distribution; (b) Mean age; (c) Mean life expectancy; (d) Mean total transit time.

Services (http://tidesandcurrents.noaa.gov/index.html) for the Station at Redwood City, California. A portion of the raw data file (`redwood_hl_dec12006.orig`) is shown here:

```
Station ID: 9414523 Page Help

Historic Tide Data
Station Date      Time  Vrfy 6
DCP#:
Units:                  Meters
Data%:  MSL        LST  98.92
Maximum:                1.545
Minimum:               -1.903
------- -------- ----- -------
9414523 20061201 00:00
9414523 20061201 00:06
...
9414523 20061201 02:18
9414523 20061201 02:24  -1.033
9414523 20061201 02:30
...
```

The header contains important information about the data, such as the units (metres) and the reference elevation (MSL or mean sea level). This data file contains daily minimum and maximum tide elevations at 6-minute intervals so many of the records do not contain an elevation value. These records are ignored by **grok**.

This data can be easily modified for use with **grok** by stripping out the header and footer information and leaving only the data records. This has been done in file `redwood_hl_dec12006.tide_data`. The beginning of the file is shown here:

```
9414523 20061201 00:00   0.0
9414523 20061201 00:06
...
9414523 20061201 02:18
9414523 20061201 02:24  -1.033
9414523 20061201 02:30
...
```

Note that we set the initial tide elevation value to zero in the first record of the data.

Figure 2.3 shows the surface water domain and finite-element mesh. It is a tilted strip 100 m long and 1 m wide, which slopes from $z = -2$ m at $x = 0$ to $z = 2$ m at $x = 100$ m.

Here is a portion of the main input file, `tide.grok`, where we assign the tidal boundary condition:

```
clear chosen nodes
```
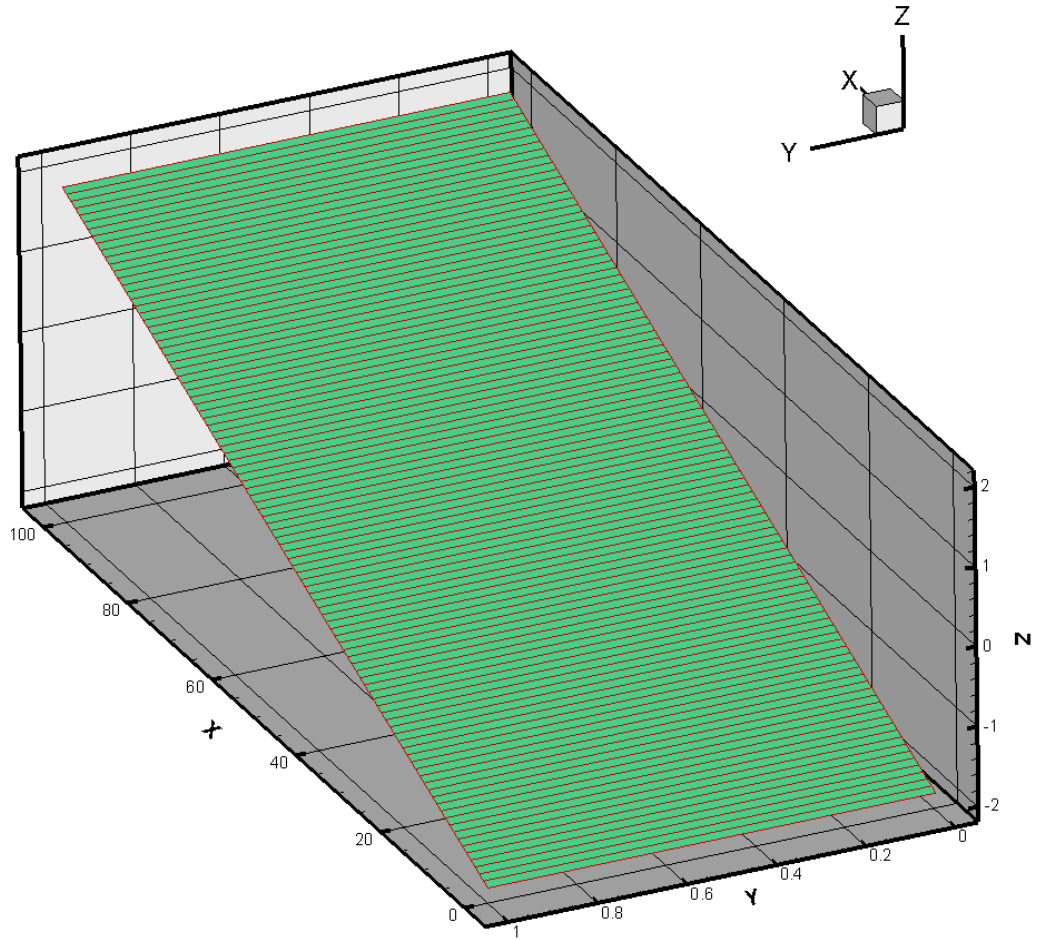
Figure 2.3: Surface domain and mesh.

```
      choose nodes block
      0.0 0.0
      0.0 1.0
      -2.0 -2.0

      interpolate specified head
      true

      specified head from tidal data
      redwood_hl_dec12006.tide_data
      20061201 00:00

      echo flow boundary conditions

      output times
      4.7
      end
```

Note that we have chosen to index the time to zero at `20061201 00:00`, the first record.

We have chosen to end the simulation at time 4.7 days, as defined by the final (and only) entry to the Output times instruction.

In this problem, time units are in days because we included the instruction Units: kilogram-metre-day.

The resulting head function can be examined by inserting the instruction Echo flow boundary conditions, which gives the following output:

```
INSTRUCTION: echo flow boundary conditions
 Number of prescribed head nodes              2
    Node       Head          Time on         Time off
     203     0.0000         0.0000         0.10001
            -1.0330         0.10001         0.36667
             1.2350         0.36667         0.66251

             ...
            -1.8740          4.8000         0.10000E+21
     304     0.0000         0.0000         0.10001
            -1.0330         0.10001         0.36667
             1.2350         0.36667         0.66251

             ...
            -1.5220         0.66251         0.92084
            -1.8740          4.8000         0.10000E+21
 No prescribed flux nodes
 No prescribed time-varying flux faces
```

Figure 2.4 shows the initial water surface (translucent blue) superimposed on the ground
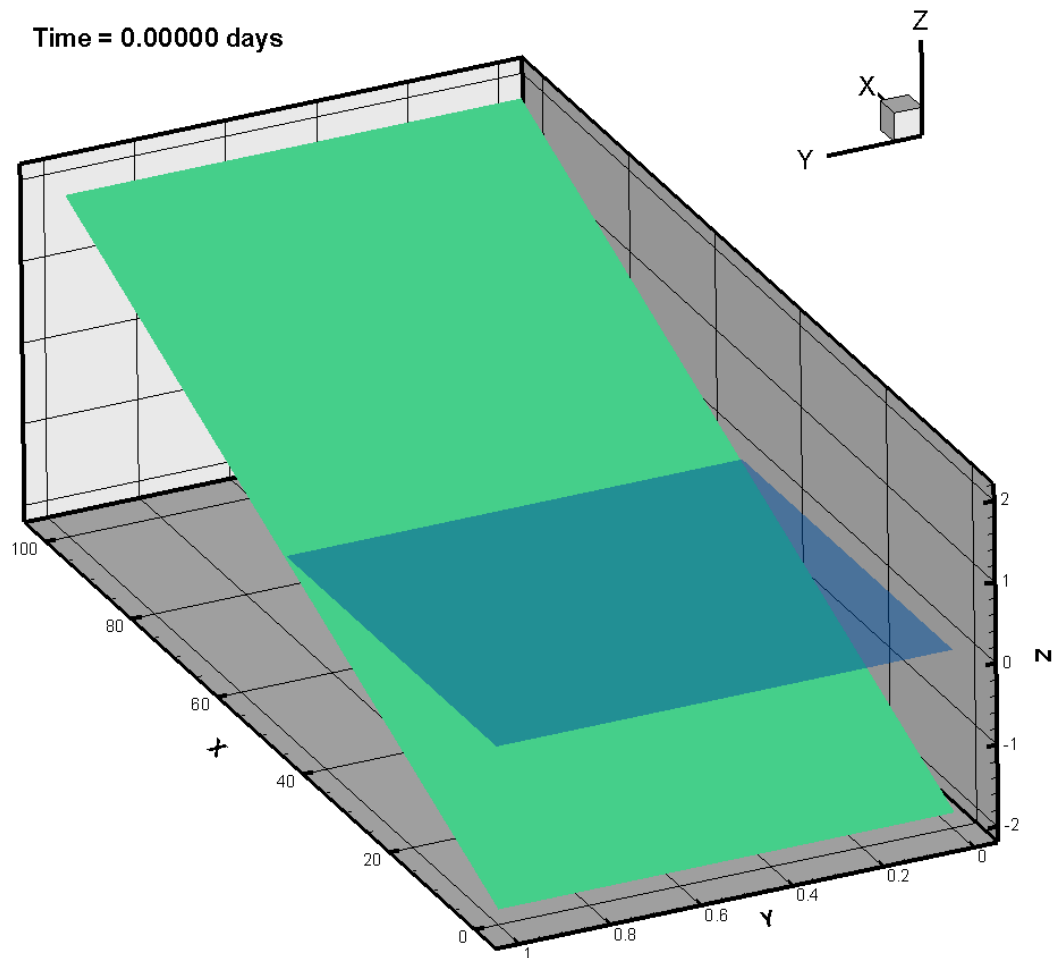
Figure 2.4: Tide level.

surface (green). This figure was produced by Tecplot using the layout file `tide.lay`. It consists of two identical frames which are superimposed. The background frame contains the ground surface, which is just the finite element mesh shaded green. The foremost frame, representing the water surface, has no background (so it doesn't obscure the ground surface) and was created by assigning the surface domain head as the z-coordinate and value blanking for surface water depths less than 1 cm.

An animated movie of the tidal fluctuation can be found in the file `tide.avi`. Rather than produce multiple output files by adding output times, we modified the `debug.control` file so that an output file was produced for each timestep.

References

Abdul, A. S. (1985). *Experimental and numerical studies of the effect of the capillary fringe on streamflow generation.* PhD thesis, University of Waterloo, Waterloo, Ontario, Canada.

Akan, A. O. and Yen, B. C. (1981). Mathematical model of shallow water flow over porous media. *Journal of the Hydraulics Division*, 107(4):479–494.

Barlow, P. M. and Moench, A. F. (2011). WTAQ version 2—A computer program for analysis of aquifer tests in confined and water-table aquifers with alternative representations of drainage from the unsaturated zone. Technical Report Techniques and Methods 3-B9, U. S. Geological Survey.

Biot, M. A. (1941). General theory of three-dimensional consolidation. *J. Applied Physics*, 12(2):155–164.

Davison, C. C., Brown, A., Everitt, R. A., Gascoyne, M., Kozak, E. T., Lodha, G. S., Martin, C. D., Soonawala, N. M., Stevenson, D. R., Thorne, G. A., and Whitaker, S. H. (1994). The disposal of Canada's nuclear fuel waste: Site screening and site evaluation technology. Technical Report AECL–10713, Atomic Energy of Canada Limited, Pinawa, Manitoba, Canada.

Di Giammarco, P., Todini, E., and Lamberti, P. (1996). A conservative finite element approach to overland flow: The control volume finite element formulation. *Journal of Hydrology*, 175:267–291.

Diersch, H. J. G. and Kolditz, O. (2002). Variable-density flow and transport in porous media: approaches and challenges. *Adv. Water Resour.*, 25(8–12):899–944.

Elder, J. W. (1967). Transient convection in a porous medium. *J. Fluid Mech.*, 27:609–623.

Faust, C. R., Sims, P. N., Spalding, C. P., Andersen, P. F., and Stephenson, D. E. (1990). FTWORK: A three-dimensional groudwater flow and solute transport code. Technical Report WSRC-RP-89-1085, ON: DE90008007, Westinghouse Savannah River Co., Aiken, SC.

Fipps, G. and Skaggs, R. W. (1991). Simple methods for predicting flow to drain. *ASCE J. Irrig. Drain. Div. Am. Soc. Civ. Eng.*, 117(6):881–896.

Fipps, G., Skaggs, R. W., and Nieber, J. L. (1986). Drains as a boundary condition in finite elements. *Water Resour. Res.*, 22(11):1613–2621.

Forsyth, P. A., Wu, Y. S., and Pruess, K. (1995). Robust numerical methods for saturated-unsaturated flow with dry initial conditions in heterogeneous media. *Adv. Water Res.*, 18(1):25–38.

Freeze, R. A. and Cherry, J. A. (1979). *Groundwater*. Prentice-Hall, Inc., Englewood Cliffs, NJ.

Frolkovič, P. and De Schepper, H. (2001). Numerical modelling of convection dominated transport coupled with density driven flow in porous media. *Adv. Water Resour.*, 24:63–72.

Gelhar, L. W. and Collins, M. A. (1971). General analysis of longitudinal dispersion in nonuniform flow. *Water Resour. Res.*, 7(6):1511–1521.

Gerke, H. H. and van Genuchten, M. T. (1993). A dual-porosity model for simulating the preferential movement of water and solutes in structured porous media. *Water Resour. Res.*, 29(2):305–319.

Govindaraju, R. S., Jones, S. E., and Kavvas, K. L. (1988a). On the diffusion wave model for overland flow: 1. Solution for steep slopes. *Water Resour. Res.*, 24(5):734–744.

Govindaraju, R. S., Jones, S. E., and Kavvas, K. L. (1988b). On the diffusion wave model for overland flow: 2. Steady state analysis. *Water Resour. Res.*, 24(5):745–754.

Govindaraju, R. S. and Kavvas, M. L. (1991). Dynamics of moving overland flows over infiltrating surfaces at hillslopes. *Water Resour. Res.*, 27(8):1885–1898.

Guvanasen, V. (2007). FRAC3DVS Enhancements: Subgridding, Hydromechanical Deformation, and Anisotropic Molecular Diffusion. Technical Report NWMO TR-2007-05, Nuclear Waste Management Organization, Toronto, Ontario, Canada.

Hoopes, J. A. and Harleman, D. R. (1967). Wastewater recharge and dispersion in porous media. *Journal of the Hydraulics Division*, 93:51–71.

Huyakorn, P. S., Springer, E. P., Guvanasen, V., and Wadsworth, T. D. (1986). A three-dimensional finite-element model for simulating water flow in variably saturated porous media. *Water Resour. Res.*, 22(13):1790–1808.

Huyakorn, P. S., Thomas, S. D., and Thompson, B. M. (1984). Testing and Validation of Models for Simulating Solute Transport in Groundwater: Development, Evaluation and Comparison of Benchmark Techniques. Technical Report 35, International Groundwater Modeling Center, Holcolm Research Institute, Butler University, Indianapolis, Indiana.

HydroGeoLogic, Inc. (1996). *MODFLOW-SURFACT ver. 2.2 User's manual. A three dimensional fully integrated finite difference code for simulating fluid flow and transport of contaminant in saturated-unsaturated porous media*. Herndon, VA.

Johannsen, K., Kinzelbach, W., Oswald, S. E., and Wittum, G. (2002). The saltpool benchmark problem—numerical simulation of saltwater upcoming in a porous medium. *Adv. Water Resour.*, 25(3):335–348.

Kirkham, D. (1949). Flow of ponded water into drain tubes in soil overlying an impervious layer. *Eos Trans. AGU*, 30(3):369–385.

Lemieux, J. M. (2006). *Impact of the Wisconsinian glaciation on Canadian continental groundwater flow.* PhD thesis, University of Waterloo, Waterloo, Ontario, Canada.

MacQuarrie, K. T. B. and Sudicky, E. A. (1996). On the incorporation of drains into three-dimensional variably saturated groundwater flow models. *Water Resour. Res.*, 32(3):477–482.

Mathias, S. A. and Butler, A. P. (2006). Linearized Richards' equation approach to pumping test analysis in compressible aquifers. *Water Resour. Res.*, 42(6).

Meyer, J. R. (2004). Development of a heat transport analytical model for a single fracture in a porous media. Project report of the course Earth 661, Analytical Solutions in Hydrogeology, submitted to E. A. Sudicky and C. J. Neville. University of Waterloo Center for Groundwater Research.

Mishra, P. K. and Neuman, S. P. (2010). Improved forward and inverse analyses of saturated-unsaturated flow toward a well in a compressible unconfined aquifer. *Water Resour. Res.*, 46(7).

Molson, J. W., Frind, E. O., and Palmer, C. D. (1992). Thermal energy storage in an unconfined aquifer: 2. Model development, validation and application. *Water Resour. Res.*, 28(10):2857–2867.

Neville, C. Personal communication.

Ogata, A. and Banks, R. B. (1961). A solution of the differential equation of longitudinal dispersion in porous media. Technical Report Professional Paper 411-A, U. S. Geological Survey.

Oswald, S. E. (1999). *Dichteströmungen in porösen Medien: Dreidimensionale Experimente und Modellierung.* PhD thesis, Institut für Hydromechanik und Wasserwirtschaft, ETH Zürich, Zürich, Switzerland.

Oswald, S. E. and Kinzelbach, W. (2004). Three-dimensional physical benchmark experiments to test variable-density flow models. *J. Hydrol.*, 290:22–42.

Palmer, C. D., Blowes, D. W., Frind, E. O., and Molson, J. W. (1992). Thermal energy storage in an unconfined aquifer: 1. Field injection experiment. *Water Resour. Res.*, 28:2845–2856.

Panday, S. and Huyakorn, P. S. (2004). A fully coupled physically-based spatially-distributed model for evaluating surface/subsurface flow. *Adv. Water Resour.*, 27:361–382.

Perlmutter, N. M. and Lieber, M. (1970). Dispersal of plating wastes and sewage contaminants in ground water and surface water, South Farmingdale-Massapequa area, Nassau County, New York. Technical Report Water Supply paper 1879-G, U. S. Geological Survey.

Shikaze, S. G., Sudicky, E. A., and Schwartz, F. W. (1998). Density-dependent solute transport in discretely-fractured geologic media: is prediction possible? *J. Contam. Hydrol.*, 34(10):273–291.

Singh, V. and Bhallamudi, S. M. (1998). Conjunctive surface-subsurface modeling of overland flow. *Adv. Water Resour.*, 21:567–579.

Smith, R. E. and Woolhiser, D. A. (1971). Overland flow on an infiltrating surface. *Water Resour. Res.*, 7(4):899–913.

Sudicky, E. A. (1986). Personal communication.

Sudicky, E. A. (1991). CMM: A semi-analytical computer model for simulating ground water fate and transport of contaminants subject to chained-decay reactions. Report prepared for Dr. Zubair Saleem, US EPA Office of Solid Waste, Hydrogeologic Inc., Contract No. 68-WO-0029.

Sudicky, E. A. (1994). Personal communication.

Sudicky, E. A., Hwang, H.-T., Illman, W. A., Wu, Y. S., Kool, J. B., and Huyakorn, P. A. (2013). A semi-analytical solution for simulating contaminant transport subject to chain-decay reactions. *J. Contam. Hydrol.*, 144(1):20–45.

Tang, D. H., Frind, E. O., and Sudicky, E. A. (1981). Contaminant transport in fractured porous media: Analytical solution for a single fracture. *Water Resour. Res.*, 17(3):555–564.

Theis, C. V. (1935). The relation between the lowering of the Piezometric surface and the rate and duration of discharge of a well using ground-water storage. *Eos, Transactions American Geophysical Union*, 16(2):519–524.

VanderKwaak, J. (1999). *Numerical simulation of flow and chemical transport in integrated surface-subsurface hydrologic systems*. PhD thesis, University of Waterloo, Waterloo, Ontario, Canada.

Wang, J. S. Y. and Narasimhan, T. N. (1985). Hydrologic mechanisms governing fluid flow in a partially saturated, fractured, porous medium. *Water Resour. Res.*, 21(12):1861–1874.

Ward, D. S., Reeves, M., and Duda, L. E. (1984). Verification and field comparison of the Sandia waste-isolation flow and transport (SWIFT) model. Technical Report NUREG/CR-3316, Sandia National Laboratories, Albuquerque, NM.

Wilson, J. L. and Miller, P. J. (1978). Two-dimensional plume in uniform groundwater flow. *Journal of the Hydraulics Division*, 104(HY4):503–514.

Yang, J. and Edwards, R. N. (2000). Predicted groundwater circulation in fractured and unfractured anisotropic porous media driven by nuclear fuel waste heat generation. *Can. J. Earth Sci.*, 37(9):1301–1308.

Zheng, C. (1990). MT3D, A modular three-dimensional transport model for simulation of advection, dispersion and chemical reactions of contaminants in groundwater systems. Technical report, U. S. Environmental Protection Agency, Robert S. Kerr Environmental Research Laboratory, Ada, OK.

Index